

FINAL REPORT

Project Title: S3 GUN-Sandgate Road Bridge Load Testing Report
(2016/17)

ARRB Project No: PRG16022

Author/s: Hanson Ngo, Anthony Rooke and Giovanna Zanardo

Client: Queensland Department of Transport and Main Roads

Date: 18/10/2018

SUMMARY

Queensland Department of Transport and Main Roads (TMR) engaged ARRB to conduct a behavioural load test on a span of Sandgate Road Bridge (ID 8558). The objective of the load test was to investigate the effects of the damage to the transverse stressing bars (TSB), that was applied during the test regime, on the structural behaviour of the bridge superstructure. TMR desires to gain confidence in the load distribution behaviour when the TSBs are damaged or there is substantial loss of the section. This will allow a wider application of findings across the state on the numerous existing deck unit bridges, in the development of mitigation strategies for the TSB deficiency issues.

The Sandgate Road Bridge, built in 1985, consists of ten simply-supported spans and carries the Gateway Motorway across Sandgate Road. Each span is composed of 15 deck units, transversely stressed by TSBs spaced every 2.0 metres in the longitudinal direction. The effects of the applied TSB damage on the bridge superstructure was investigated via in-service monitoring and controlled load testing. The in-service data were used to benchmark the structural behaviour under operational loads, and to assess the properties of the traffic carried by the northbound lane of the bridge. The controlled load test data were analysed to assess the changes in the behaviour of the bridge superstructure due to various levels of damage applied to the TSBs during the test regime.

It was found that the incrementally induced damage resulted in a reduction in the overall capacity of the structure, as well as an increase in the measured structural responses (e.g. deflections and strains) and a reduction in the lateral load distribution capability. The magnitude of these effects is in proportion to the reduction of the mortar joint areas between the deck units rather than to the level of applied TSB damage. The loss of the transverse prestress and damage of the mortar joints at various locations resulted in the reduced level of structural integrity and the onset of propagation of failure of the lateral load transfer mechanism.

The integrity of the mortar joints plays a critical role in the transverse load transfer mechanism of the bridge superstructure, while the TSBs contribute to the integrity of the mortar joints under loads. For a deck unit bridge with TSB deficiency, damage to the mortar joints is highly likely due to some overload events and may also occur under service loads. This damage would propagate further under service loads. Eventually, the mortar joints would be lost to a state in which each deck unit carries loads separately, i.e. a transverse load transfer mechanism is no longer present. The integrity of the overall structure would be lost, and the overall capacity of the structure would be dependant on the capacity of each individual deck unit, which may result in structural failure under service loads.

Since the load test was carried out in a short time period, no detailed assessment of the long-term effects of the TSB deficiencies on the performance of the bridge has been undertaken. It is recommended that further investigation and research be conducted to establish a knowledge base for TMR to develop appropriate mitigation measures for deck unit bridges with TSB deficiencies.

This report should be read in conjunction with the accompanying document titled '*AS/ISO 13822 Framing investigation into the assessment of deck unit bridge and transverse stressing bar deficiencies*'.

Although the Report is believed to be correct at the time of publication, ARRB, to the extent lawful, excludes all liability for loss (whether arising under contract, tort, statute or otherwise) arising from the contents of the Report or from its use. Where such liability cannot be excluded, it is reduced to the full extent lawful. Without limiting the foregoing, people should apply their own skill and judgement when using the information contained in the Report.

Queensland Department of Transport and Main Roads Disclaimer

While every care has been taken in preparing this publication, the State of Queensland accepts no responsibility for decisions or actions taken as a result of any data, information, statement or advice, expressed or implied, contained within. To the best of our knowledge, the content was correct at the time of publishing.

ACKNOWLEDGEMENTS

The authors acknowledge the support provided by staff across TMR's Engineering & Technology, and Program Delivery & Operations Branches, and the assistance of Lend Lease staff, as well as the NSW Roads and Maritime Services for the operation of the proof load vehicle during the site testing.

CONTENTS

1	INTRODUCTION	1
2	DETAILS OF SANDGATE ROAD BRIDGE	2
2.1	Reference Information	2
2.2	Characteristics of Existing Structure	2
2.3	Characteristics of Span 9	3
3	OBJECTIVES OF TESTING	6
4	STAGES OF STRUCTURAL DAMAGE	7
5	LOAD CASES AND CONFIGURATION	8
6	LOAD TEST PROGRAM	11
7	SITE MEASUREMENTS	12
7.1	Instrumentation	12
8	TEST SCHEDULE	16
9	ROLES AND RESPONSIBILITY	17
10	DATA ANALYSIS	18
10.1	In-service Monitoring	18
10.1.1	<i>Measurement Settings and Data Processing</i>	18
10.1.2	<i>Event Statistics</i>	18
10.1.3	<i>Strain Distribution</i>	19
10.1.4	<i>Load Distribution Factors</i>	21
10.2	Load Tests	25
10.2.1	<i>Measurement Settings and Data Processing</i>	25
10.2.2	<i>Strain Distribution</i>	25
10.2.3	<i>Load Distribution Factors</i>	33
10.2.4	<i>Neutral Axis</i>	33
10.2.5	<i>Deck Movements</i>	38
11	DISCUSSION	40
11.1	Observations Based on In-service Monitoring	40
11.2	Effects of the Applied TSBs Damage	40
12	CONCLUSIONS AND RECOMMENDATIONS	42
12.1	Conclusions	42
12.2	Recommendations	43
	REFERENCES	44
APPENDIX A	BRIDGE AS-CONSTRUCTED DRAWINGS	45
APPENDIX B	CRACKING OF DU IN SPAN 9	48
APPENDIX C	PHOTOGRAPHS OF BRIDGES	49
APPENDIX D	RMS PROOF LOAD TRUCK	51
APPENDIX E	INSTRUMENTATION AND SEVERING OF TSBS	52

APPENDIX F	SENSOR SPECIFICATIONS.....	56
APPENDIX G	IN-SERVICE MONITORING – KEY EVENTS.....	59
APPENDIX H	LOAD TESTING – SUPPLEMENTARY INFORMATION	80

TABLES

Table 2.1:	Summary of characteristics of Bridge No. 8558	3
Table 2.2:	Summary of characteristics of Span 9	3
Table 4.1:	Severing of TSBs in stages	7
Table 5.1:	RMS vehicle axle loads	10
Table 6.1:	Load test sequence	11
Table 7.1:	Summary of sensor system	13
Table 8.1:	Activity schedule	16
Table 9.1:	Tasks and responsibilities	17

FIGURES

Figure 2.1:	Deck cross-section	2
Figure 2.2:	View of Span 9 from the bridge soffit (Pier 8 is on the left-hand side)	4
Figure 2.3:	Layout of Span 9 with overlaid traffic lanes	4
Figure 2.4:	Crack map of Span 9 – simplified from the latest Level 2 inspection report (Appendix B)	5
Figure 4.1:	Color-coded TSBs severing stages	7
Figure 5.1:	Configuration of RMS proof load vehicle	8
Figure 5.2:	Layout of Span 9 with test vehicle running paths	9
Figure 5.3:	Configurations of test vehicle in load cases	10
Figure 7.1:	Sensor arrangement on a part of the bridge cross-section	13
Figure 7.2:	Milling of the DWS	14
Figure 7.3:	Arrangement of SGs	14
Figure 7.4:	Arrangement of string pots and proximity probes	15
Figure 10.1:	Strain intensity maps for random traffic	19
Figure 10.2:	Event count distribution	20
Figure 10.3:	Event distribution over 24 hour period	21
Figure 10.4:	Event distribution across the deck	21
Figure 10.5:	Event #17	23
Figure 10.6:	Event #26	24
Figure 10.7:	LDF distribution for random traffic	25
Figure 10.8:	Strain intensity maps for load tests, undamaged stages	27
Figure 10.9:	Strain intensity maps for load tests (1 of 3)	28
Figure 10.10:	Strain intensity maps for load tests (2 of 3)	29
Figure 10.11:	Strain intensity maps for load tests (3 of 3)	30
Figure 10.12:	Tensile strains in undamaged stage	31
Figure 10.13:	Tensile strains in last damaged stage	32
Figure 10.14:	LDF distribution for load tests	33
Figure 10.15:	NA position, DU1–6	34
Figure 10.16:	NA position, DU7–14	35
Figure 10.17:	NA position for each damaged stage	36
Figure 10.18:	NA position variation, DU4–9	37
Figure 10.19:	NA position variation, DU10–14	38
Figure 10.20:	Maximum deck movements	39

1 INTRODUCTION

Transversely stressed precast concrete deck unit bridges (TSDUB's) have been in service since the late 1950's and represent a dominant and large portion of the road bridges in Queensland for small and medium spans. Despite their widespread use, the behaviour of these bridges is not fully understood.

The performance of TSDUB has been the focus of a 4-year research program with the National Asset Centre of Excellence (NACOE) (Ngo, Pape & Kotze 2015; Ngo & Pape 2015; Ngo 2017a and b). The project was developed to address TMR concerns regarding the safety of TSDUBs affected by corrosion or deterioration of the transverse prestressing bars (TSB) or, alternatively, constructed with a smaller number of TSBs than designed.

Following the performance assessment of a real-life bridge under operational traffic loads (Ngo et al. 2015), laboratory testing was conducted on deck units (DU) salvaged from demolished bridges, both in terms of single beam capacity (Ngo & Pape 2015) and DU behaviour as part of a re-assembled deck portion (Ngo 2017a and b). The results from both site measurements and the laboratory testing showed that the TSDUBs performed better than estimated from their design properties, while the specific contribution of the TSB to the load-carrying capacity could not be quantified.

TMR desires to gain confidence in the load distribution behaviour when the transverse bars are damaged or there is substantial loss of the section. This will allow:

- wider application across the state on the numerous existing TSDUB's
- establishment of guidelines and development of methodologies to evaluate this loss in strength to be applied on multiple bridges across the network, in preparation of maintenance strategies.

The proposed deconstruction of the Sandgate Road Northbound bridge (BIS 8558) provides an opportunity to destructively test a real-life TSDUB structure. To probe the effects of TSB damage on the behaviour of the bridge superstructure, a load test program was implemented in March 2017, including controlled load testing and in-service monitoring of one span of this bridge. Damage to the TSBs on the span under investigation was induced incrementally during the test regime.

This report presents the details of the testing program and discusses the results obtained from high-resolution measurements of the bridge response, both prior to and during the stages of incremental TSB damage.

2 DETAILS OF SANDGATE ROAD BRIDGE

2.1 Reference Information

The following references were provided by TMR:

- R1 design drawings and as-constructed plans (1985)
- R2 Level 2 – Structure condition inspection report (2013)
- R3 Level 2 – Structure condition inspection report (2017).

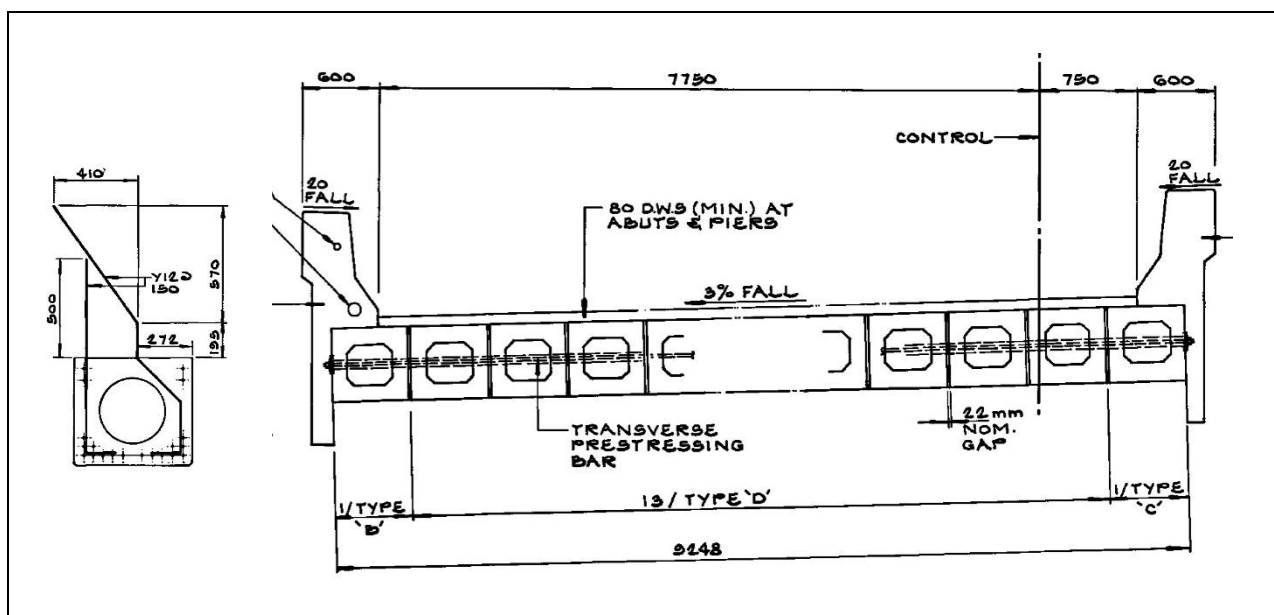
2.2 Characteristics of Existing Structure

TMR Bridge No. 8558 was constructed in 1985. It carries two northbound lanes of the Gateway Motorway (M1) across Sandgate Rd in Deagon (Brisbane). The width between kerbs is of 8.5 metres. The structure consists of ten simply-supported spans, with a span length between 14 and 18 metres. In each span, the deck is made of 15 prestressed precast concrete, voided DUs, which were transversely post-tensioned by 29 mm diameter TSBs, spaced every 2 metres, with an 80 mm thick asphalt deck wearing surface on top of the DUs (R1, see Figure 2.1 and Appendix A).

All spans have a minor skew (θ) of 13° . Except for Pier 5, where the DUs are seated on elastomeric bearings, each DU is anchored to the piers via 30–36 mm diameter dowels (galvanised bolts) 800–920 mm in length, depending on the span length. They were grouted into sockets in both the DUs and the headstocks (see Appendix A). Each pier is made of three 800 mm diameter reinforced concrete (RC) columns that connect into a 900 x 750 mm headstock. The average pier height is 7.8 metres, while the deck minimum clearance is 6.4 metres in Span 8. Piers and abutments seat on deep foundations with prestressed concrete piles (R1, see Appendix A).

A summary of the bridge characteristics is given in Table 2.1.

Figure 2.1: Deck cross-section



Source: TMR.

Table 2.1: Summary of characteristics of Bridge No. 8558

Bridge parameters	Description
As-built drawings	56731–56740, 57674, 280076
Superstructure type	10 simply-supported span prestress concrete superstructure with transverse prestressing bars
Span length (m)	13.85–8.00
Deck width (m)	9.70
Deck width between kerbs (m)	8.50
Construction history	1985/1986
Construction materials	Prestressed concrete deck, reinforced concrete substructure
Supports	Dowels cast into the deck units and grouted in sockets in the piers

2.3 Characteristics of Span 9

Given the simply-supported deck system and constraints due to the construction schedules, performance testing was carried out on a single span. The 16 metre long Span 9 (see Table 2.2) was instrumented for in-service monitoring and load testing.

A view of Span 9 from the ground is shown in Figure 2.2, while a schematic layout of the DUs with overlay of the two lanes of northbound traffic is shown in Figure 2.3.

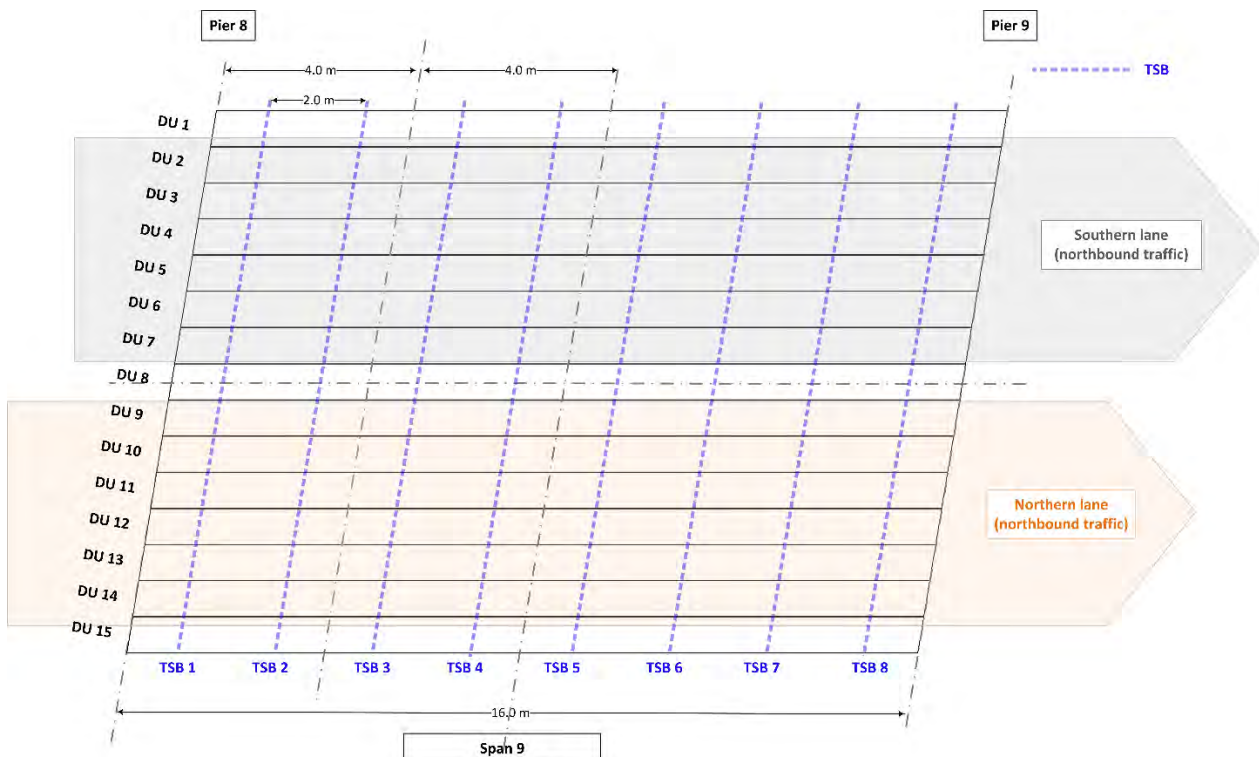
Table 2.2: Summary of characteristics of Span 9

Bridge parameters	Descriptions
Deck type	15 prestressed DUs with cast-in situ parapets
Span length (m)	16.00
Deck width o/a (m)	9.70
Deck width between kerbs (m)	8.50
DUs with concrete cracking	DU1: longitudinal crack running across the entire span length DU2, 5, 7, 8, 11, 13, 15: minor longitudinal cracks within 0.7–2.8 m from the supports
DUs w/o concrete cracking	DU3, 4, 6, 12
Supports	Dowels cast into the DUs and grouted in sockets in the piers
Bridge piers/foundations	Deed foundations, prestressed concrete piles

Figure 2.2: View of Span 9 from the bridge soffit (Pier 8 is on the left-hand side)



Figure 2.3: Layout of Span 9 with overlaid traffic lanes

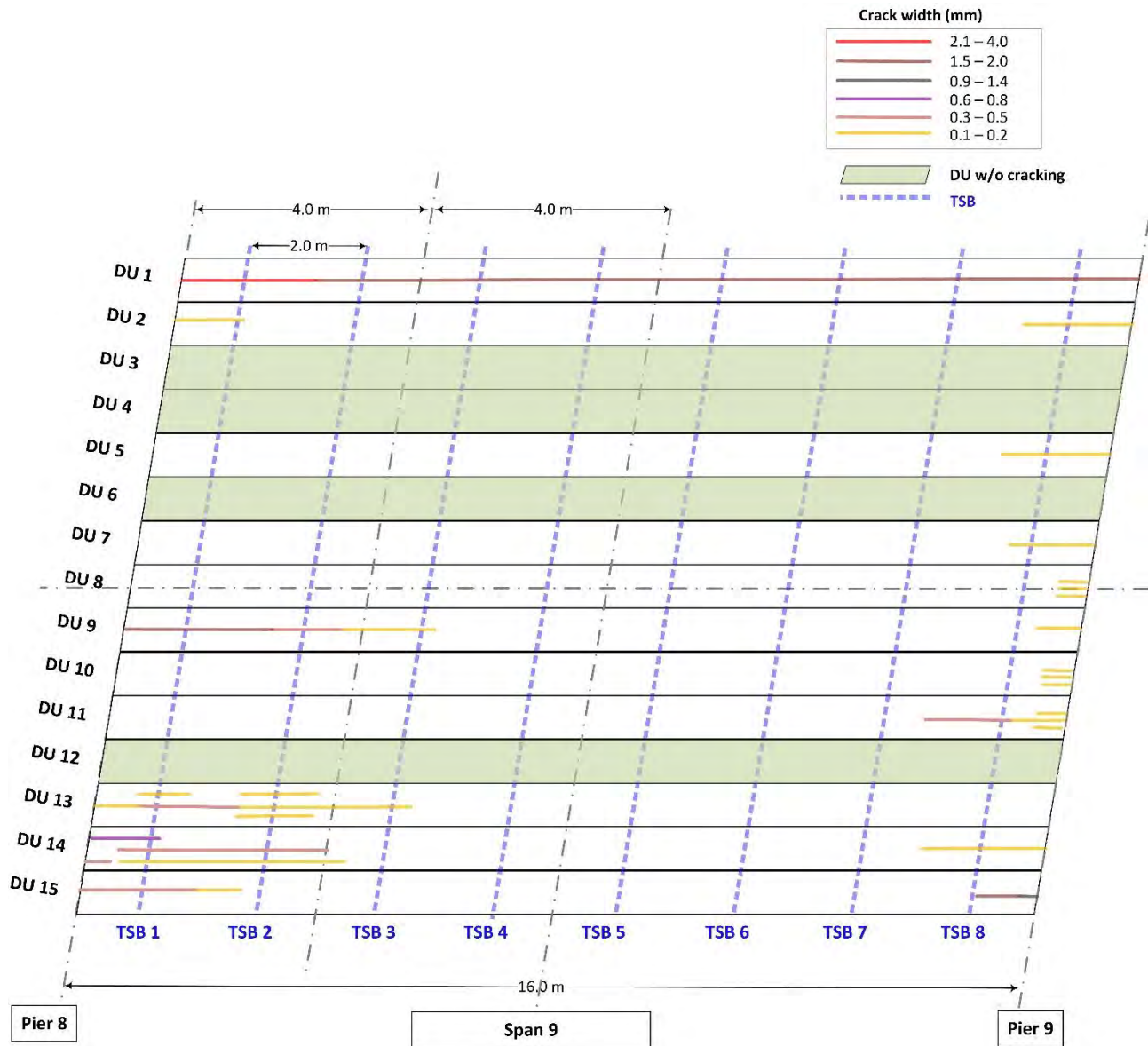


At the time of the sensor installation, as noted in the Level 2 inspections (R2, R3), 11 out of the 15 DUs in Span 9 exhibited longitudinal cracking to a varying extent. This was likely caused by alkali-silica reaction (ASR), and mostly localised within 2.8 metres from the supports (see Appendix B).

The condition of the structure at the time of testing is summarised in Table 2.2, while the crack layout refers to the R3 map reported in Appendix B. The southernmost unit, DU1, had a 1.5–4.0 mm wide crack across the entire span due to defective drainage. As for R3, most of the

other DUs exhibited minor longitudinal cracking 2.0–2.8 metres from the supports, with a crack width ranging from 0.1–0.9 mm (see Figure 2.4).

Figure 2.4: Crack map of Span 9 – simplified from the latest Level 2 inspection report (Appendix B)



3 OBJECTIVES OF TESTING

As discussed in Section 1, the main objective of the bridge testing was to identify the impact of TSB deterioration on the bridge performance. In light of this, the following site measurements were taken:

- Load testing phase 1 (S1): continuous monitoring of the bridge response under operational traffic (i.e. random traffic loads)
- Load testing phase 2 (S2): monitoring of the structural performance under known quasi-static loads before and after the introduction of gradually-increasing levels of damage to the TSBs.

The purpose of the testing was to assess the:

1. maximum DU concrete strains
2. load distribution factor
3. maximum deck movements.

Due to limitations in the instrumentation, tensile strains only were measured in the S1 phase, while both compressive and tensile strains were measured during the load testing phase (S2).

The derivation of the load transfer distribution, or LDF, based on field data under different loading scenarios and for varying structural condition provides an important indication of the actual performance and, therefore, of any structural alteration that may affect the bridge capacity (S2). On the other hand, the LDFs measured under operational traffic allow an evaluation of whether the internal and external girders are more sensitive to a specific load configuration, such as a single lane being loaded or all lanes being loaded (S1).

Ultimately, the direct measurement of the bridge response and, especially, of the contribution of the TSBs to the structural capacity, can provide important information in terms of defining the transverse elements in either grillage or finite element models of TSDUBs. The implementation of calibrated or benchmarked numerical models is critical for bridge analysis and related load ratings.

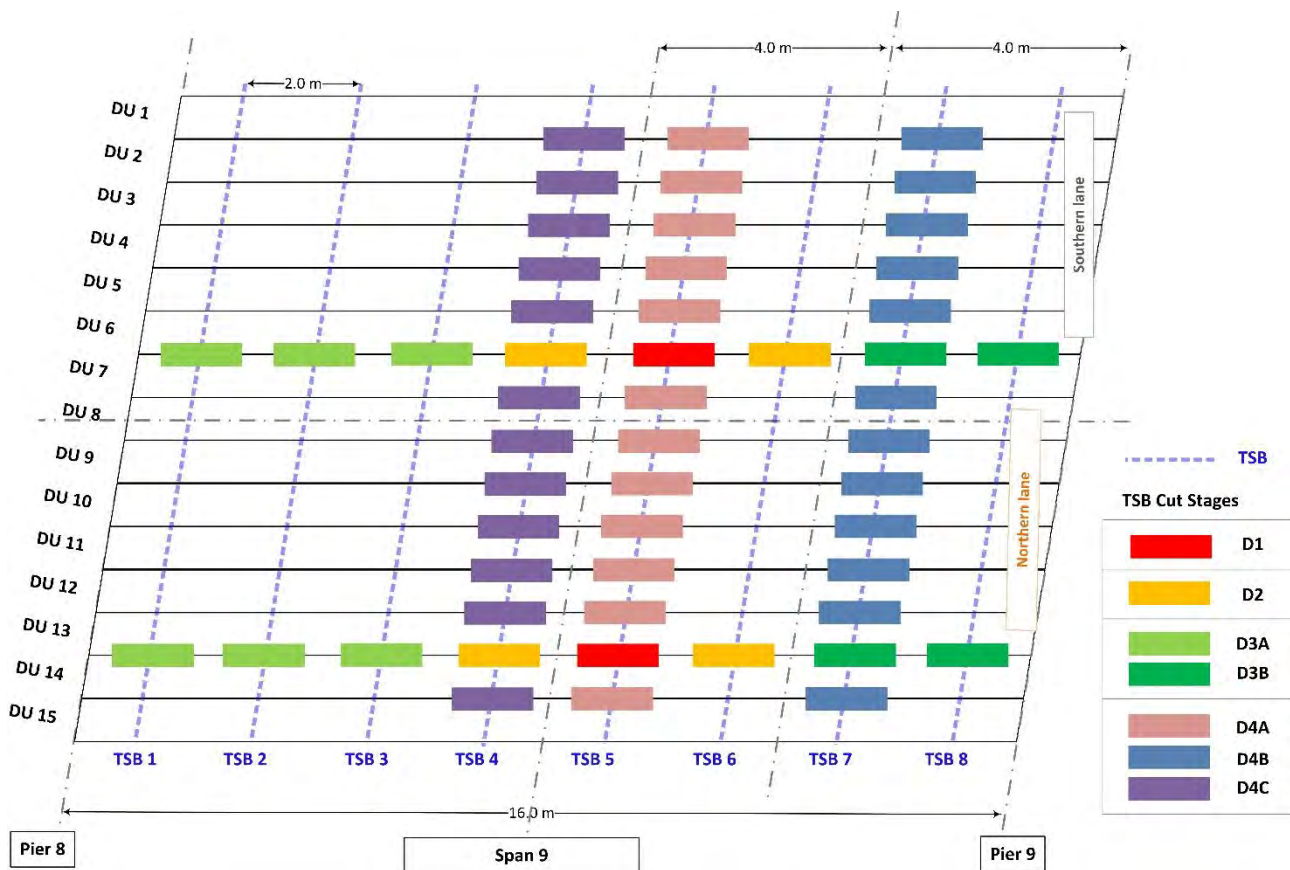
4 STAGES OF STRUCTURAL DAMAGE

The level of damage in the TSBs on Span 9 was gradually increased by severing the TSBs in different locations as shown in Table 4.1. This process is also graphically presented in Figure 4.1.

Table 4.1: Severing of TSBs in stages

Stage	Descriptions
D0	TSBs in their original state – or undamaged – across all deck locations
D1	Severing of TSB 5 in two locations – between DU6 and DU7 and between DU13 and DU14 (red marks)
D2	Severing of TSBs 4 and 6 in two locations – between DU6 and DU7 and between DU13 and DU14 (yellow marks)
D3A	Severing of TSBs 1, 2, 3, in two locations – between DU6 and DU7 and between DU13 and DU14 (light green marks)
D3B	Severing of TSBs 7 and 8 in two locations – between DU6 and DU7 and between DU13 and DU14 (dark green marks)
D4A	Severing of TSB 5 at the remaining 12 DU interfaces (pink marks)
D4B	Severing of TSB 7 at the remaining 12 DU interfaces (blue marks)
D4C	Severing of TSB 4 at the remaining 12 DU interfaces (purple marks)

Figure 4.1: Color-coded TSBs severing stages



5 LOAD CASES AND CONFIGURATION

To assess the bridge response after the introduction of each stage of TSB damage, the Roads and Maritime Services, New South Wales (RMS) proof load vehicle (see configuration in Figure 5.1) was set up to cross Span 9 in nearly static conditions, i.e. at a speed of 2–5 km/h. It was initially planned that the RMS vehicle would travel along the bridge centreline and on the northern lane, including a path adjacent to the northern kerb. However, due to concerns associated with load transfer after the TSBs were severed, the vehicle movements were restricted away from the kerbs in all load tests.

The test truck was scheduled to cross the deck along two paths, running from Pier 9 to Pier 8. Based on the two test lanes indicated in Figure 5.2, the vehicle was set to run along the following paths:

1. central path – the vehicle positioned for central movement, i.e. the test truck travelled along the deck centreline
2. northern path – the vehicle travelled along a path that was offset by about 1.0 metre north of the bridge centreline.

For measurement verification, the RMS vehicle travelled forward (i.e. from Pier 9 to Pier 8) and backward three times, i.e. a total of six crossings (runs) along each path.

Figure 5.1: Configuration of RMS proof load vehicle

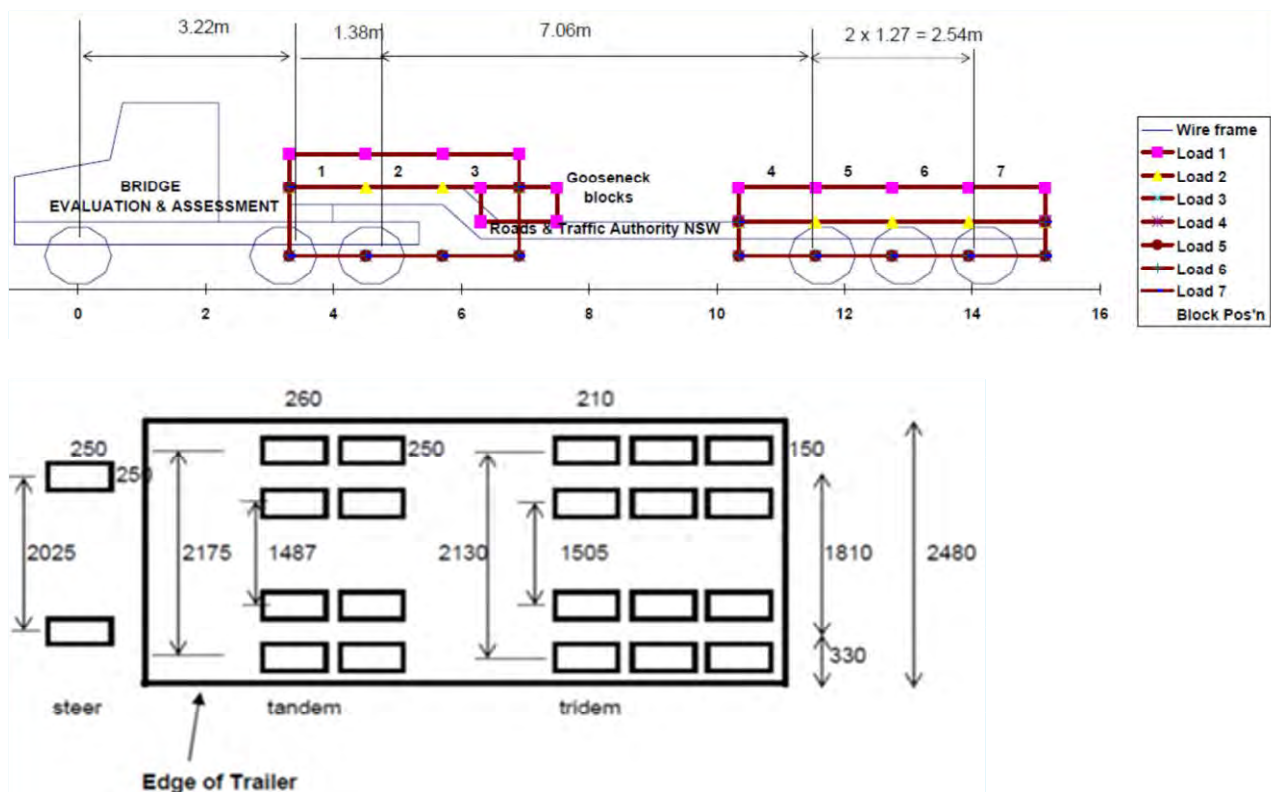
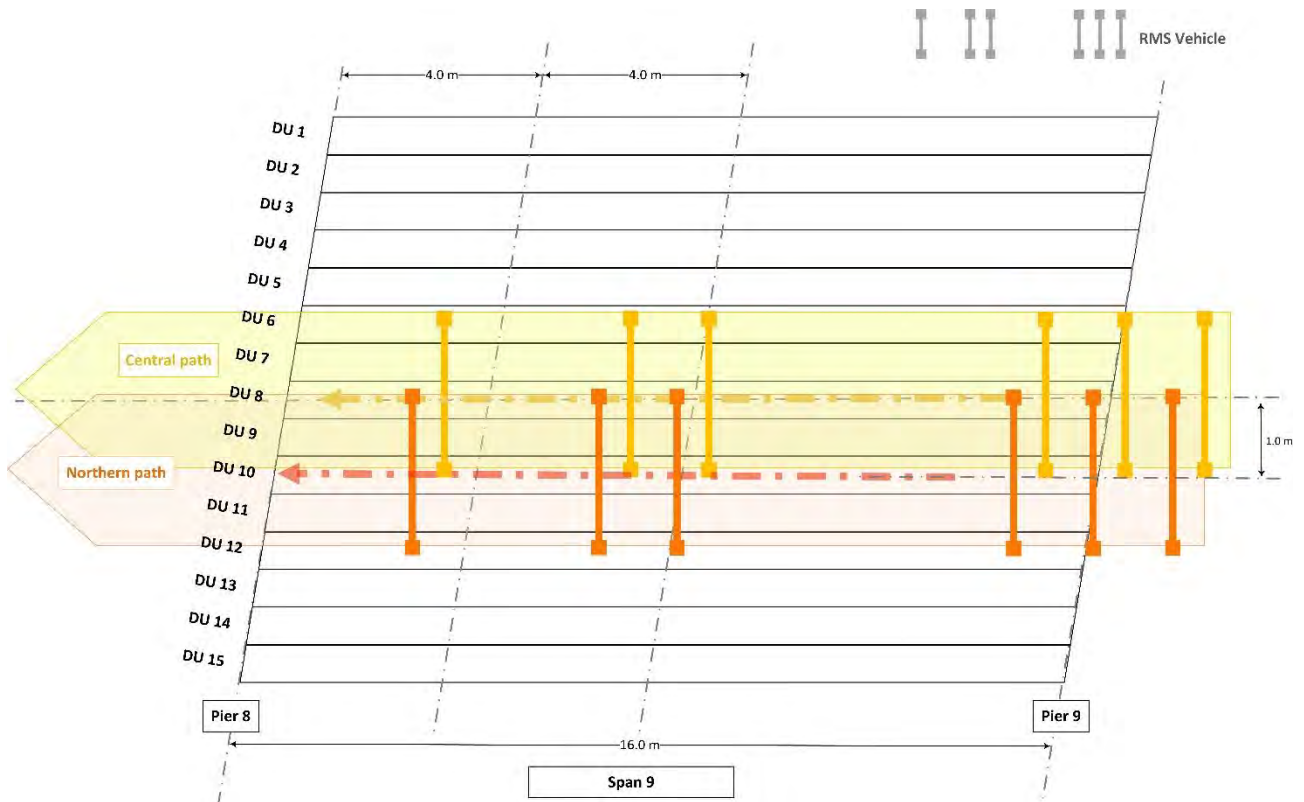


Figure 5.2: Layout of Span 9 with test vehicle running paths



The test truck was set to be loaded in accordance with three incremental load cases (LC) (see Figure 5.3 and Table 5.1):

- LC1: total load 42.5 tonne: load on tandem $LC1_2 = 16.5$ tonne; load on triaxle group $LC1_3 = 20$ tonne
- LC2: total load 62.5 tonne: $LC2_2 = 1.6 \times LC1_2$; $LC2_3 = 1.5 \times LC1_3$
- LC3: total load 82.5 tonne: $LC3_2 = 2.2 \times LC1_2$; $LC3_3 = 2.0 \times LC1_3$.

The following should be noted:

- Due to concerns regarding the overall performance of the bridge, LC3 was used only to test the deck in its undamaged state (D0). For the damaged stages D1–D4C, only LC2 was applied.
- The RMS vehicle only travelled along the bridge centreline ('Central path') and along the 'Northern path' (see Figure 5.2), due to concerns about the load-carrying capacity of DU1, which had significant longitudinal cracking (Figure 2.4). Thus, for the sequence of damaged stages D1–D4C, a total of 12 runs were performed while testing the bridge for LC2 only.

Photographs of the test vehicle with different load configurations are shown in Appendix D.

Figure 5.3: Configurations of test vehicle in load cases

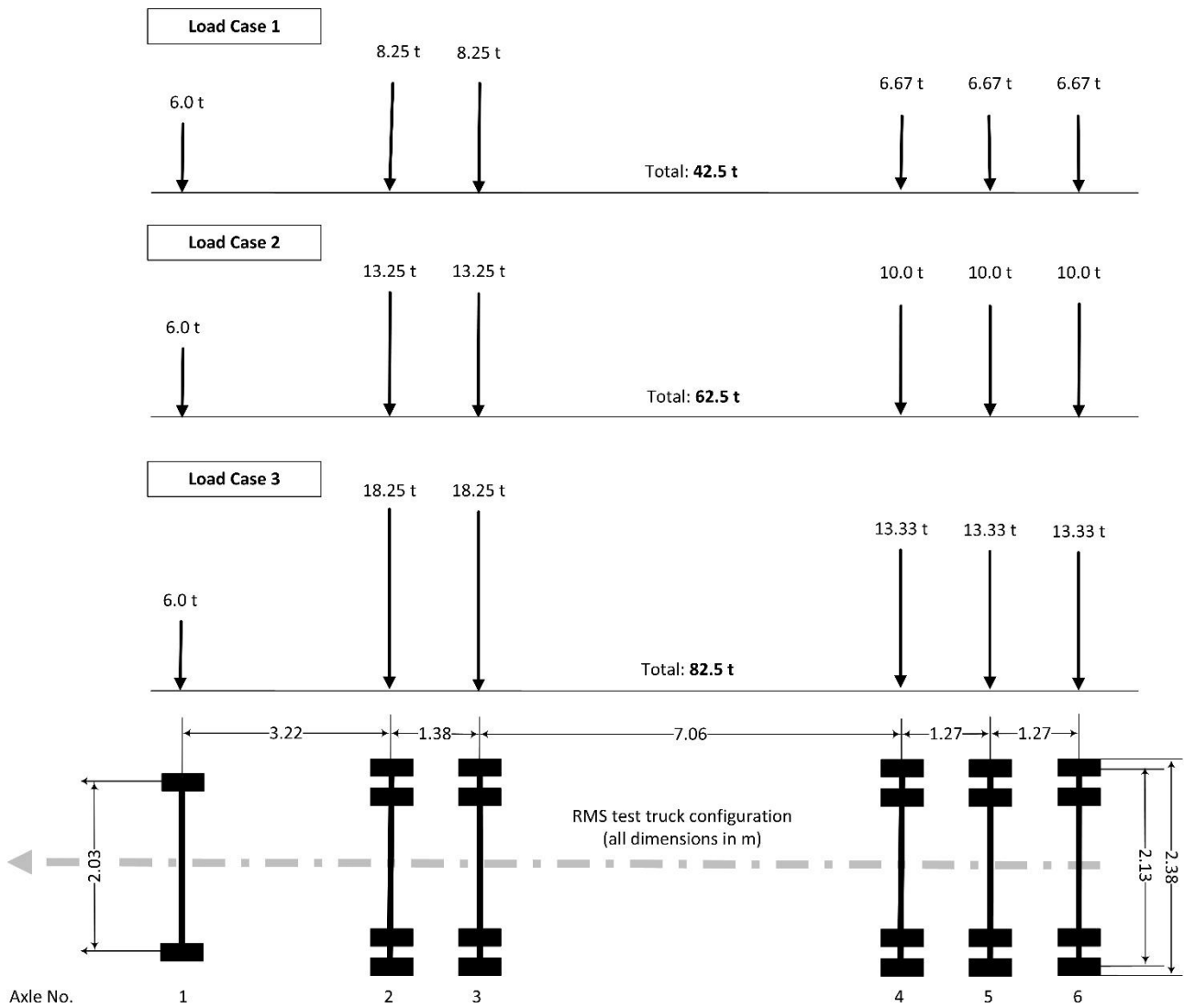


Table 5.1: RMS vehicle axle loads

Axle groups	Axle no.	Tyres	Single axle load (t)			Axle group load (t)		
			LC1	LC2	LC3	LC1	LC2	LC3
Single steer	1	2	6.00	6.00	6.00	6.0	6.0	6.0
Tandem axle dual tyres	2	4	8.25	13.25	18.25	16.5	26.5	36.5
	3	4	8.25	13.25	18.25			
Tri-axle dual tyres	4	4	6.67	10.00	13.33	20.0	30.0	40.0
	5	4	6.67	10.00	13.33			
	6	4	6.67	10.00	13.33			
Total load (t)						42.5	62.5	82.5

6 LOAD TEST PROGRAM

In the light of the discussion in Section 4 and Section 5, the test loading sequence is shown in Table 6.1.

Table 6.1: Load test sequence

Damaged stage	Load case	Total load (t)	Run path ¹	Run ID N ²	Description ³	No. total cuts
D0 1	LC1	42.5	Central path	1.1, 1.2, 1.3	Undamaged stage (no cuts)	-
			Northern path	1.4, 1.5, 1.6		-
D0 2	LC2	62.5	Central path	2.1, 2.2, 2.3		-
			Northern path	2.4, 2.5, 2.6		-
D0 3	LC3	82.5	Central path	3.1, 3.2, 3.3		-
			Northern path	3.4, 3.5, 3.6		-
D1	LC2	62.5	Central path	4.1, 4.2, 4.3	Localised severing of TSB5	2
Northern path			4.4, 4.5, 4.6			
D2			Central path	5.1, 5.2, 5.3	Localised severing of TSB4 and TSB6	6
			Northern path	5.4, 5.5, 5.6		
D3A			Central path	6.1, 6.2, 6.3	Localised severing of TSBs 1, 2 and 3	12
			Northern path	6.4, 6.5, 6.6		
D3B			Central path	7.1, 7.2, 7.3	Localised severing of TSBs 7 and 8	16
			Northern path	7.4, 7.5, 7.6		
D4A			Central path	8.1, 8.2, 8.3	Severing of TSB 5 at all joints	28
			Northern path	8.4, 8.5, 8.6		
D4B			Central path	9.1, 9.2, 9.3	Severing of TSB 7 at all joints	40
			Northern path	9.4, 9.5, 9.6		
D4C			Central path	10.1, 10.3, 10.3	Severing of TSB 4 at all joints	52
			Northern path	10.4, 10.5, 10.6		

1 See Figure 5.2.

2 Each Run ID N. includes both the forward (from Pier 9 to Pier 8) and backward movements (from Pier 8 to Pier 9).

3 See Figure 4.1.

7 SITE MEASUREMENTS

The structural performance was recorded in two stages:

- Stage 1 (S1): in-service monitoring of structural performance – response of deck to ongoing traffic/ambient excitation, recorded from the 28 February to 8 March.
- Stage 2 (S2): load testing – response of deck response to controlled load tests before and after introducing TSB damage, recorded from the 9–13 March 2017.

7.1 Instrumentation

The deck in Span 9 was instrumented with 87 sensors to measure the following (see Figure 7.1):

- strains in the concrete at the top and bottom of the DUs using foil-type strain gauges (SG)
- differential displacements between adjacent DUs using proximity probes (PP) located between adjacent DUs across the mortar joints
- vertical deflections of each DU using string potentiometers (SP).

In addition, to assess the impact of temperature variations on the measured strains, a SG was placed on top of the northern kerb, close to the support on Pier 9. As the kerb is discontinuous, the sensor was not influenced by load effects.

It is noted that the strain measurements for in-service monitoring relied on the SGs installed on the deck soffit. The installation of SGs on the top of each DU was only possible after the deck wearing surface (DWS) was removed in two locations: midspan and quarterspan near Pier 9 (see Figure 7.2).

As shown in the layout schematic in Figure 7.3 and Figure 7.4, the instrumentation included:

Midspan

- 15 SGs on the bottom of each DU (SGB1–15)
- 15 SGs on the top of each DU (SGT1–15; installed after DWS removal)
- 15 SPs attached to the bottom of each DU (SP1–15)
- 10 PPs placed between adjacent DUs (PP1–10)
- one temperature sensor placed on one kerb.

Quarterspan

- eight SGs on the bottom of every second DU (SGB16–23)
- eight SGs on the top of each DU (SGT16–23; installed after DWS removal)
- 15 SPs attached to the bottom of each DU (SP16–30).

A summary of the sensor system is provided in Table 7.1, while the sensor specifications are provided in Appendix F.

Figure 7.1: Sensor arrangement on a part of the bridge cross-section

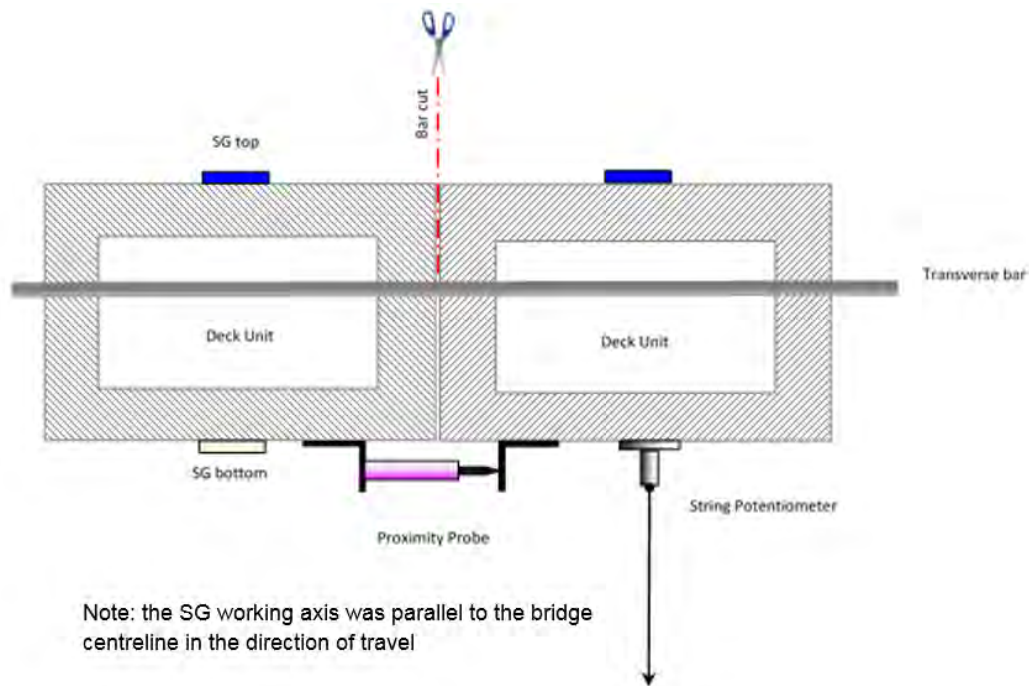


Table 7.1: Summary of sensor system

Sensor type	Location	Sensor label	Measurement	Specifications ¹	No.
Strain gauge	DU top ² (mid-width)	SG	Concrete strain	Uniaxial, prewired Gauge length: 30 mm	23
Strain gauge	DU soffit (mid-width)	SG	Concrete strain	Uniaxial, prewired Gauge length: 30 mm	23
Strain gauge	Northern kerb (top surface)	SG	Temperature-induced strain	Uniaxial, prewired Gauge length: 30 mm	1
String potentiometer	DU soffit (mid-width)	SP	DU deflections	Range: 0-300 mm Resolution: infinite	30
Proximity probe	DU soffit (between joints)	PP	DU Joint gap	Range: 0 – 5 mm Resolution: $\leq 1 \mu\text{m}$	10

¹ Refer to Appendix F for details.

² Installed prior to load testing, i.e. after removal of the asphalt wearing surface.

Figure 7.2: Milling of the DWS

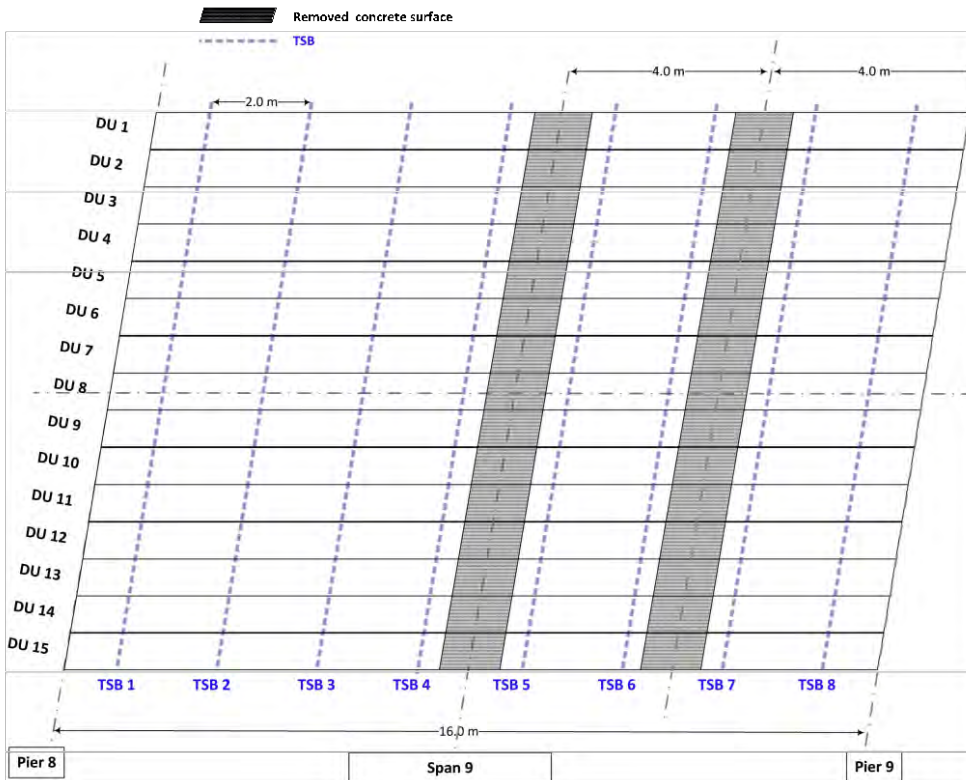


Figure 7.3: Arrangement of SGs

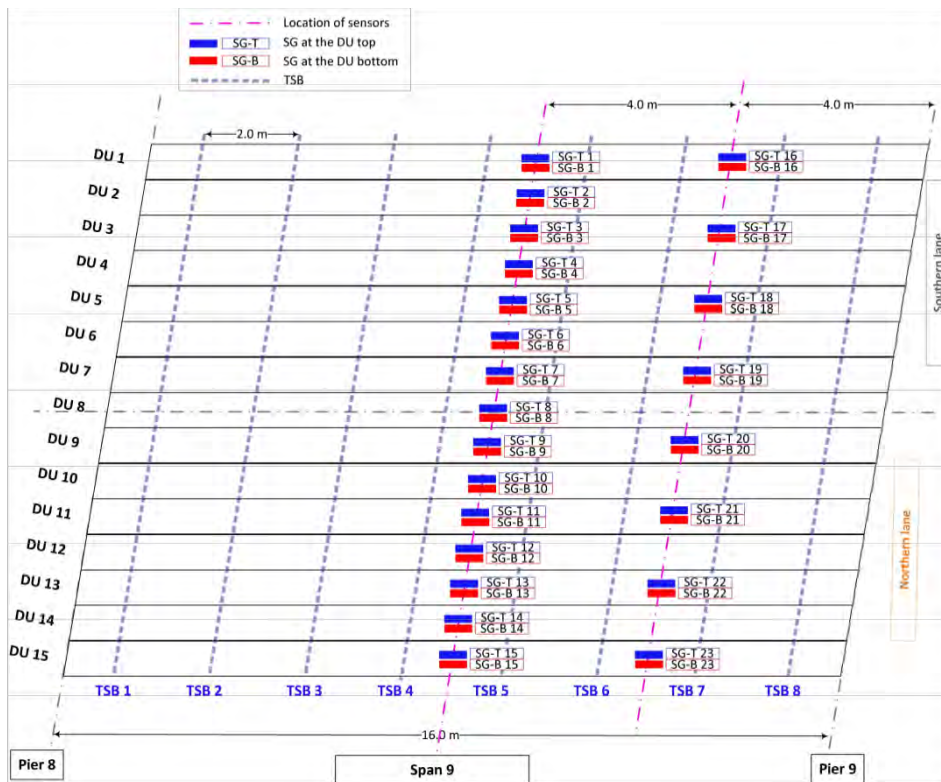
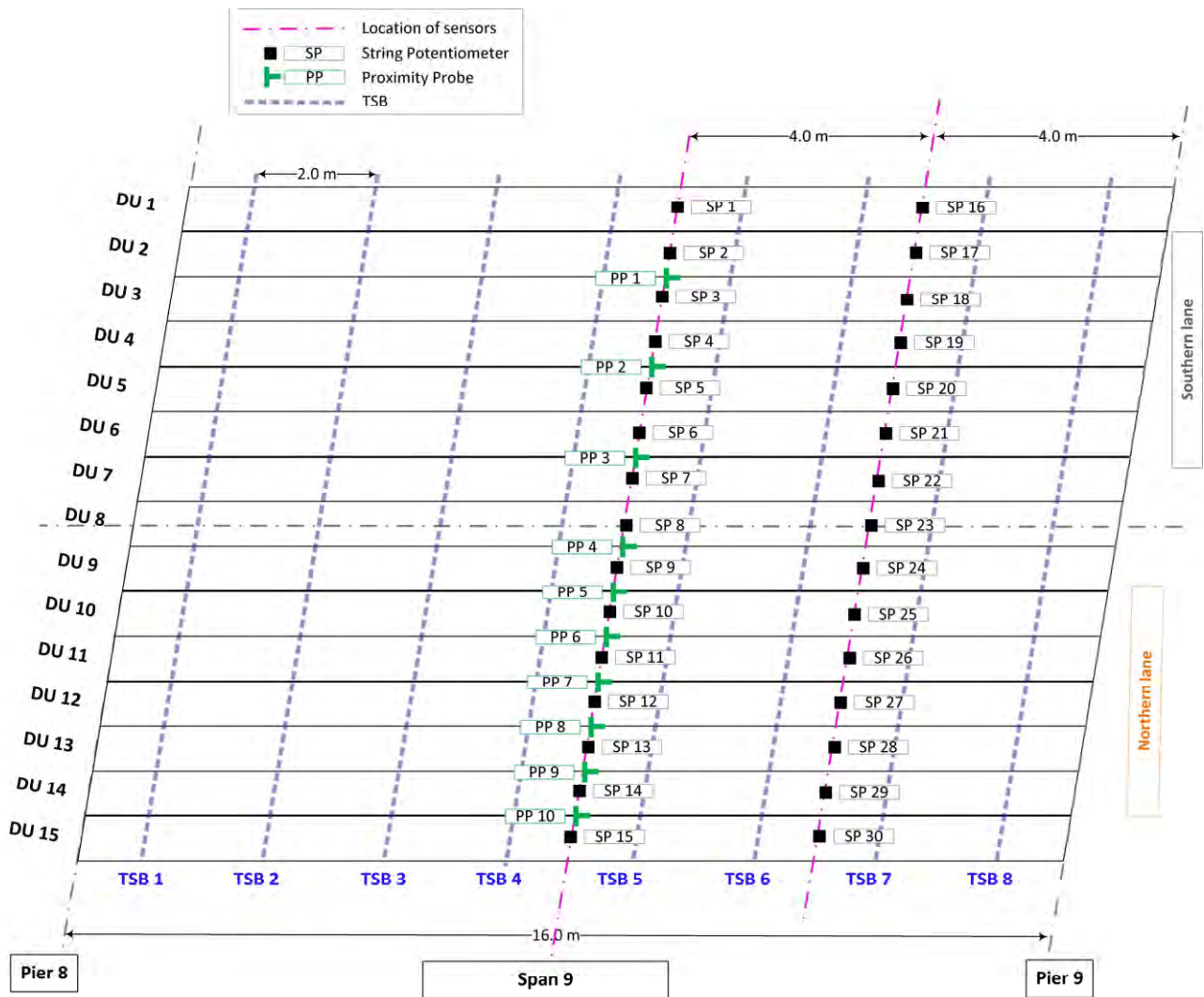


Figure 7.4: Arrangement of string pots and proximity probes



8 TEST SCHEDULE

The schedule for the in-service monitoring carried out on Span 9 is summarised in Table 8.1.

Table 8.1: Activity schedule

Step	Activity	Notes
1	Treating/polishing of concrete surface on deck soffit for application of SGs, SPs, and PPs	Monitoring of the bridge response under ongoing traffic
2	Milling of the deck-wearing surface (DWS) (Figure 7.2) at midspan and quarterspan sections	Exposure of the top of all DUs for direct application of SGs
3	Treating/polishing of concrete surface on top of the DUs for SG application in midspan and quarterspan (Figure 7.3 and Figure 7.4)	Strain measurement at the top and bottom of the DUs to localise the neutral axis of each section
4	Slow rolls of RMS vehicle along the centre and northern paths ¹ . The test vehicle runs ¹ in 3 load configurations ²	Assessment of the undamaged deck 18 test runs: 1.1–3.3 ²
5	Localised severing of TSB5 (near midspan location)	Damage scenario: D1 ³
6	Slow rolls of RMS vehicle along the centre and northern paths ¹ , in L2 configuration only, i.e. total load of 62.5 t	12 runs: 4.1–4.6 ²
7	Localised severing of TSBs 4 & 6 (near midspan location)	Damage scenario: D2 ³
8	Slow rolls of RMS vehicle along the centre and northern paths, in L2 configuration only	12 runs: 5.1–5.6 ²
9	Localised severing of TSBs 1, 2 & 3 (near Pier 8)	Damage scenario: D3A ³
10	Slow rolls of RMS vehicle along the centre and northern paths ¹ , in L2 configuration only	12 runs: 6.1–6.6 ²
11	Localised severing of TSBs 6, 7 & 8 (near Pier 9)	Damage scenario: D3B ³
12	Slow rolls of RMS vehicle along the centre and northern paths ¹ , in L2 configuration only	12 runs: 7.1–6.6 ²
13	Severing of TSB5 at all DU joints	Damage scenario: D4A ³
14	Slow rolls of RMS vehicle along the centre and northern paths ¹ , in L2 configuration only	12 runs: 8.1–8.6 ²
15	Severing of TSB7 at all DU joints	Damage scenario: D4B ³
16	Slow rolls of RMS vehicle along the centre and northern paths ¹ , in L2 configuration only	12 runs: 9.1–9.6 ²
17	Severing of TSB4 at all DU joints	Damage scenario: D4B ³
18	Slow rolls of RMS vehicle along the centre and northern paths ¹ , in L2 configuration only	12 runs: 10.1–10.6 ²
19	Removal of all instrumentation	

¹ See vehicle crossing paths in Figure 5.2.

² See damaged stage description in Table 4.1.

³ See the full list of vehicle runs in Section 4.

9 ROLES AND RESPONSIBILITY

The project execution required close collaboration between ARRB and TMR. The roles and responsibilities assigned to the ARRB and TMR teams are outlined in Table 9.1.

Table 9.1: Tasks and responsibilities

Step	Tasks	Responsibility	Notes
1	Scope development	ARRB/TMR	
2	Test concept and implementation	ARRB/TMR	
2.1	Design of test procedure (vehicle runs, severing of TSBs, coordination of testing and preparation stages)	ARRB/TMR	
2.2	Instrumentation system	ARRB	Reviewed by TMR
2.3	Numerical modelling/performance prediction	TMR	Engagement of an independent consultant (KBR) and reviewer (AECOM)
3	Removal of DWS to allow SG installation	TMR	
4	Sensor system installation	ARRB	Assisted by TMR (arrangements for access, relevant method statement, etc.)
5	Load testing	ARRB/TMR	
5.1	Test vehicle and load configurations	TMR	
5.2	Test schedule	ARRB/TMR	Schedule implementation based on sensor measurements during runs and after each damaged stages
6	Decommissioning of instrumentation	ARRB	
7	Data processing and analysis	ARRB	
8	Reporting	ARRB	Reviewed by TMR

10 DATA ANALYSIS

The bridge response was monitored to assess the operational condition of Span 9 and the effects of increasing the damage to the TSBs. The following parameters were measured in all damaged stages:

- tensile and compressive strain in each DU
- deflection of each DU
- gap opening at the joints between adjacent DUs.

All data were recorded at a sampling rate of 100 Hz. Details of the data analysis from the two phases of the testing exercise, i.e. in-service monitoring and load testing, are now presented.

10.1 In-service Monitoring

10.1.1 Measurement Settings and Data Processing

The measurements were recorded with a sufficiently high resolution that data from the vehicles travelling at operational speeds could be captured and the response of the bridge during trafficking, including temperature variations, mapped. The strain data were recorded by the SGs placed on the bridge soffit (see Figure 7.3) continuously for 24 hours.

It is noted that all measurements are affected by errors. Apart from the instrument noise errors, systematic errors that affect longer recordings are also present, mostly due to variations in the electrical supply, thermal expansion of the connecting cables and voltage and resistance drifts (which are predominantly unidirectional). The combination of these effects results in an instrumental baseline drift or unstable baseline (e.g. see Zhang et al. 2010).

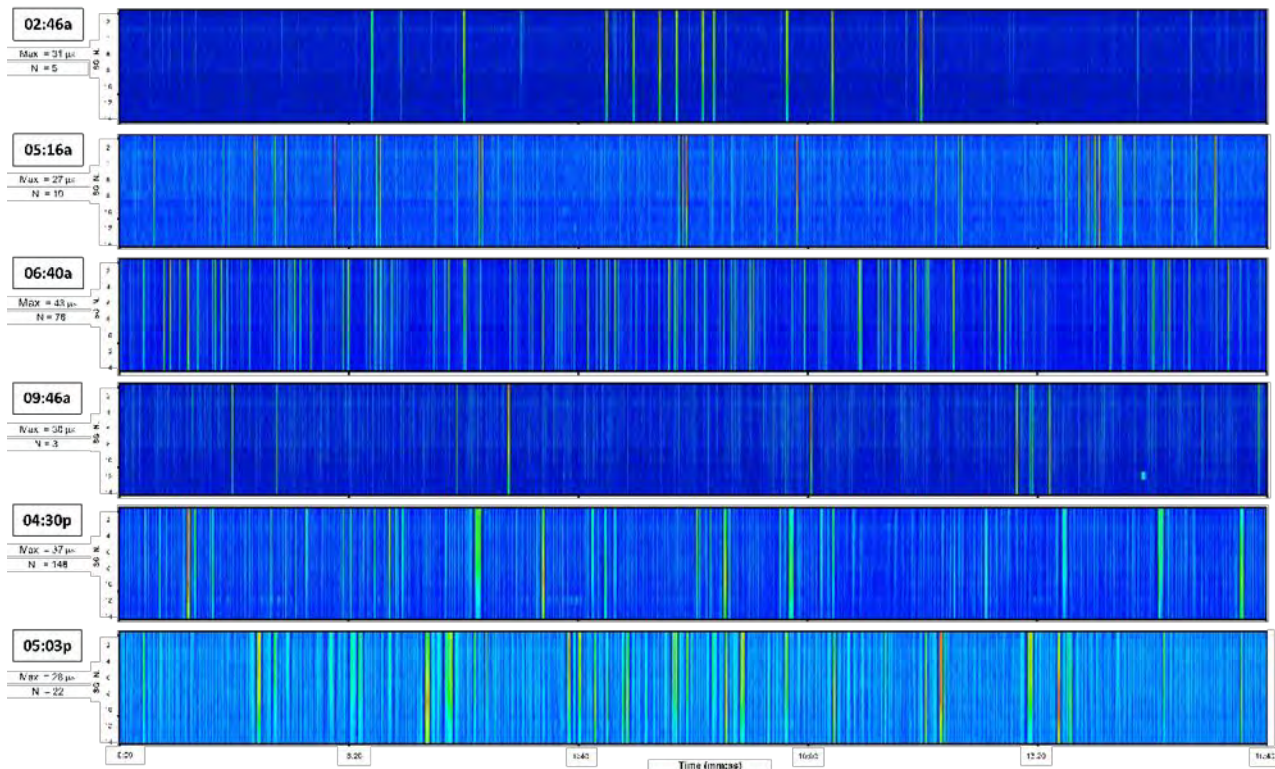
The error on a variable is defined as the algebraic difference between the actual or baselined value and the measured value. Therefore, all data collected during continuous in-service monitoring has to be corrected via subtraction of the least-squares smoothing fit of the baseline drift. Light smoothing was also used to remove noise and other signal interferences (e.g. see Omenzetter & Brownjohn 2006; Chakraborty & DeWolf 2006).

10.1.2 Event Statistics

In order to investigate in detail the volume of traffic and the distribution of vehicles that generated a significant bridge response, the data was split into time histories of 100 000 points (about 17 minutes recording). The passage of a vehicle, or a group of vehicles, that resulted in a short (0.1–3.0 seconds) deck excitation above the noise level ($\approx 3\sigma$, with $\sigma \approx 2.5 \mu\epsilon$), is defined here as an *event*.

The timeframes most representative of the varying event distribution across the bridge are shown in Figure 10.1 for a 24 hour cycle of a weekday (Thursday). As expected, the type and number of events changed significantly within and outside peak hours, which are usually between 6:00 am–9:00 am and 3:00 pm–6:00 pm. The intensity maps in Figure 10.1 use a colour scale which identifies the highest strain with red pixels. As for the sensor layout (see Figure 7.3), the southern lane appears to be affected by the majority of the higher-strain events. The number of events that induced strains (ϵ) $\geq 25 \mu\epsilon$ peaked at around 4:30 pm, with 148 events recorded between 4:30 pm and 4:45 pm. The maximum strain recorded during this period was $37 \mu\epsilon$, while the highest strain measured in the morning peak hour, i.e. between 6:30 am and 7:00 am, was $43 \mu\epsilon$.

Figure 10.1: Strain intensity maps for random traffic



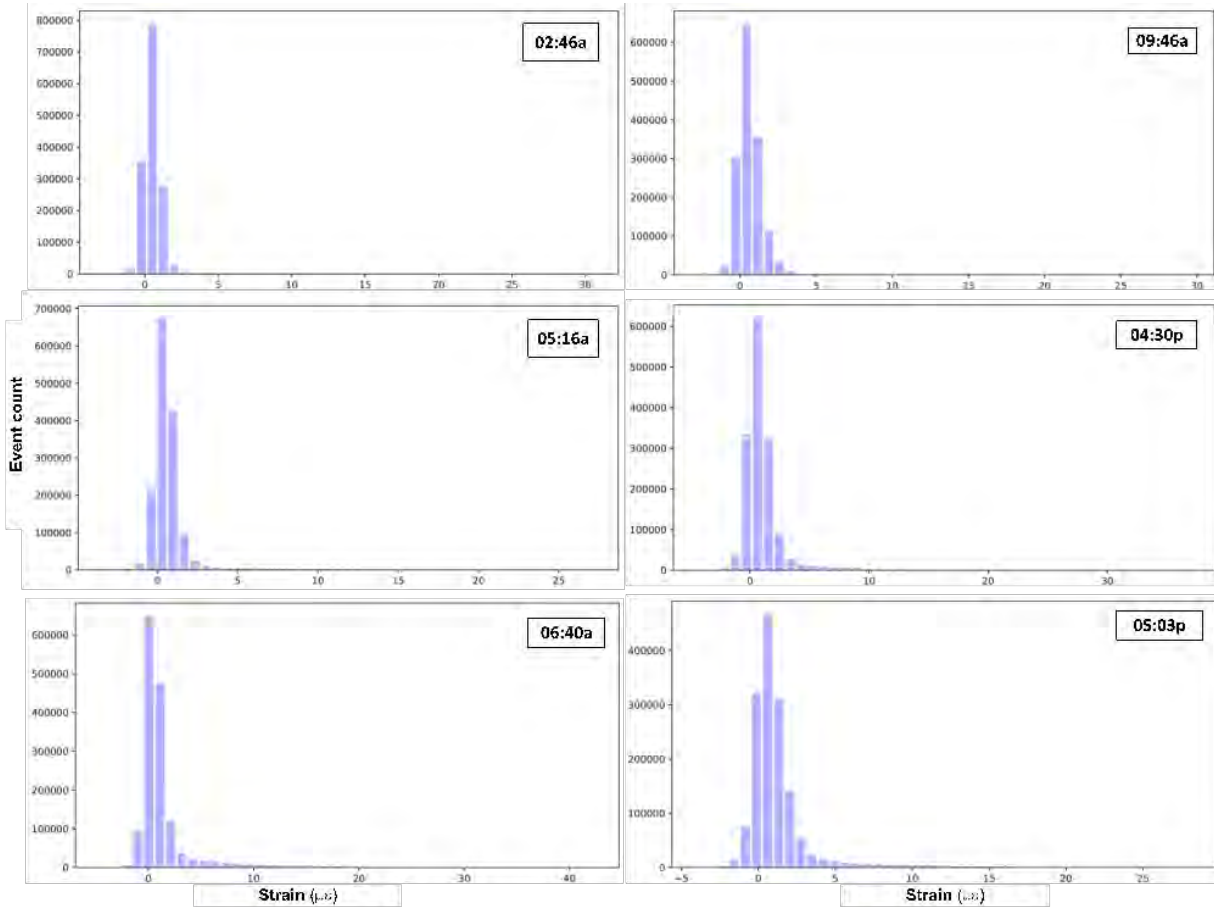
Notes: Heat maps of the strain in Span 9 under ongoing traffic, during selected time slots, on a weekday. Each map shows the strain recorded in the midspan across the deck soffit. As shown in Figure 7.3, SGB1–8 capture the strain in DU1–8, i.e. in the southern (slower) traffic lane, while SGB9–14 capture the traffic movements in the northern lane. Vertical lines flag the passage of vehicles (events) while, in the blue-to-red colour scheme, the red pixels identify the maximum strain levels (Max), as indicated on the left of each map. The number of traffic events inducing tensile strains $\epsilon > 25 \mu\epsilon$ is indicated for each timeframe (N).

10.1.3 Strain Distribution

The event distribution based on the strain values, with reference to the time frames selected in Figure 10.1, is detailed in Figure 10.2. For all recorded data the 95 percentile (P_{95}) is $4 \mu\epsilon$. The number of daily events, N , that induced tensile strains (ϵ) $> 25 \mu\epsilon$, was 1 340 around 4:30 pm, when 10 such events occurred every minute. The strain distribution over a 24 hour cycle is shown in Figure 10.3, overlaid with the maximum strain recorded within each 17 minute time slot. The overall maximum strain (ϵ_{max}) during the 24 hour cycle was $43 \mu\epsilon$. Strain values above $40 \mu\epsilon$ were measured between 06:30 am and 08:30 am and, outside peak hours, around 02:00 pm and 08:00 pm.

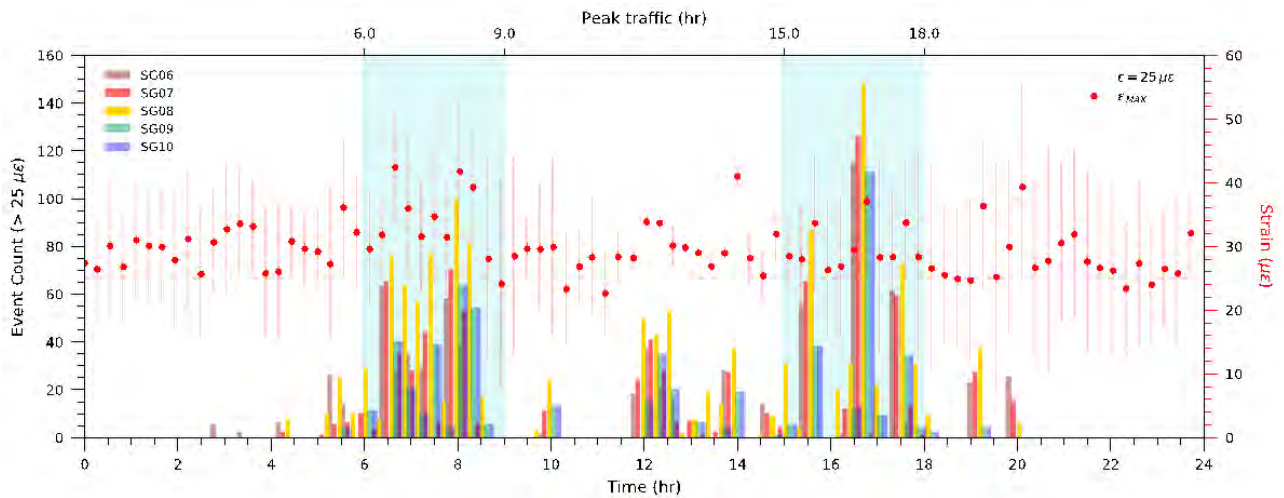
Given the large amount of data recorded, the data from DU6–10 was selected as typical of the behaviour of the entire deck. In light of this, Figure 10.4 shows the event count mapped over the busiest day of the working week for SG6–10 only, i.e. the SGs in the central section of the span soffit (see Figure 7.3). As indicated in Figure 10.1, the map in Figure 10.3 clearly shows that most of the traffic was confined to the southern lane, which is likely the lane that carries the slower and heavier vehicles.

Figure 10.2: Event count distribution



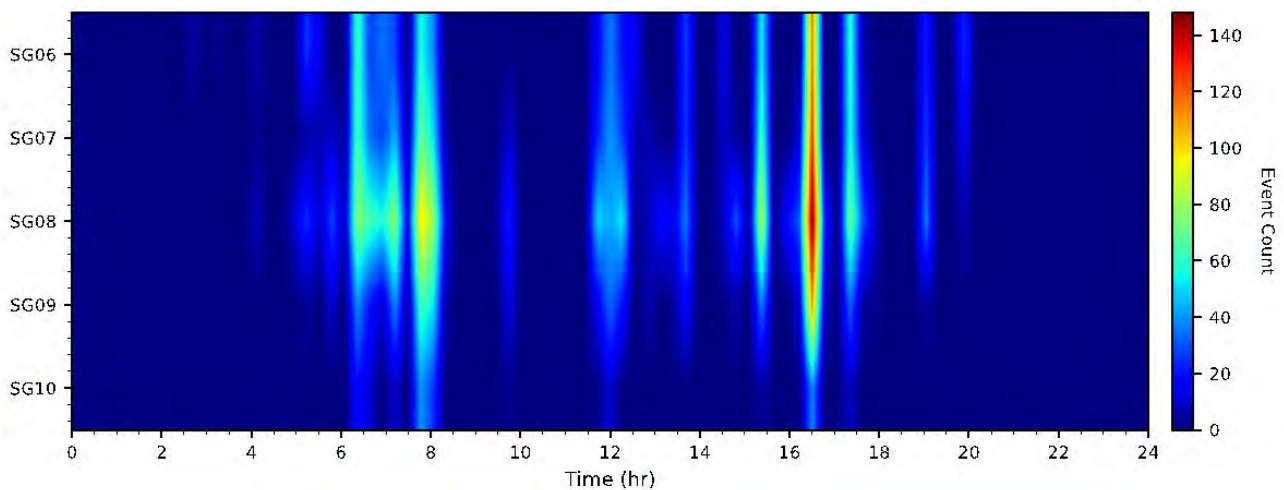
Notes: Histograms of selected timeslots during the 24 hour cycle of a weekday (Thursday). The 6 selected time slots are the same selected for the maps in Figure 10.1 and the top left label indicates the start time of the recording. The maximum strain is reached at 43 µε at 06:40:36 am, i.e. within the '06:40 am' time slot. The highest number of relevant strain events (i.e. $\epsilon > 25 \mu\epsilon$) is counted in the '04:30 pm' timeslot.

Figure 10.3: Event distribution over 24 hour period



Notes: Distribution of events inducing tensile strain $\epsilon > 25 \mu\epsilon$ over a week day cycle (24 hours), as measured by SGB6–10 (see Figure 7.3). The strain data were binned every 17 minutes. The maximum strain measured within each bin is indicated by the red dots (RHS vertical axis). The error bars are a result of the unstable baseline intrinsic to long-term instrumental measurements. The overall maximum recorded for the baselined strains, over the 24 hour cycle, is $43 \mu\epsilon$. The plot regions shaded in light blue highlight the standard peak traffic hours (6:00 am–9:00 am, 3:00 pm–6:00 pm).

Figure 10.4: Event distribution across the deck



Notes: Distribution of the count of events inducing tensile strains $\epsilon > 25 \mu\epsilon$, as measured across the midspan of the inner DUs (SGB6–10), over the 24-hour cycle of a weekday (Thursday). With reference to the sensor layout (Figure 7.3), the central/southern side of the deck is mapped by SGB6–8.

10.1.4 Load Distribution Factors

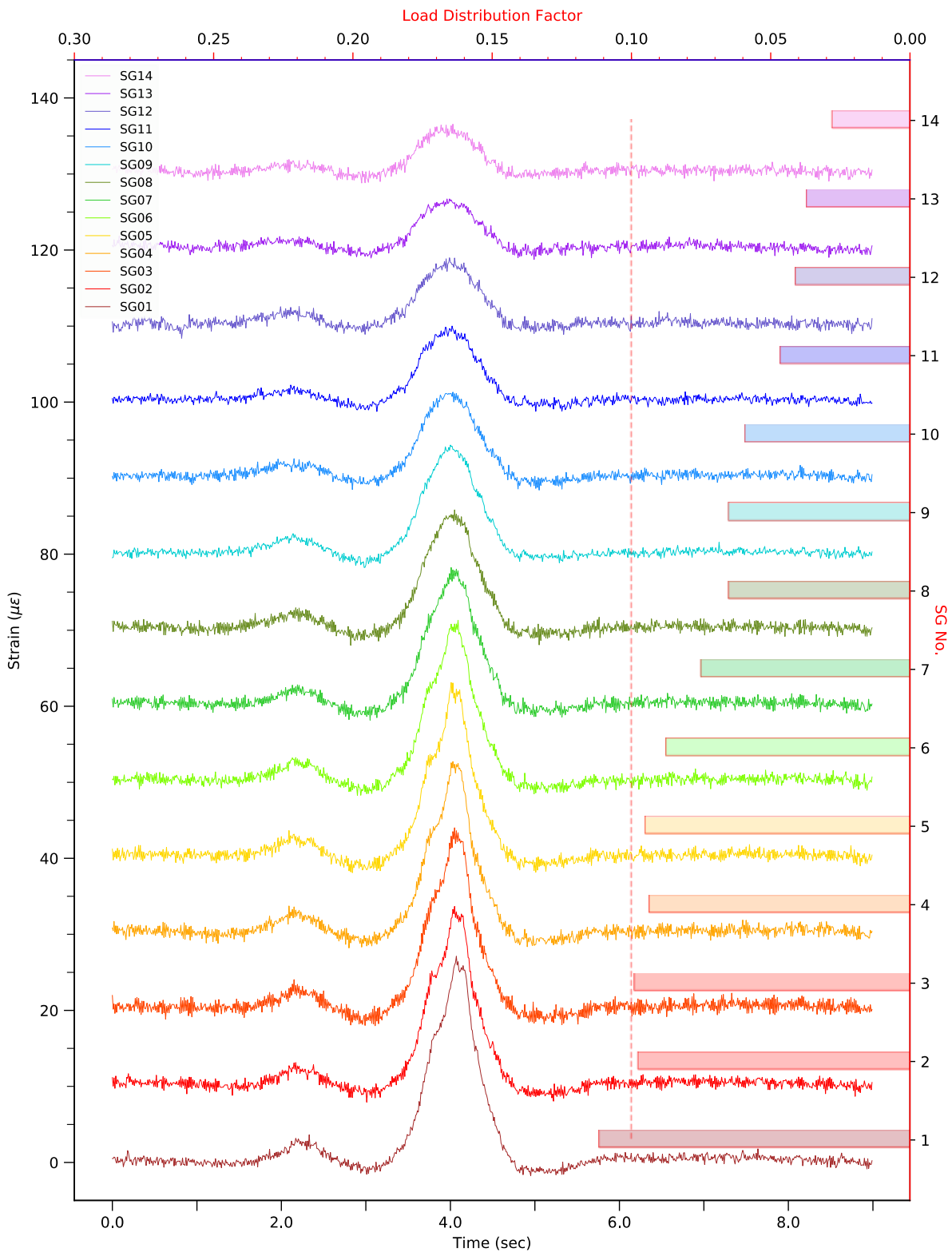
The load distribution across the deck longitudinal elements is primarily governed by the transverse position of the vehicle. Two typical examples of the traffic events over Span 9 are shown in Figure 10.5 and Figure 10.6.

In detail, the strain measured for Event #17 (Figure 10.5) points to the presence of a single heavy vehicle positioned within the southern lane (DU1–8), as the strain peaked within SGB1–8, with the maximum portion of load taken by DU1 (LDF = 11.15%). The fact that the LDF for DU1 is approximately 15% higher than the LDF associated with DU2 is likely due to the significant longitudinal cracking in DU1 (see Figure 2.4). The resultant LDF of 11.15% is the highest value derived from the in-service monitoring measurements. Figure 10.6 shows a different load distribution (Event #26), when the vehicles moved along both the traffic lanes simultaneously, with the heavier vehicle positioned in the northern lane. In this case, the load configuration results in the

maximum load distribution across all DUs. As a result, the maximum strain ($\epsilon_{\max} = 43 \mu\epsilon$) was measured in DU10, while the highest LDF of 8.49% (associated with DU10) is within the lower LDF limit (see Figure 10.7).

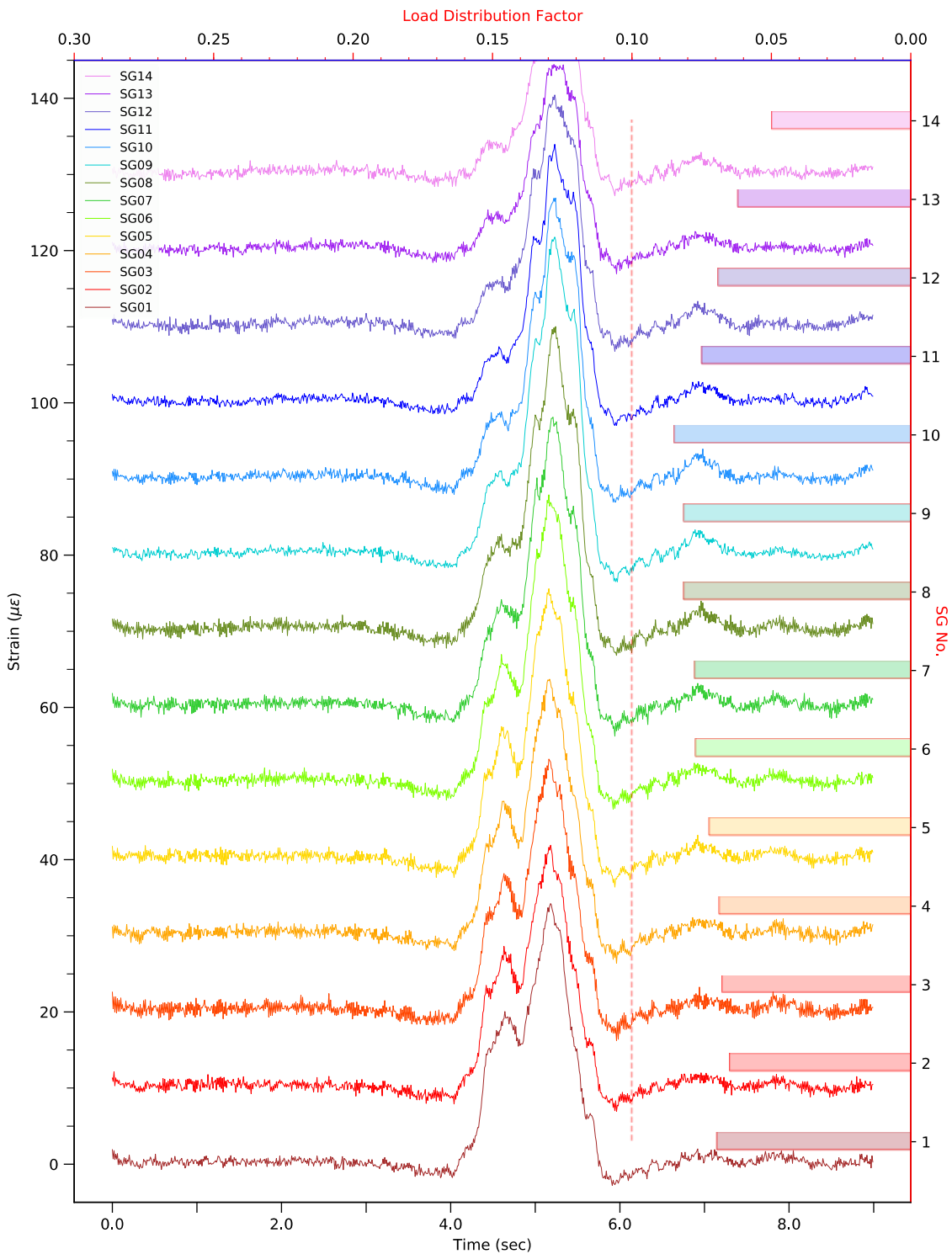
The LDF distribution derived from a sample of significant events recorded over the 24 hour cycle of a weekday is shown in Figure 10.7, while the most representative events are reported in Appendix G. It can be seen that higher LDF values are typical of the quiet or off-peak hours (night and early morning), while lower LDFs are characteristic of busier hours or daytime. As shown with the pilot events shown in Figure 10.5 and Figure 10.6, higher LDFs are associated with traffic on a single lane, while the lower LDFs point to the presence of traffic on all lanes, i.e. the moving loads are distributed across the deck width.

Figure 10.5: Event #17



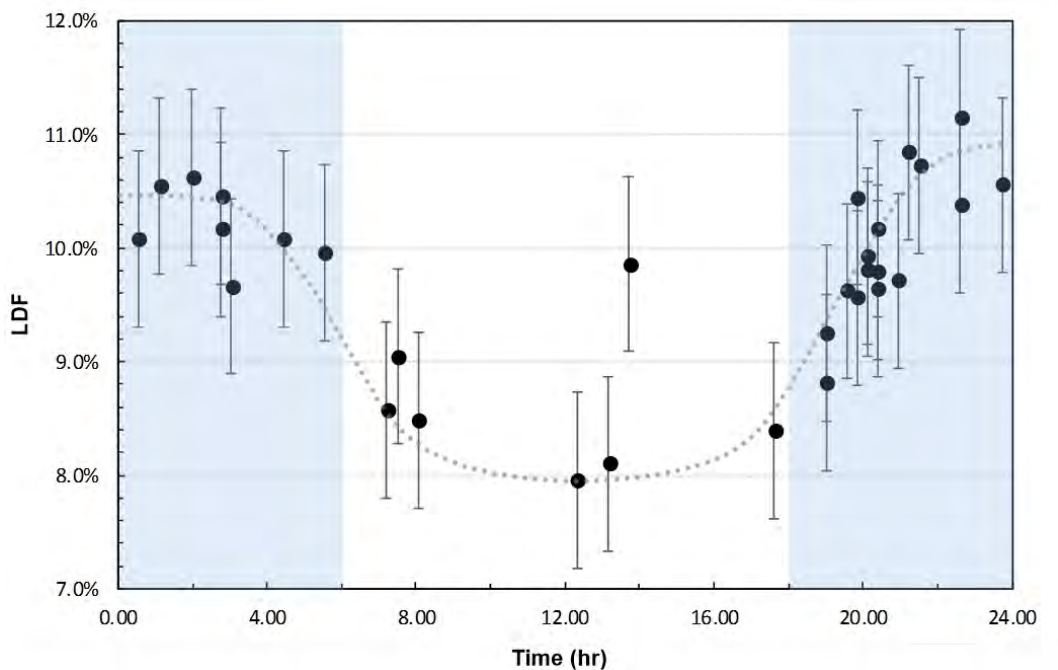
Notes: This Figure shows the strains measured for Event # 17 on Thursday 2 March 2017. Start time 10:41:18 pm – Peak strain: 27 µε – Maximum LDF = 11.15% (DU1). The strain time histories recorded by each SG on the deck soffit in midspan (SG1–14) are stacked with an offset of 10 µε, with SGB1 at the bottom of the plot. Each SG number matches the DU number to which it is attached to, as indicated by the labels on the right vertical axis. The related LDF was plotted on the right with values indicated by the top horizontal axis. The vertical red dashed line marks LDF = 10%. For SGs layout see Figure 7.3.

Figure 10.6: Event #26



Notes: This Figure shows the strains measured for Event # 26 on Friday 3 March 2017. Start time 08:18:13 am – Maximum strain: 43 µε. LDF = 8.49% (DU10). The strain time histories recorded by each SG on the deck soffit in midspan (SGB1–15) are stacked with an offset of 10 µε, with SG1 at the bottom of the plot. Each SG number matches the DU number to which it is attached, as indicated by the labels on the right vertical axis. The related LDF was plotted on the right with values indicated by the top horizontal axis. The vertical red dashed line marks LDF = 10%. For SGs layout see Figure 7.3.

Figure 10.7: LDF distribution for random traffic



Notes: This Figure shows the distribution of the LDF derived from in-service monitoring data over the 24 hour cycle of a weekday (Thursday). A sample of the most relevant events used to derive the LDF distribution is shown in Appendix G.

10.2 Load Tests

10.2.1 Measurement Settings and Data Processing

The load data was recorded using a sampling rate of 100 Hz, while the sensor system included SGs placed on top of each DU (see Figure 7.3).

As discussed in Section 10.1.1, longer measurements were corrected for baseline drift. The error in the measurements is therefore defined as the algebraic difference between the actual, or baselined value, and the measured value.

10.2.2 Strain Distribution

In the 'undamaged' stage (before severing TSBs) (see stages D01–D03 in Table 6.1), the strain under increased truck loading underwent a linear increase across all DUs, i.e. the strain scaled elastically with the added load. The variation of the strain distribution across the DUs under increasing loads, with the truck travelling along the central path (see Figure 5.2), is shown in Figure 10.8. It can be seen that the distribution pattern did not change when the load changed from 42.5 to 82.5 tonne, while the strain in each DU increased by the same fraction.

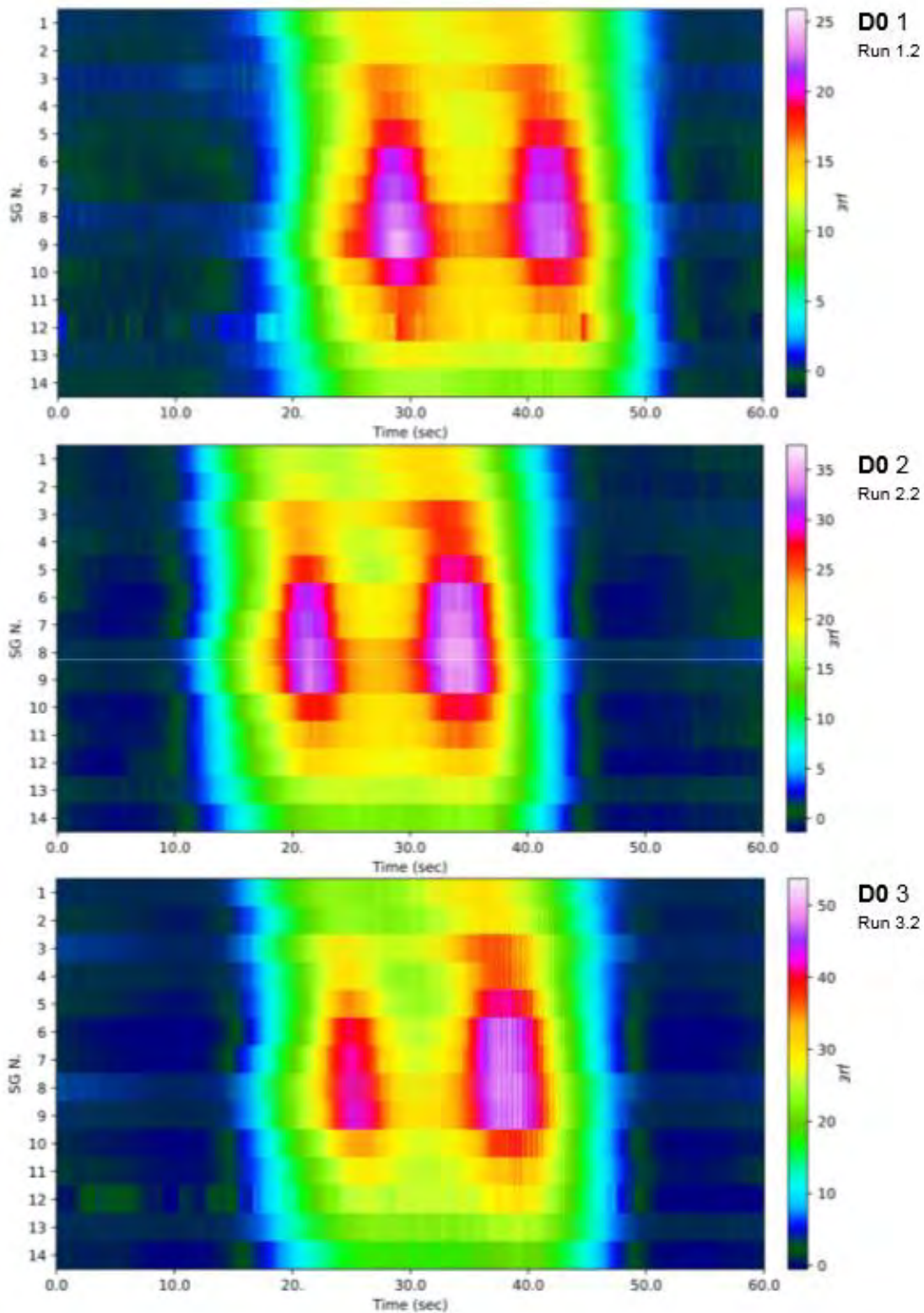
On the other hand, as TSB severing was introduced, the strain distribution pattern varied between adjacent units, and the changes became more significant as the TSBs were severed in more locations (Figure 10.9, Figure 10.10 and Figure 10.11). At the damaged stage D2, the central DUs, DU7–10, were already taking approximately 25% more load than in the undamaged stage (see Figure 10.9). At the last stages of TSB severing (D4B to D4C), DU6–12 appeared to take all the loads (see Figure 10.11).

The maximum tensile strain ($53.7 \mu\epsilon$) was reached with the heaviest load in D0, i.e. when the 82.5 tonne truck crossed the undamaged bridge. In the presence of TSB severing, the maximum tensile strain (ϵ_{max}) recorded by the most loaded DU was $49.6 \mu\epsilon$ (DU7) at stage D4C. A view of the significant change in the amount of strain taken by each DU, between the undamaged stage

D02 and last damaged stage D4C is shown in Figure 10.12 and Figure 10.13 respectively. The maximum compressive strain (ϵ_{min}) measured in the damaged deck was $58.9 \mu\epsilon$ (DU7; D4C).

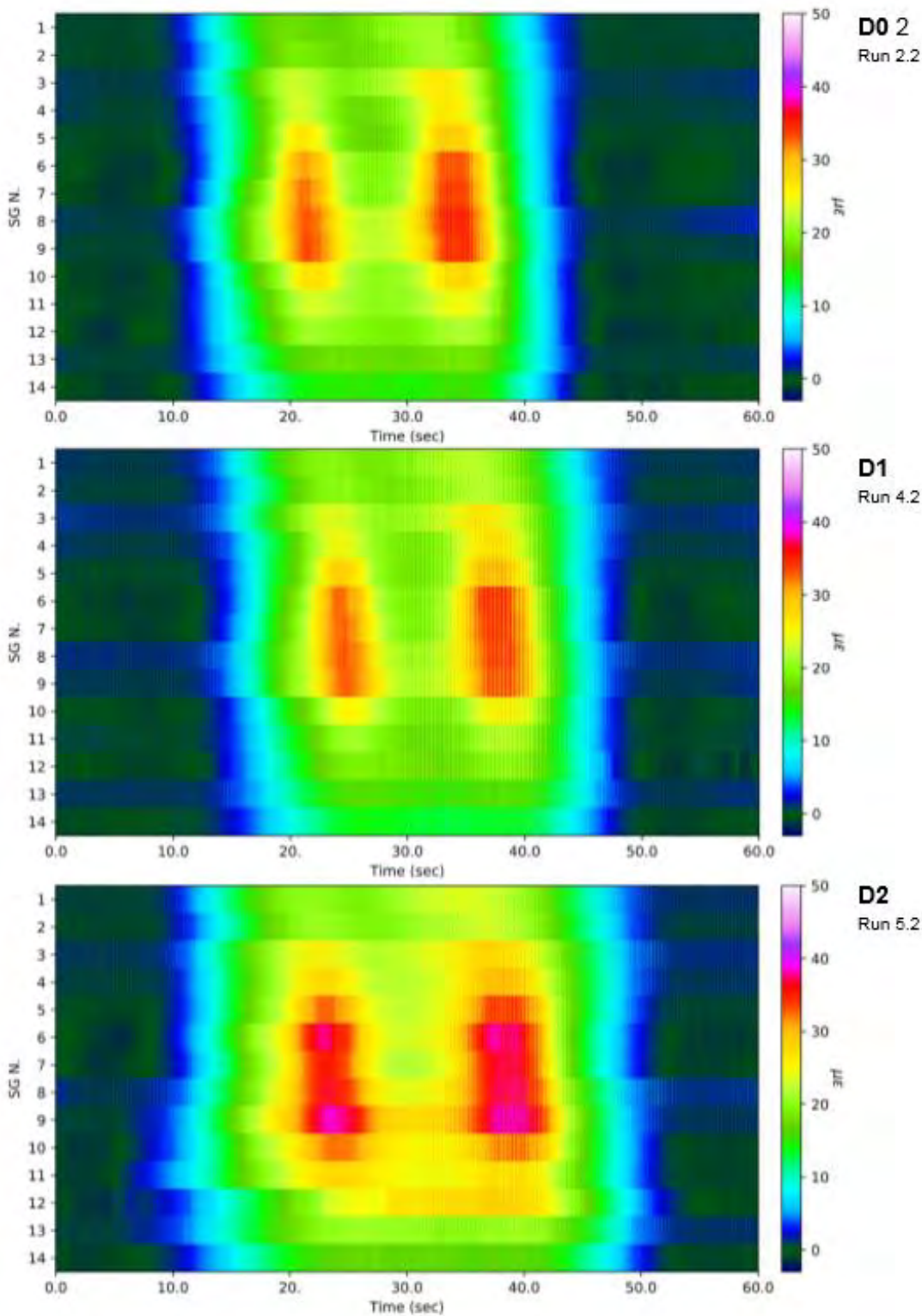
A summary of the maximum tensile strains recorded in all the tests, with the truck running along the central path, is plotted in Figure 10.14. It can be seen that, after TSB damage, the deck behaviour departed from the linear response measured in the undamaged state. The TSB severing resulted in a strain increase in the most loaded DUs, from D0 to D4C, of 32%. Such an increase is less than the 43% strain increment measured under the 82.5 tonne truck, i.e. right after the 62.5 tonne run in the initial tests (D02 and D03). Using the linear fit of the D0 strains, the undamaged bridge would reach a maximum strain of $49.6 \mu\epsilon$ under a load of 75.6 tonne, or approximately 1.21×62.5 tonne.

Figure 10.8: Strain intensity maps for load tests, undamaged stages



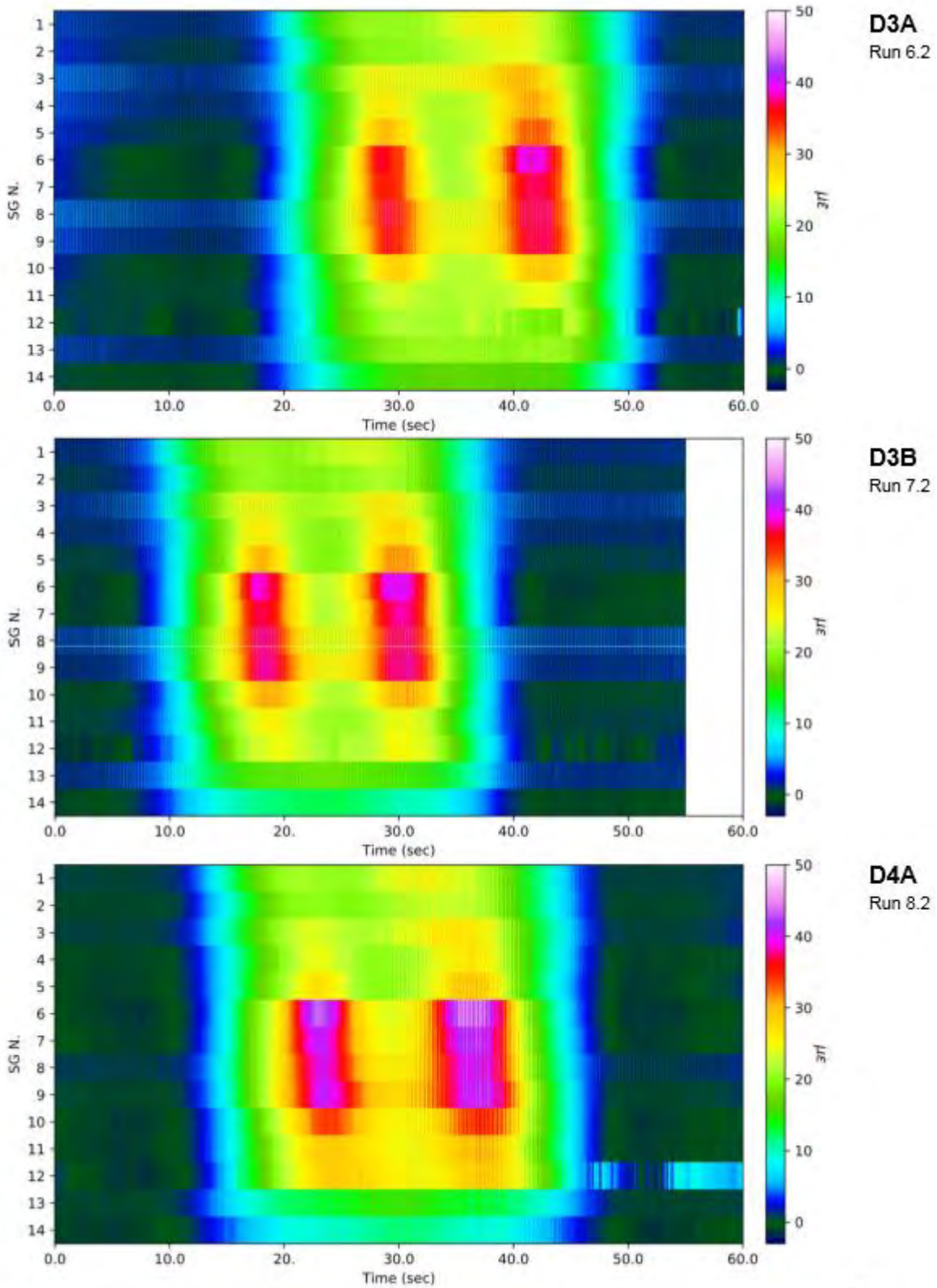
Notes: This Figure shows maps of the strain intensity and distribution across Span 9 during the load tests in the undamaged stage (D01, D02 and D03), with the 42.5, 62.5 and 82.5 tonne trucks crossing Span 9 along the central path, respectively. SGB1–7 captured the strain in the northern lane (DU1–7) and SGB8–14 mapped the strain in the southern lane (DU8–14). The truck speed was approximately 2.5 km/h.

Figure 10.9: Strain intensity maps for load tests (1 of 3)



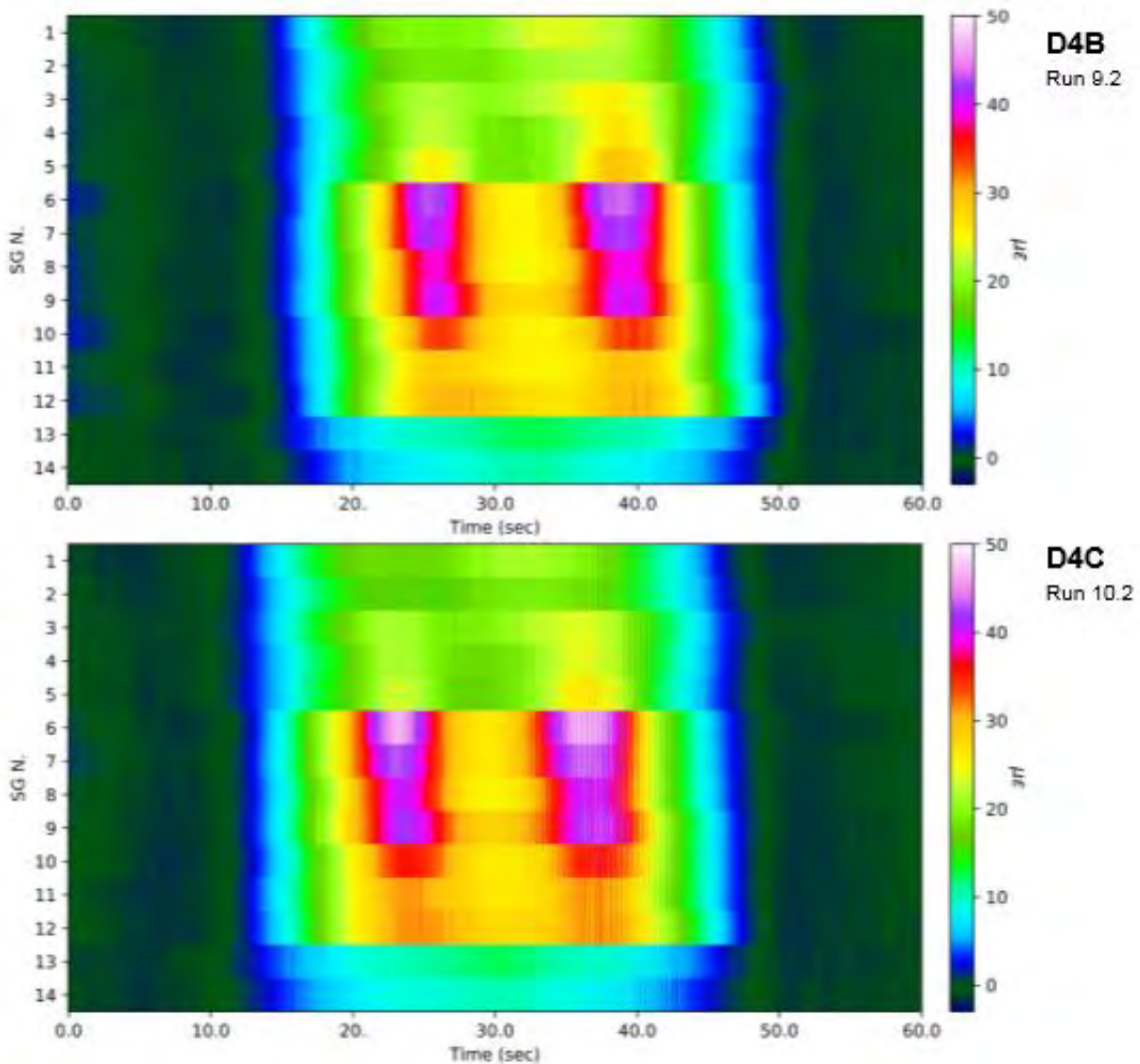
Notes: This Figure shows fixed-intensity maps of the strain distribution across Span 9 with increasing TSB severing (see Figure 4.1). The strain was measured when the 62.5 tonne truck crossed Span 9 along the central path. For comparison, the strain response of the deck in the undamaged stage (D0), under identical load configuration, is shown in the top map. SGB1–7 captured the strain in the northern lane (DU1–7) and SG8–14 mapped the strain in the southern lane (DU8–14). The truck speed was 2.5 km/h.

Figure 10.10: Strain intensity maps for load tests (2 of 3)



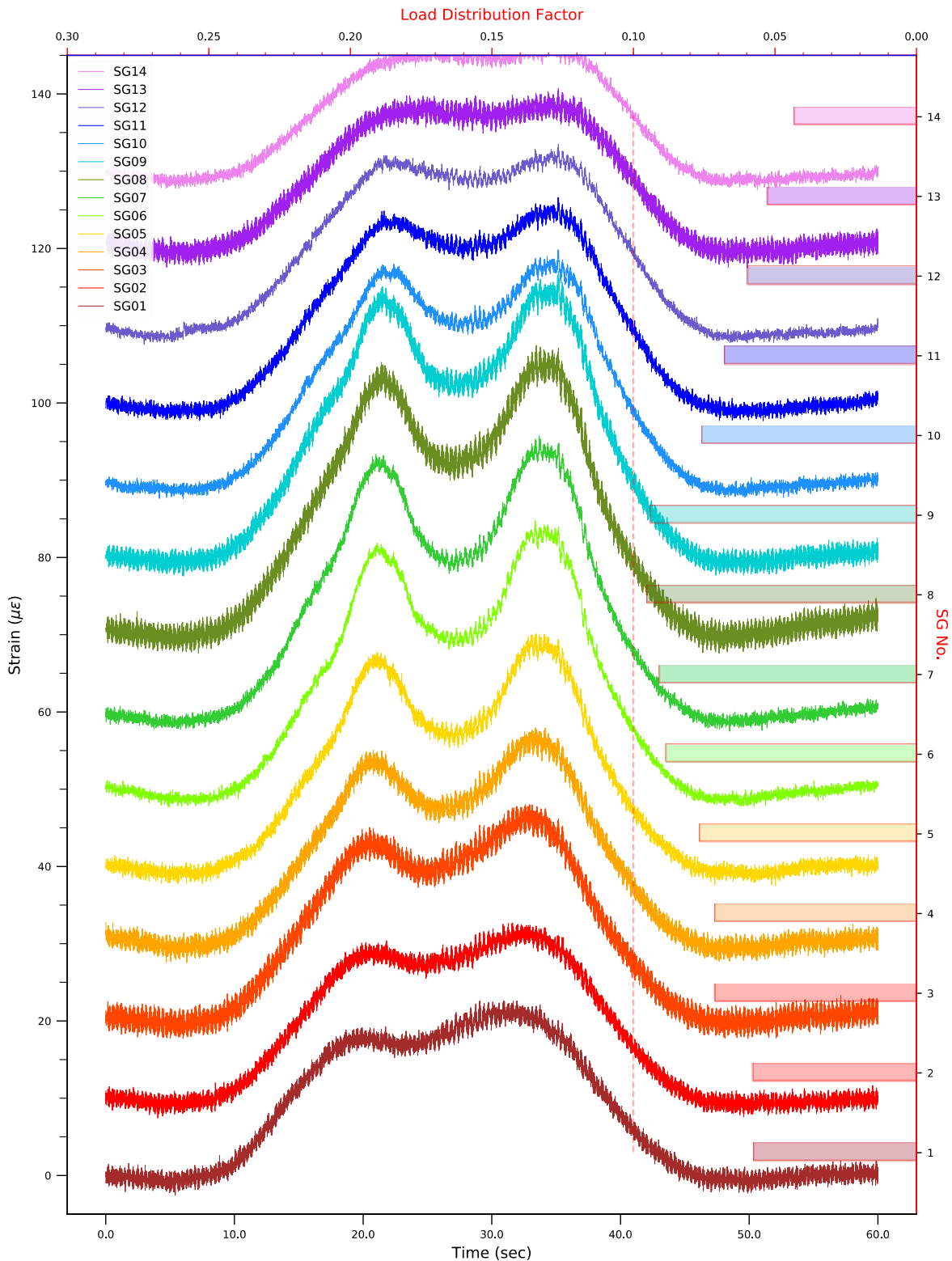
Note: see notes in Figure 10.11.

Figure 10.11: Strain intensity maps for load tests (3 of 3)



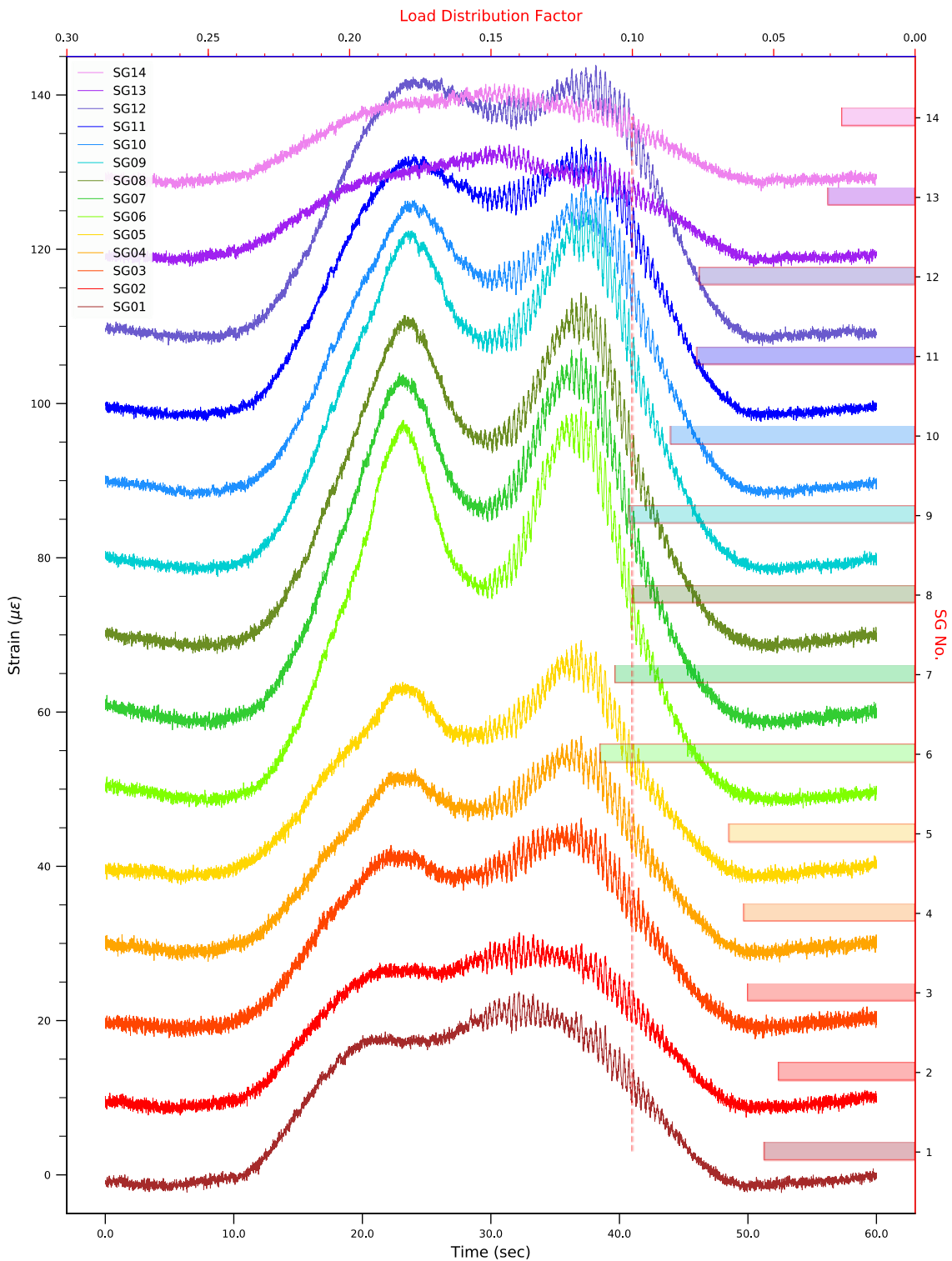
Notes: Figure 10.10 and Figure 10.11 show the fixed intensity maps of the strain distribution across Span 9 with increasing TSB severing. The strain was measured when the 62.5 tonne crossed Span 9 along the central path. The damaged stages increase in severity from top to bottom (see Figure 4.1). SGB1-7 captured the strain in the northern lane (DU1-7) and SGB8-14 mapped the strain in the southern lane (DU8-14). The truck speed was 2.5 km/h.

Figure 10.12: Tensile strains in undamaged stage



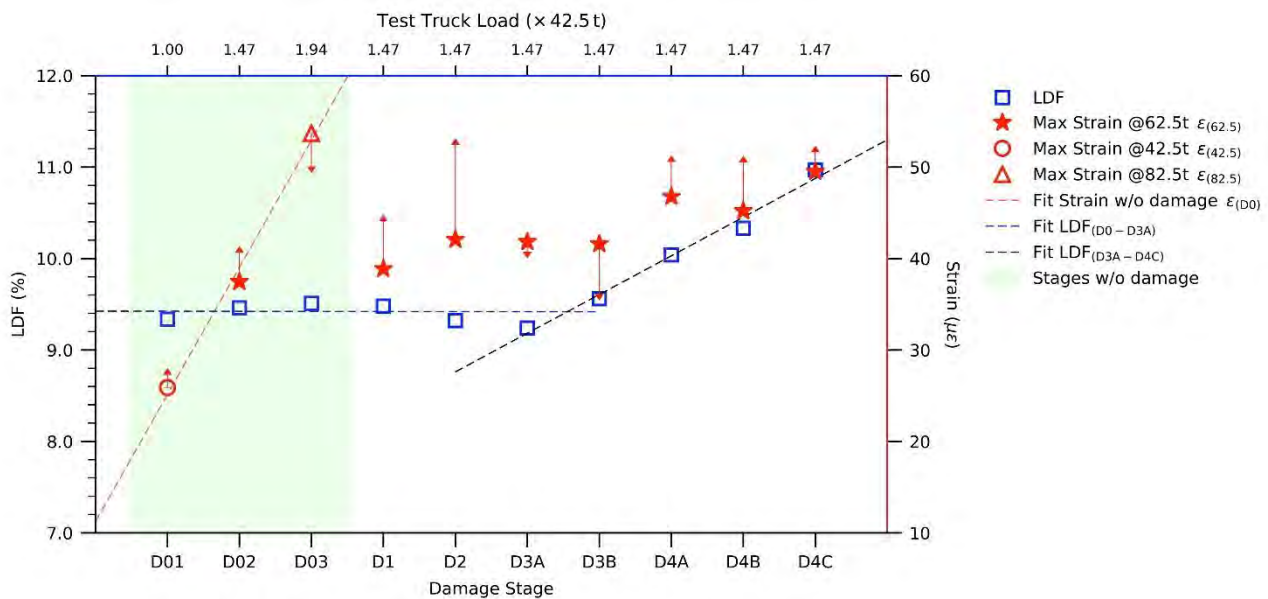
Notes: This Figure shows the strains measured for Run 2.2, i.e. with the 62.5 tonne truck travelling along the central path of the undamaged bridge (D02). The maximum strain was $37 \mu\epsilon$ (DU9) and the maximum LDF was 9.46% (DU9). The strain time-histories recorded by each SG on the deck soffit in the midspan are stacked with an offset of $10 \mu\epsilon$, with SGB1 at the bottom of the plot. Each SG number matches the DU number to which it is attached, as indicated by the labels on the right vertical axis. The related LDF is plotted on the right with values indicated by the top horizontal axis. The vertical red dashed line marks LDF = 10%. For SGs layout see Figure 7.3.

Figure 10.13: Tensile strains in last damaged stage



Notes: This Figure shows the strains measured for Run 10.2, i.e. with the 62.5 tonne truck travelling along the central path of the bridge after all TSB severing was complete (D4C). The maximum strain was 49.5 µε (DU7) and the maximum LDF was 11.10% (DU7). The strain time-histories recorded by each SG on the deck soffit at the midspan are stacked with an offset of 10 µε, with SGB1 at the bottom of the plot. Each SG number matches the DU number to which it is attached to, as indicated by the labels on the right vertical axis. The related LDF is plotted on the right with values indicated by the top horizontal axis. The vertical red dashed line marks LDF = 10% (see SGs layout in Figure 7.3).

Figure 10.14: LDF distribution for load tests



Notes: This Figure shows the distribution of the LDF values derived from the load tests (hollow blue squares). For consistency, all considered tests were carried out with the RMS test truck running along the central path. The truck load associated with each test is indicated on the top horizontal axis. The LDF values are superimposed with the maximum strains measured during each considered test (red stars), under a truck load of 62.5 tonne. The maximum strains derived for the initial runs of the 42.5 tonne and 82.5 tonne loaded truck are indicated by a hollow red circle and a hollow red triangle, respectively. The error bars attached to the strain values indicate the measurement drift before the baselining process. Fits of LDF values for increasing TSB damage are shown by the blue dashed line, for stages without or with minor damage (D0–D3A), and by the black dashed line for stages of significant TSB damage (D3B–D4C). The green-shaded region highlights the testing stages without TSB damage.

10.2.3 Load Distribution Factors

The LDF variation with increasing damage can be described in two distinct phases: before and after the damaged stage D3A. As shown in Figure 10.13, the structural load transfer mechanism changes after all the TSBs between DU6 and DU7 and between DU13 and DU14 were severed. The D3B severing stage significantly affected the load transfer mechanism of the deck, as DU7–13 ended up carrying most of the load (see Figure 10.10 and Figure 10.12). After D3A, the LDF increased linearly after successive TSB cuts, with an overall increase of 18% from the undamaged stage to the last severing stage. However, in contrast with the LDF measured for each DU prior to TSB severing, given the absence of TSB connections, four DUs (DU7–10) exceeded the LDF of 10% threshold in D4C, contemporaneously. The maximum LDF measured was 11.10% in D4C (Figure 10.12).

The LDF values derived from the load tests along the northern path (and related strain distribution), including the measurements in the quarterspan section, are detailed in Appendix H¹.

10.2.4 Neutral Axis

The position of the neutral axis (NA) in a beam cross-section is an important indicator of the beam's performance under load and, in turn, of the beam integrity. Therefore, a change in the NA position from the design value flags a change in the position of the centroid of stiffness. The stiffness of a bridge beam would change if its cross-section undergoes strengthening or damage. In the assessment of standard bridge superstructures (e.g. see Sigurdardottir & Glisic 2013), a variation of the NA position can be mainly explained as due to: (a) a change in the force normal to the beam longitudinal axis; (b) construction tolerance; and (c) reduced width/depth of the effective area.

¹ The data reported in Appendix H has not been corrected for baseline drift.

The NA positions derived for DU1–14 under the vehicle along the central path, for the initial condition and each damaged stage, are shown in Figure 10.15 and Figure 10.16. The location of the NA position, before and after TSB severing, is shown in Figure 10.17, where the internal DUs characterised by a more stable NA (DU5–11) are highlighted. It is noted that the SG placed on the top of DU13 (SGT13), after milling of the DWS, appeared to have undergone some damage during installation.

Figure 10.15: NA position, DU1–6

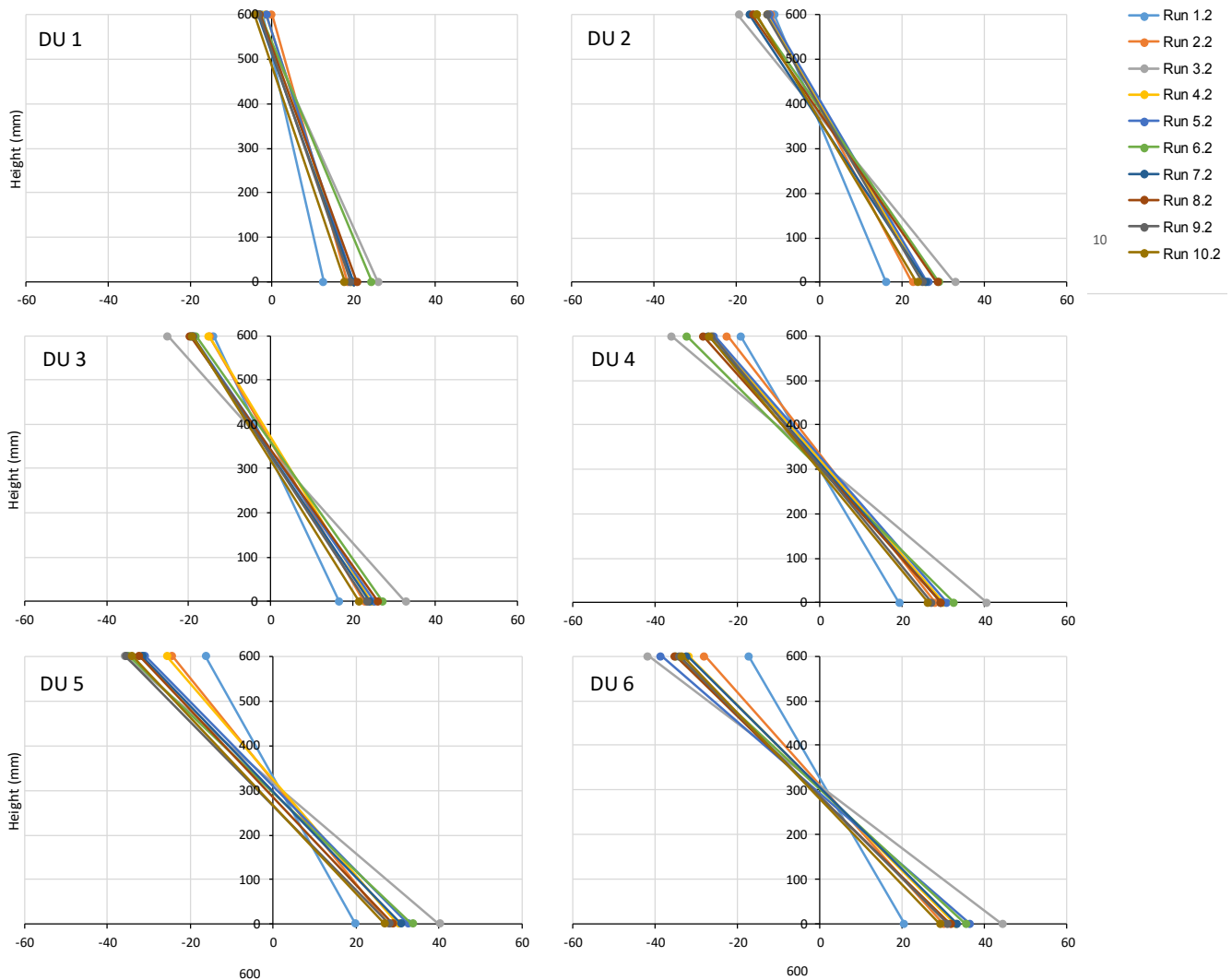


Figure 10.16: NA position, DU7-14

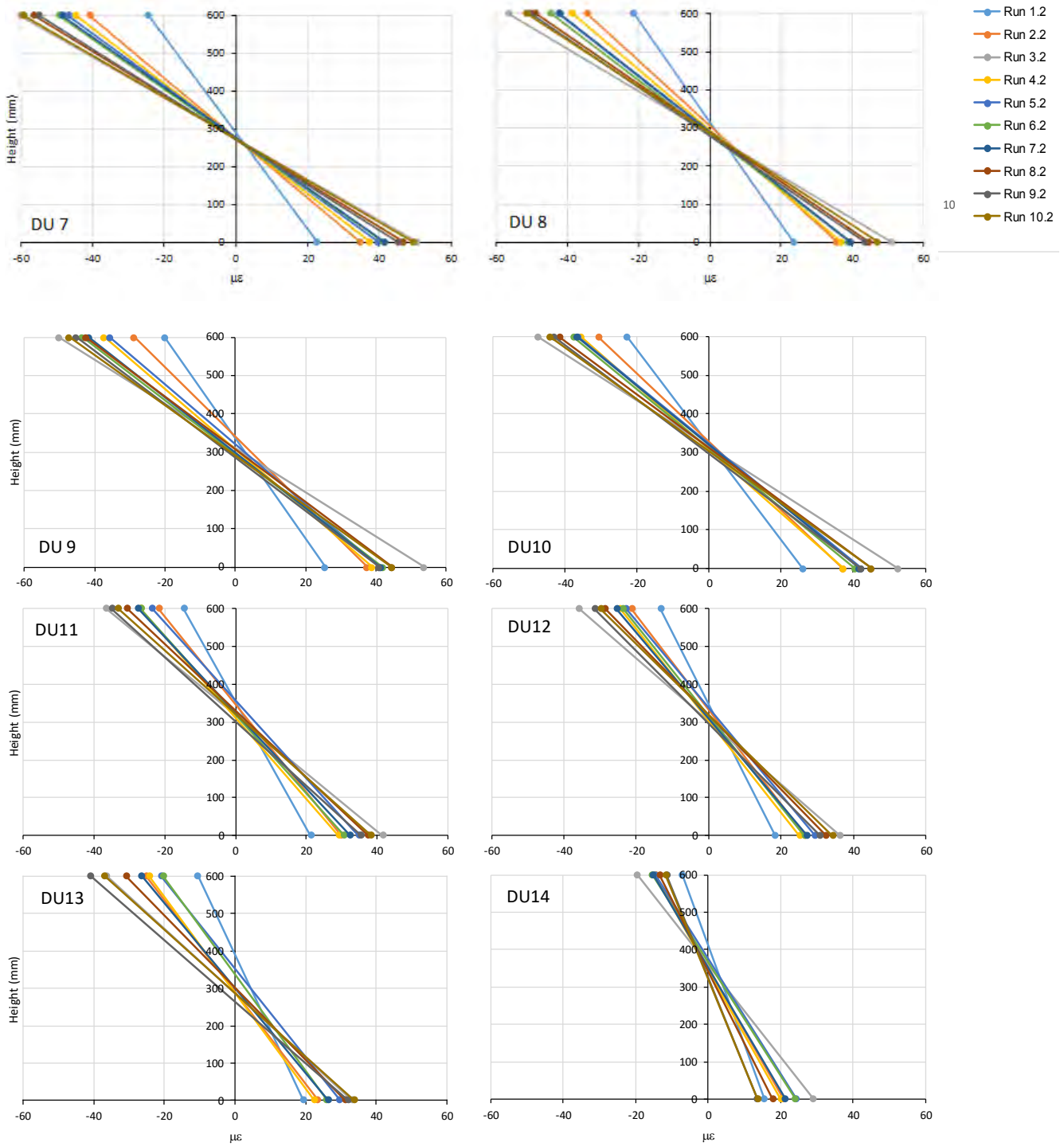
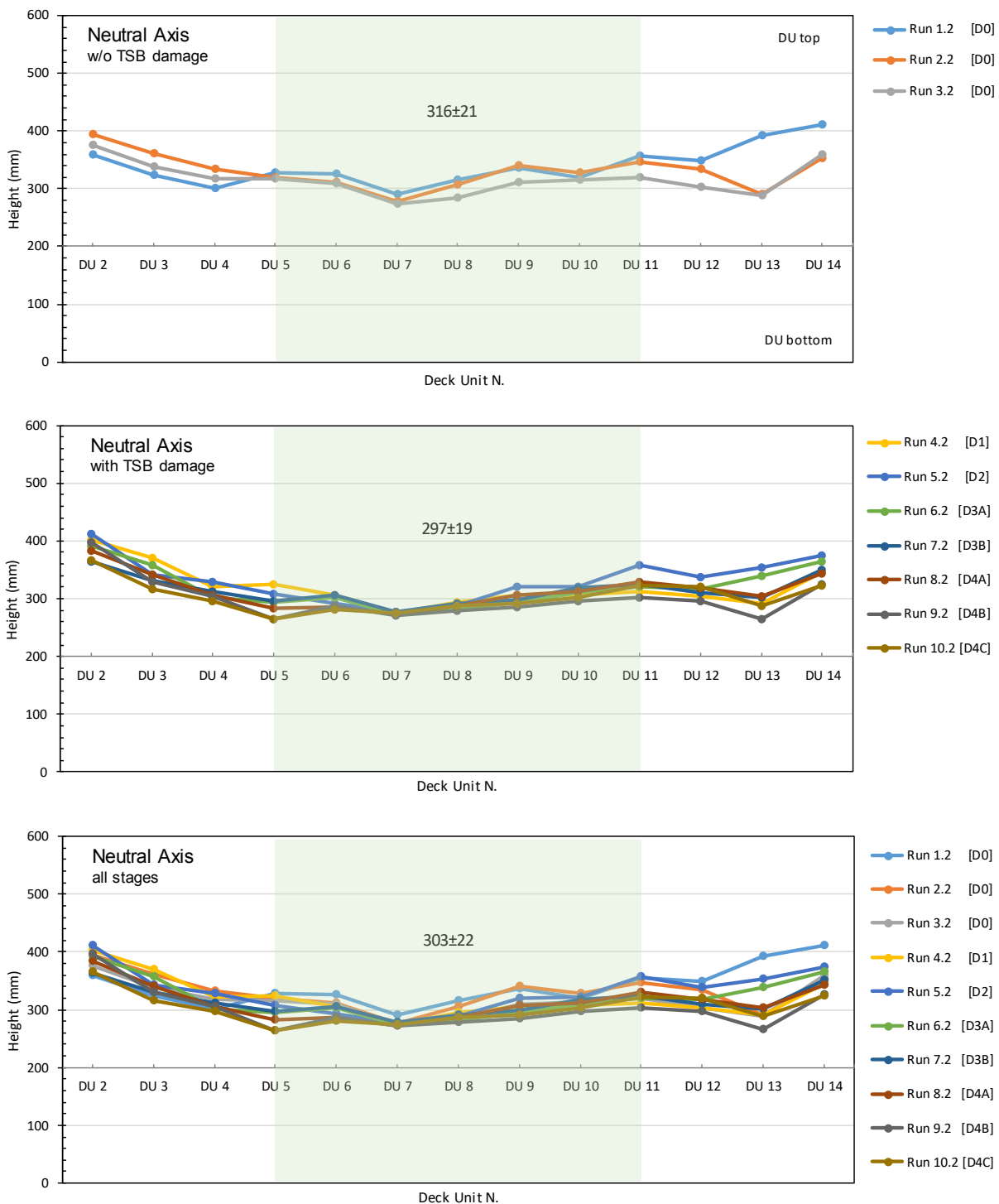


Figure 10.17: NA position for each damaged stage



Notes: This Figure shows the location of the neutral axis (NA) in each beam for each damaged stage, as derived for the load tests with the truck crossing the deck along the central path. The top Figure shows the NA derived for the load tests prior to TSB severing (D01–3), the central Figure shows the NA position after each stage of TSB severing, and the bottom Figure shows the NA position for all tests combined. The light-green shaded area highlights the DUs characterised by a more 'stable' NA, with indication of the average NA value (in mm) for DU5–11.

As an index of the variation of the NA position across the tests, the ratio, $RNA = NA(D)/NA$, of the NA position was derived for the middle DUs (DU4–14) after ($NA(D)$) and before (NA) the TSB severing, i.e. in the undamaged state, is reported in Figure 10.18 and Figure 10.19. The symbol D indicates a damaged stage, and NA is defined as the average of the values obtained from tests D0 1–3 (or Runs 1.2, 2.2, 3.2; see Table 6.1).

The assessment of the NA position, shown in Figure 10.15 to Figure 10.17, indicates an overall downward change of the NA as the TSB severing becomes more widespread.

The change of the normal force due to the increasing loads in the D0 tests (i.e. prior to TSB severing), produced a marginal variation of the NA position, i.e. it did not significantly affect the cross-sectional behaviour. Therefore, the NA position derived from the tests D01–3 is a reliable reference for the initial properties of each DU, as part of an undamaged deck effectively sharing and transferring the load (see Figure 10.17).

In the absence of observable transverse cracking during or after the damaged stages (see R3, and Appendix B), the change of the NA position by 10–18% (Figure 10.18 and Figure 10.19), downward from the initially identified location, is primarily due to an increase of the normal forces. As expected, the severing of the TSBs forced the few DUs, within the load pattern, to take the majority of the normal forces. Since the NA position is critical to the cross-sectional capacity, the measured change in the load transfer mechanism ultimately resulted in a deck characterised by a load bearing capacity of approximately 18% less than that of the original superstructure, this being the decrease in capacity controlled by the most loaded unit.

Figure 10.18: NA position variation, DU4–9

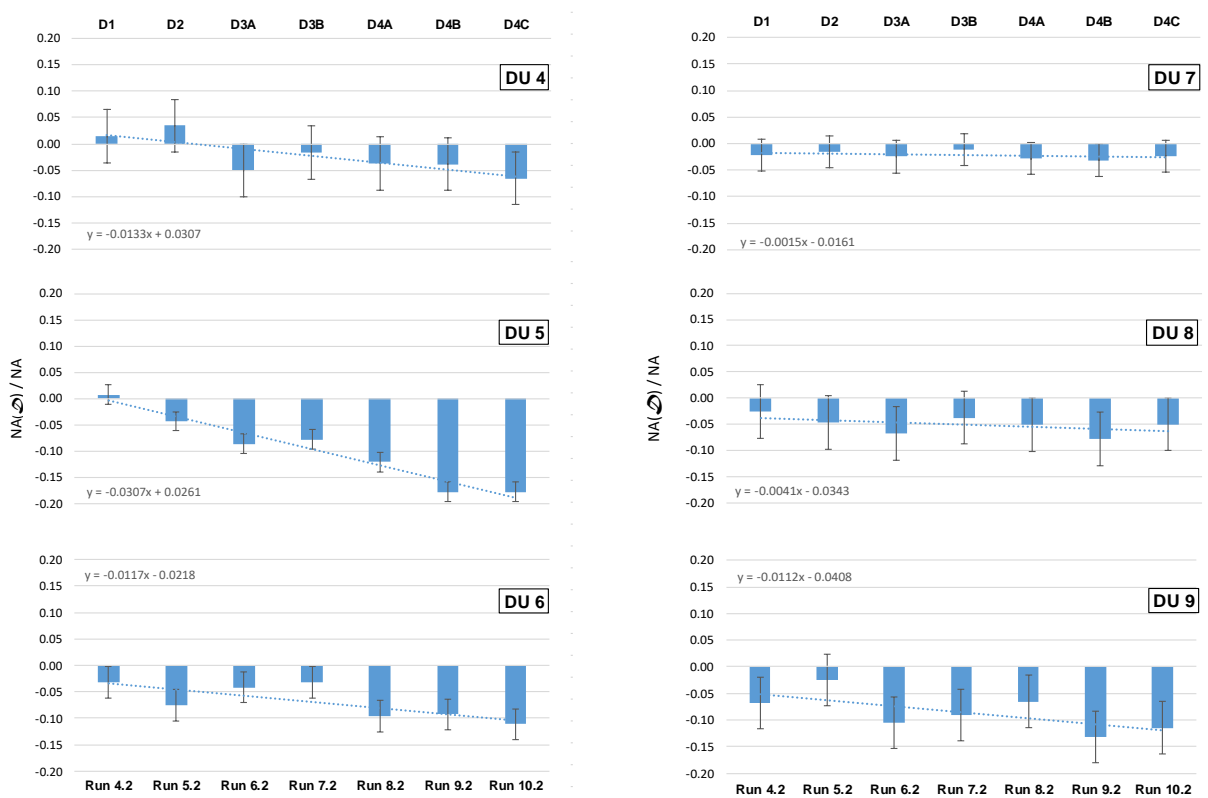
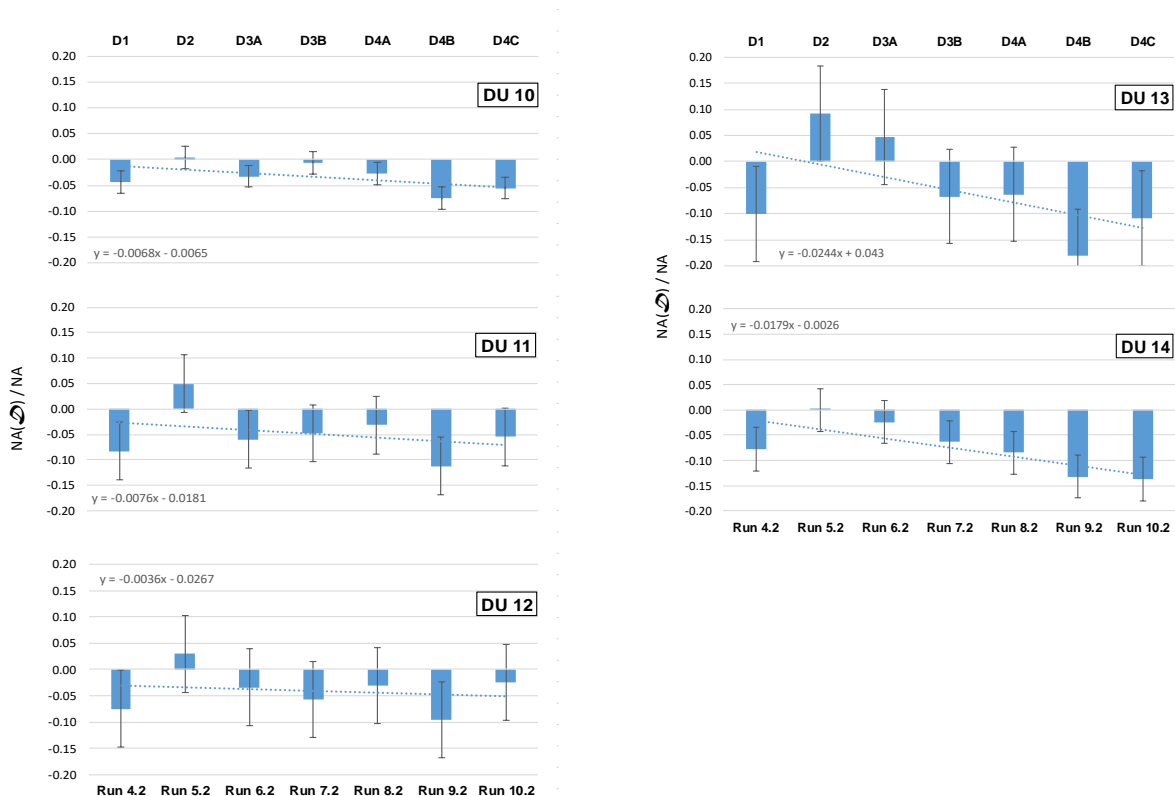


Figure 10.19: NA position variation, DU10–14



Notes: Figure 10.18 and Figure 10.19 show the variation of the neutral axis position across the tests for DU4–14. The neutral axis variation is expressed as the ratio, $NA(\delta) / NA$, where $NA(\delta)$ is the neutral axis position derived after each stage (δ) of TSB severing, and NA is the neutral axis position derived, for each DU, from the load tests carried out in the undamaged state. All data refer to vehicle runs along the central path with a load of 62.5 tonne. The error bars indicate the standard deviation.

As for Section 10.2.3, the upper limit of RNA of 18% appears to match the LDF increase derived for the deck structure after the last damaged stage (see Figure 10.13).

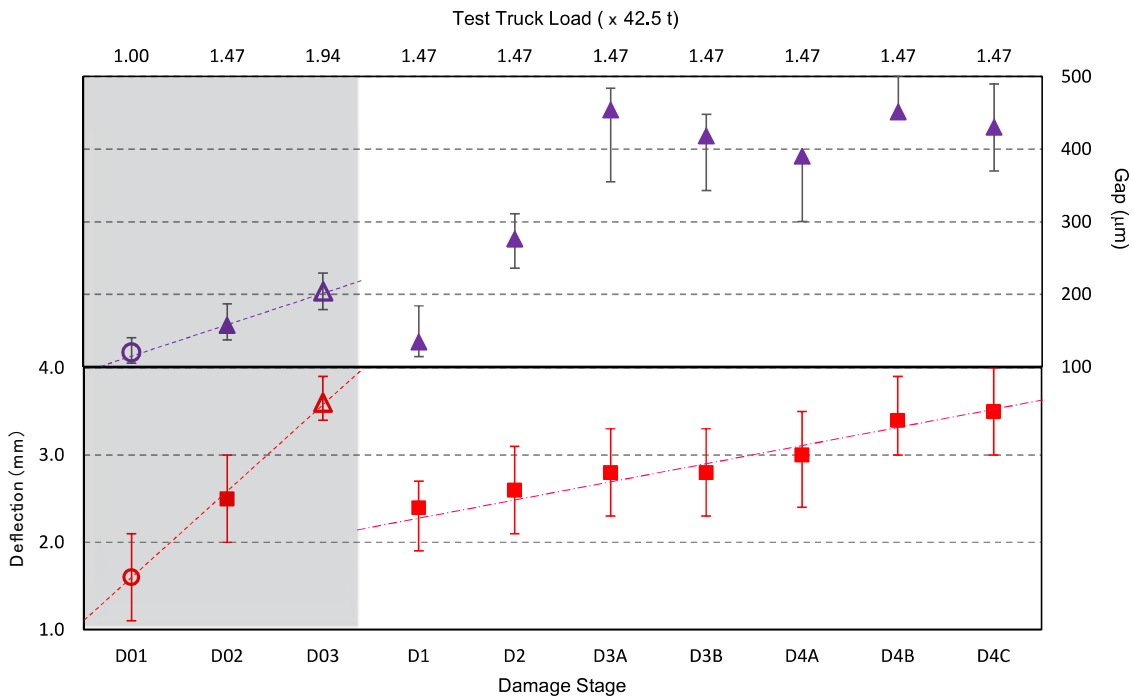
It is noted that the variation of the NA position could have also been induced by the ambient temperature. However, the temperature variation would have been only relevant when the top SGs were directly exposed to the sun. To allow the vehicle passage without damaging the sensors on top of the DUs, the top SGs, which were placed in the recess created by the DWS milling, were covered by steel sheets during the tests and for the related preparation. The temperature variation resulted in negligible effects, as the temperature gauge measured maximum concrete strains of 2.5–3.0 $\mu\epsilon$.

10.2.5 Deck Movements

The deck movements were measured in terms of vertical deflections (via SPs) and relative gaps between adjacent DUs, i.e. at the DU joints, via PPs (see Figure 7.4). The most significant results are summarised in Figure 10.20, while all measurements, including from sensor locations in the quarterspan section, are detailed in Appendix H.

The maximum measured deflection (δ_{max}) was 3.5 mm in stage D4C for DU7. The data from D1 to D4C could be fit either with a bilinear (as seen for LDF values in Figure 10.13) or a linear fit. However, an overall increase was measured with the gradual TSB damage, with a final deflection $30 \pm 8\%$ greater than the correspondent measurement in the undamaged stage. Similarly to the maximum strains, the deflection associated with the final damaged stage was close to that measured in D03, i.e. under a load that is 30% greater than what was used in D4C.

Figure 10.20: Maximum deck movements



Notes: This Figure shows the maximum DU displacements derived in midspan from tests carried out with the RMS truck running along the central path. The relative movements measured with the PP are shown on the top plot (purple markers), while the deflections measured with the SP are shown in the bottom plot (red markers). The truck load associated with each test is indicated via the top horizontal axis. All the filled markers indicate measurements taken with the truck load of 62.5 tonne. The maximum movements measured for the initial runs of the 42.5 tonne and 82.5 tonne truck are indicated by a hollow circle and a hollow triangle, respectively. The error bars attached to the movement values indicate the measurement drift before the baselining process. The linear fit of the deflections measured for increasing TSB damage is shown by the magenta dash-dotted line (D1–D4C). The dashed lines are fitting the data for the stages without TSB damage (also shaded in light blue). For PP and SP layout see Figure 7.4.

In terms of the relative movements between adjacent DUs, the relation with the deterioration of the TSBs could possibly match a bilinear fit, with yielding point in D3A. It is noted that given the µm scale of these measurements, the derived values are more sensitive to installation defects and systematic errors. The maximum gap opening reached 0.45 mm in test D4B between DU12 and DU13, while the gap opening was estimated at 0.12 mm in D02. Details of the measurements derived in all the tests are provided in Appendix H.

11 DISCUSSION

11.1 Observations Based on In-service Monitoring

The analysis of the in-service data was primarily focused on identifying the strain distribution and load transfer characteristics for a typical weekday, i.e. over a 24 hour cycle. The key findings from the monitoring exercise are as follows:

- The maximum strain measured under traffic was $43 \mu\epsilon$. According to the linear strain-load relationship derived from the D0 load tests (see Figure 10.13), $\epsilon = 43 \mu\epsilon$ corresponds to an equivalent static load of 68 tonne, or a 50 tonne travelling vehicle with a DLA of approximately 1.35. Strain values above $40 \mu\epsilon$ were measured both within and outside peak hours.
- The maximum LDF derived from traffic events was 11.2%. Daytime and night-time traffic can be characterised by lower (8.0–9.0%) and higher (9.0–11.0%) LDF values, respectively. Higher LDFs are associated with traffic positioned on a single lane only.
- The majority of the heavy traffic (which induced strains higher than $25 \mu\epsilon$) was localised on the southern lane (i.e. carried by DU1–8), and peaked at 4:30 pm on weekdays, when the structure sustained strains between 25 and $35 \mu\epsilon$ about ten times each minute.

11.2 Effects of the Applied TSBs Damage

This section discusses the observations made with respect to the effects of the applied TSB damage on the structural performance of the bridge superstructure. It should be noted that the TSB damage were applied during the testing regime, i.e. with a short term nature.

The analysis of the data from the controlled load tests yielded the following results:

- The maximum tensile strain measured during the last damaged stage (D4C) was $49.6 \mu\epsilon$. This value was 32% greater than the strain measured under equivalent load in the undamaged state (D02).
- The maximum LDF measured was 11.1% in the last damaged stage (D4C). The LDF increased by 18% from the undamaged stage to the last stage of TSB severing. The increase in LDF was evident only when the TSB severing was carried out in several longitudinal locations (D3A). The most loaded DUs, after extensive TSB severing (D4C), carried approximately 20% more load than in the undamaged stage.
- The NA position was lowered with incremental TSB severing. The maximum downward change of the NA position corresponded to an 18% reduction in the initial NA height, as measured from the bottom fibre.
- The maximum measured deflection was 3.5 mm in stage D4C for DU7, which was 30% greater than the maximum deflection measured in the undamaged state.
- The maximum gap opening beneath units reached 0.45 mm in stage D4B between DU6 and DU7, while the gap opening was estimated to be 0.12 mm in stage D02.

In light of the above findings, the following comments are made:

- During the testing regime, the test vehicle travelled back and forth on the bridge in a short period of time. Therefore, the behaviour of the bridge superstructure was investigated with a very low number of load cycles (about 60 runs in 2 days).

- When a TSB was severed, the mortar joint area on top of the TSB was also cut (noting that a 1.0 m dia. rotary blade was used to saw cut the mortar and TSB). The mortar joints away from the cutting areas remained intact, therefore they still contribute to the load transfer mechanism between the DUs.
- In the final testing stage (Stage D4C – see Figure 4.1), all bars along 2 mortar joints (out of 14 joints) and all joints along 3 TSBs (of out 8 TSBs) were cut. The reduction in the area of mortar along a joint is 34%. In comparison to the whole deck, the reduction in the area of mortar joint is 16%.
- In addition, observations from the lab test as part of the previous year project program (see Ngo 2017b) indicate that the TSBs did not engage in taking load at service load levels (due to its location at the mid-depth of the DUs). They only started taking loads at very high load levels which are close to the ultimate load. Therefore, at service loads, the main transverse load transfer mechanism was through the mortar joint.
- Given the above observations, for Sandgate Rd at the final testing stage (Stage D4C), where all TSBs were damaged, there were still substantial areas of mortar joints remained intact (86%). Although the load transfer was reduced to some extent as evidenced by the increase in the measured deflections and strains, the stiffness in the transverse direction which relies on the remaining mortar joint areas was still sufficient to provide a high level of load transfer capacity between the DUs. Therefore, it supports the observations and measured data from the tests.
- However, it is likely that the integrity of the uncut TSB sections and mortar joints would be lost gradually under the dynamic impact of traffic, should the bridge continue to be open for traffic after the test was completed. Since the TSBs were already cut, there was nothing to hold the units together, further failure of the mortar joints would likely propagate from the cutting areas under service loads. DUs would eventually work individually and might fail under service loads.

12 CONCLUSIONS AND RECOMMENDATIONS

12.1 Conclusions

The effect of the applied TSB damage on the behaviour of a simply-supported TSDUB was investigated via in-service monitoring and controlled load testing of one span of Sandgate Road Bridge. In-service monitoring data was recorded in two weeks under random traffic before the bridge was closed. The load tests were performed during a short period of time on the undamaged superstructure and when damage was incrementally applied to the TSBs on the span under investigation. The in-service data were used to benchmark the structural behaviour under operational loads, and to assess the properties of the traffic carried by the northbound section of the Gateway Motorway that crosses Sandgate Road. The controlled load test data were analysed to assess the changes in the behaviour of the bridge superstructure due to various levels of damage applied to the TSBs during the test regime.

Key findings from this investigation include:

1. The induced damage on the test span included (i) TSBs were cut, and (ii) the mortar joint areas surrounding the severed TSBs were lost. As observed from the test results, the incrementally induced damages resulted in a reduction in the overall capacity of the structure, as well as an increase in the measured structural responses (deflections and strains) and a reduction in the lateral load distribution. Apparently, the loss of the transverse prestress and damage of the mortar joints at various locations resulted in the reduced level of structural integrity and the onset of propagation of failure of the lateral load transfer mechanism.
2. The changes in the load transfer between the DUs in different TSB damaged stages are proportional to the reduction in the areas of mortar joints rather than on the level of the applied TSB damage. This is due to the fact that the mortar joints between the DUs are the key contributor to the transverse load transfer mechanism between the DUs. The reduction in the mortar joint areas in different damaged stages is insignificant in comparison to the total remaining intact mortar joint areas. As a matter of fact, a substantial portion of the mortar joint areas (86%) still remained intact at the most damaged stage.
3. The integrity of the mortar joints plays a critical role in the transverse load transfer mechanism of the bridge superstructure, while the TSBs contribute to the integrity of the mortar joints under loads. For a deck unit bridge with TSB deficiency, damage to the mortar joints is highly likely due to some overload events and may also occur under service loads. This damage would propagate further under service loads. Eventually, the mortar joints would be lost to a state in which each DU carries loads separately, i.e. a transverse load transfer mechanism is no longer present. The integrity of the overall structure would be lost, and the overall capacity of the structure would be dependant on the capacity of each individual deck unit, which may result in structural failure under service loads.

The assessment of the TSDUBs when TSB deficiencies are present has been part of the objectives of an investigation within the framework of AS/ISO 13822 *Basis for design of structures: assessment of existing structures*. The AS/ISO 13822 framework is more appropriate to the assessment of existing TSDUBs than the design philosophy stipulated in the assessment part of the bridge design code (AS 5100.7) which is more focused on design principles. AS/ISO 13822 is based on a much broader structural assessment concept than AS 5100.7 and incorporates factors such as asset business case, functional performance, understanding of risk and available precautions and mitigations, as well as operational management opportunities, including understanding and managing actual performance. An assessment scenario should be viewed in the operational, engineering and assessment contexts and take into account the specific assessment objectives. Further details of this investigation are included in the accompanying

document titled '*AS/ISO 13822 Framing investigation into the assessment of deck unit bridge and transverse stressing bar deficiencies*'.

12.2 Recommendations

The following recommendations are made:

1. This report should be read in conjunction with the accompanying document titled '*AS/ISO 13822 Framing investigation into the assessment of deck unit bridge and transverse stressing bar deficiencies*'.
2. It is essential that further investigation and research be conducted to determine the long-term effects and changes in load carrying capacity and performance of TSDUBs as a result of damaged transverse stressing bars.
3. Due to the large amount of recorded data, it is recommended that further analysis of the high-quality datasets derived from both the in-service monitoring and the load testing phases be conducted. Further work could include a more in-depth statistical analysis of the in-service monitoring datasets, which span over a two-week time window. In particular, the displacement time histories, which have not been processed for this report, are sufficiently long to be used for ambient-only dynamic analysis, e.g. via stochastic subspace identification. Similar analysis can be applied on the strain time-histories to investigate fatigue cycles.
4. In terms of the load testing data, the gradual evolution of the bridge response with increasing damage can be further investigated via dynamic analysis of the displacement and strain time histories. The highly sampled data and long recording times allow the fundamental frequency and its possible changes, especially in terms of frequency splitting, as the damage of the TSBs progresses, to be identified. Frequency splitting has been associated with the formation of microcracks, which amalgamate in visible cracks after repeated loading cycles. The displacement and strain time-histories recorded after the last stages of damage point to features in the bridge response that can be likely linked to microcracking dynamics.

REFERENCES

- Chakraborty, S & DeWolf, JT 2006, 'Development and implementation of a continuous strain monitoring system on a multi-girder composite steel bridge', *Journal of Bridge Engineering*, vol. 11, no. 6.
- Department of Transport and Main Roads 2013, 'Annexure S02 Modelling deck unit bridge superstructure for Tier 1 assessments', TMR, Brisbane, Queensland.
- Ngo, H, Pape, T & Kotze, R 2015, 'S3: Deck unit bridge deck analysis under live load: year 2 report', contract report RC007205, ARRB Group, Vermont South, Vic.
- Ngo, H & Pape, T 2015, 'BIS 7703 Canal Creek bridge: load test and in-service monitoring', contract report RC8286, ARRB Group, Vermont South, Vic.
- Ngo, H 2017a, 'S3: Deck unit bridge deck analysis under live load', NACoE S3 report, ARRB Group, Vermont South, Vic.
- Ngo, H 2017b, 'Destructive load testing of transversely stressed deck unit bridges', *Austrroads bridge conference, 10th, 2017, Melbourne, Victoria*, ARRB Group, Vermont South, Vic, 10 pp.
- Omenzetter, P & Brownjohn, JMW 2006, 'Application of time series analysis for bridge monitoring', *IOP Journal of Smart Materials and Structures*, vol. 15, no. 1.
- Rooke, A 2015, 'Network summary report: bridges and major culverts', Queensland Department of Transport and Main Roads, Brisbane, Qld.
- Sigurdardottir, DH & Glisic, B 2013, 'Neutral axis as damage sensitive feature', *IOP Journal of Smart Materials and Structures*, vol. 22, no. 7.
- Zhang, ZM, Chen, S & Liang Y-Z 2010, 'Baseline correction using adaptive iteratively reweighted penalised least squares', *Analyst*, vol. 135, no. 5, pp. 1138-46.

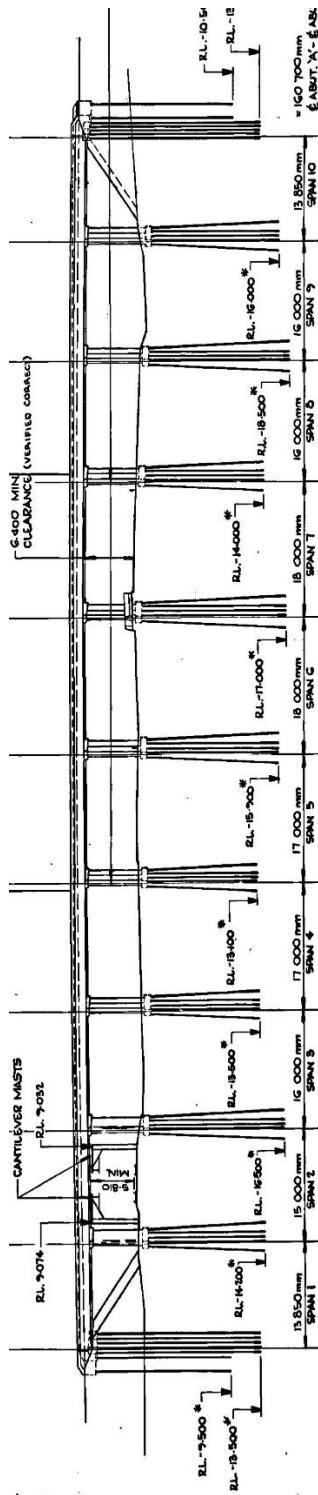
Standards Australia

AS 5100.7:2017, *Bridge design: bridge assessment*.

AS/ISO 13822:2005 (R2016), *Basis for design of structures: assessment of existing structures*.

APPENDIX A BRIDGE AS-CONSTRUCTED DRAWINGS

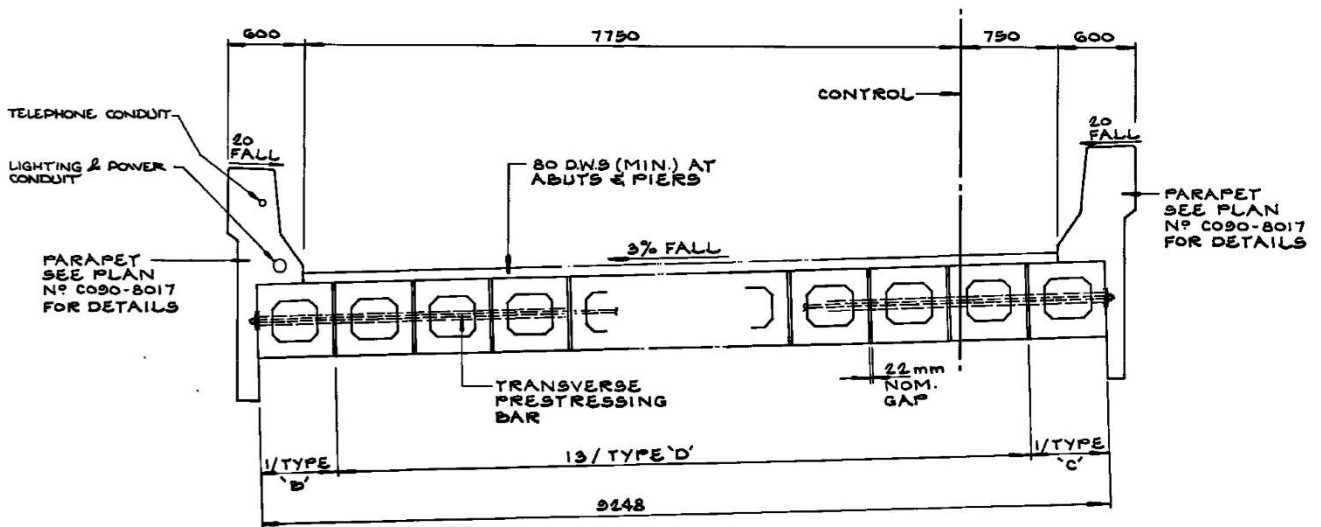
Figure A 1: Bridge profile



Notes: Elevation view of the bridge over Sandgate Road, facing south. Abutment A and Pier 1 are on the left. Span 9 is the second span from Abutment B, on the right.

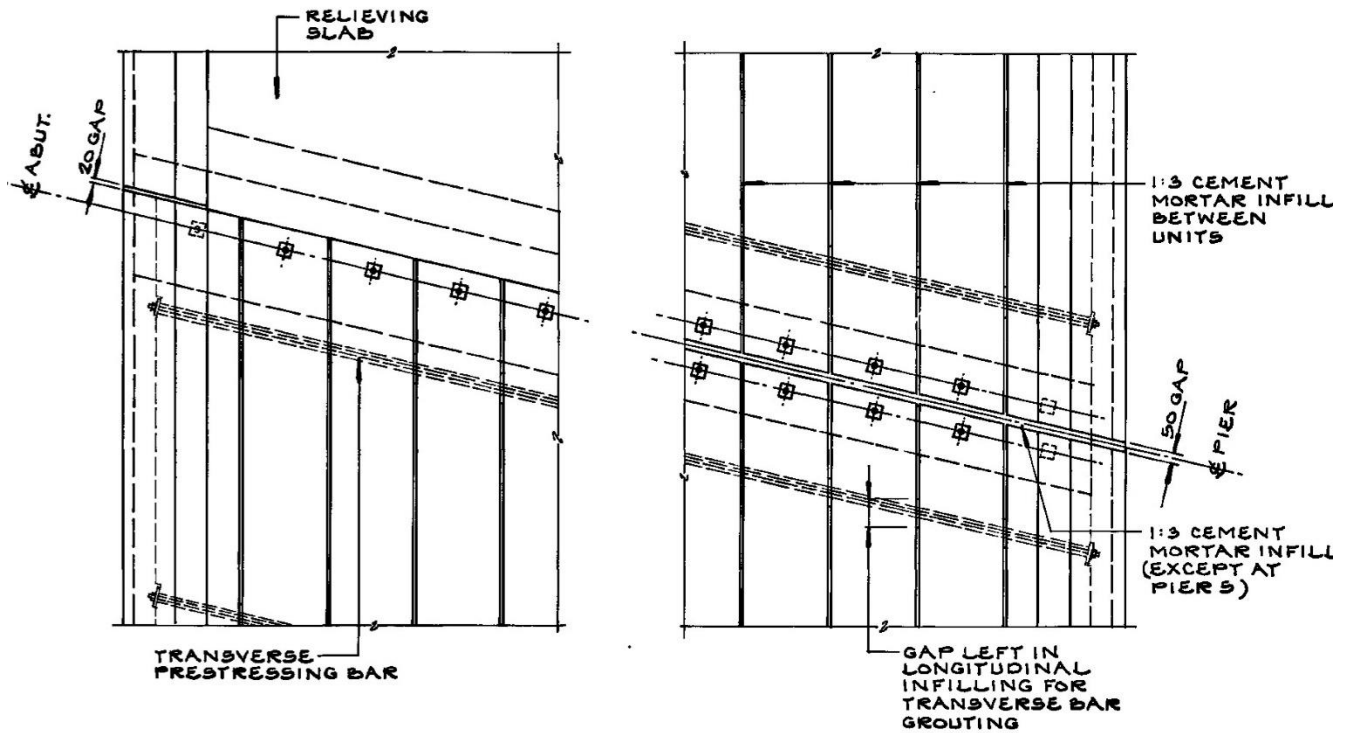
Source: TMR (DRG. No. 56731).

Figure A 2: Typical deck cross section



Source: TMR (DRG. No. 56737).

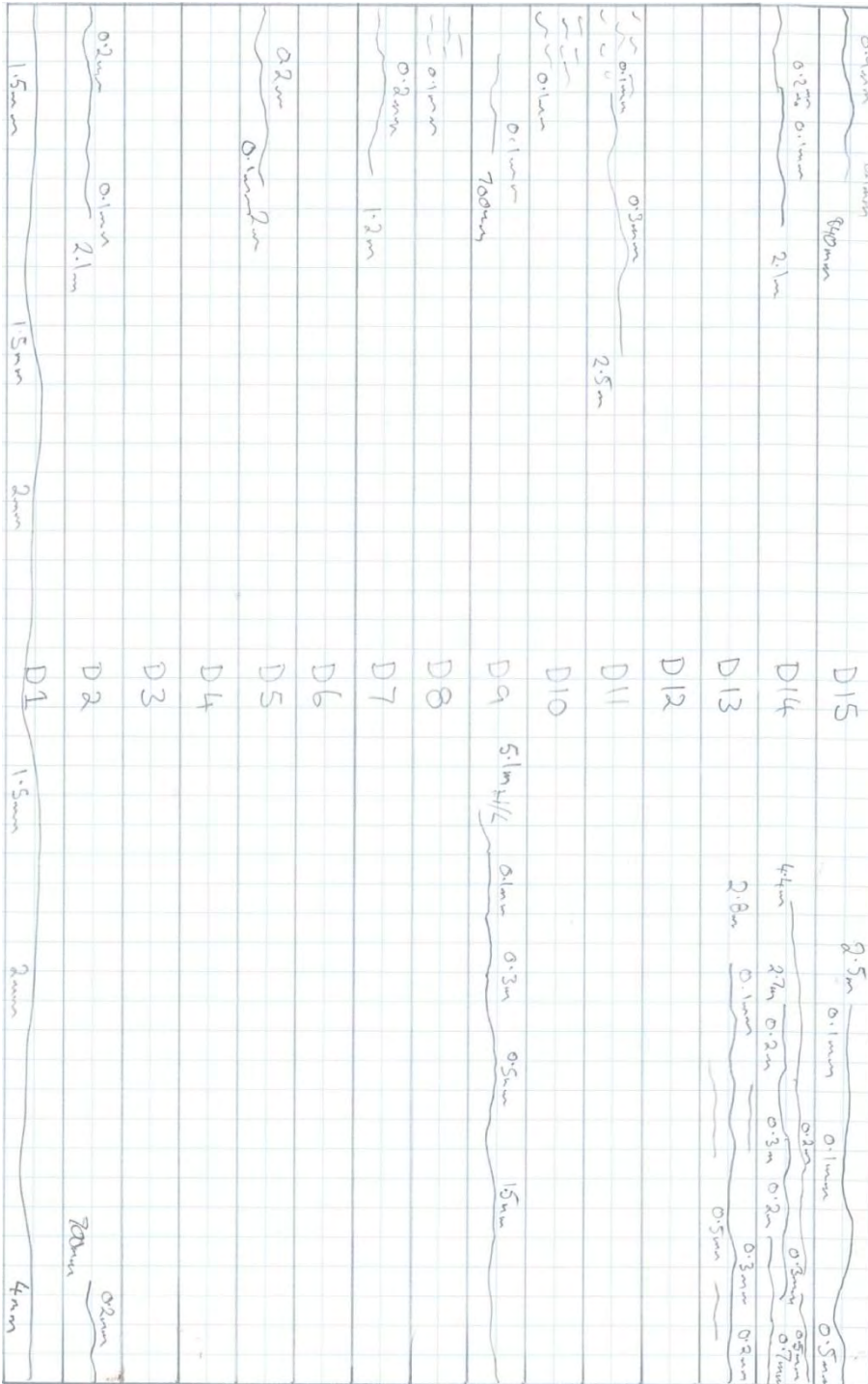
Figure A 1: Partial plan of the deck, at the abutment (right) and at the piers (left). The bridge has a skew angle of 13°



Source: TMR (DRG. No. 56737).

APPENDIX B CRACKING OF DU IN SPAN 9

Figure B 1: Cracking pattern on each DU in Span 9



Notes: The L2 inspection was carried out at the same time of the bridge testing, before and after TSB cutting. This map is reproduced, in a simplified form.
Source: TMR.

APPENDIX C PHOTOGRAPHS OF BRIDGES

Figure C 1: View of Bridge 8558 over Sandgate Rd, facing south



Figure C 2: View of Span 9 and Span 10 (on Abutment B), facing north



Notes: At the time of the photo, the bridge was undergoing load tests with the RMS truck, which is visible on the deck.

Figure C 3: View of Span 9 from the ground, facing south



Notes: DU15 is the unit near the top of the photo. Pier 8 can be seen on the left, while Pier 9 is visible on the right.

Figure C 4: Close-up view of Span 9



Notes: DU15 is the unit near the top of the photo, partially obscured by the northern parapet. DU1 can be seen near the bottom of the photo, with the drains in mid width.

APPENDIX D RMS PROOF LOAD TRUCK

Figure D 1: View of the RMS truck loaded with 62.5 t moving along the central path



Figure D 2: View of the RMS truck loaded with 82.5 t moving along the northern path

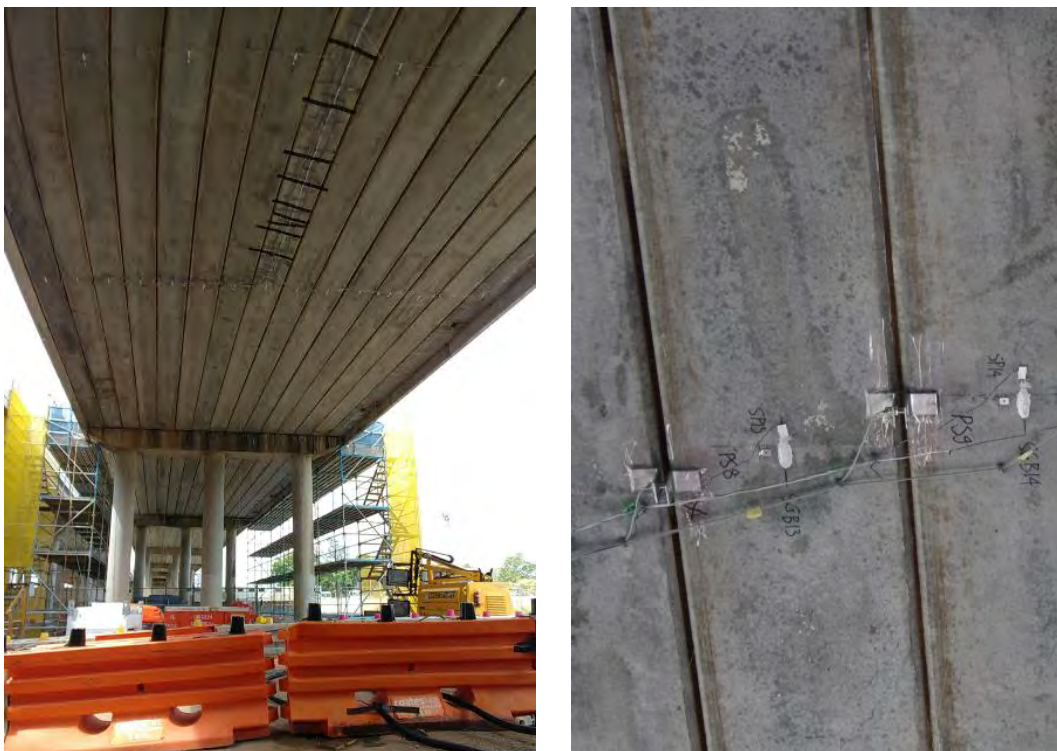


APPENDIX E INSTRUMENTATION AND SEVERING OF TSBs

Figure E 1: Instrumentation of the deck soffit – installation of a SG on the DU mid width



Figure E 2: Instrumentation of the deck soffit – layout



Notes: View of the instrumented soffit of Span 9, with SGs, PPs, and SPs installed in midspan and quarter span (right). A close-up of the attached SGs and PPs is shown on the right, including SP hooks and wire.

Figure E 3: Instrumentation of the DU top surface



Notes: View of the exposed DU after DWS milling (left), and application of SGs on the top of each DU in mid width (right).

Figure E 4: Load tests – RMS vehicle rolling over the sensor location in midspan



Figure E 5: TSB cuts – Close-up of a cut through the DWS to reach the TSBs



Figure E 6: TSB cuts – View of the bridge deck after cutting of TSB 2 (damaged stage D4A), facing south



Figure E 7: TSB cuts – View of the bridge deck after cutting of TSB 5 (damaged stage D4B), facing northeast

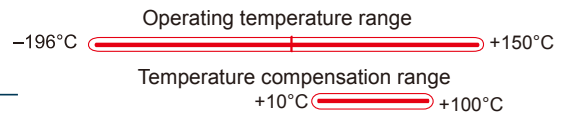


APPENDIX F SENSOR SPECIFICATIONS

Figure F 1: Strain gauges – Specifications of foil gauges TML FLA-30

FOIL STRAIN GAUGES

series F



Suffix code for temperature compensation materials
 -11: Mild steel (red square) -17: Stainless steel (orange square) -23: Aluminium (green square)
 For ordering, the above suffix code should be added to the basic gauge type.

Applicable adhesives

CN	-196 ~ +120°C
P-2	-30 ~ +150°C
EB-2	-60 ~ +150°C

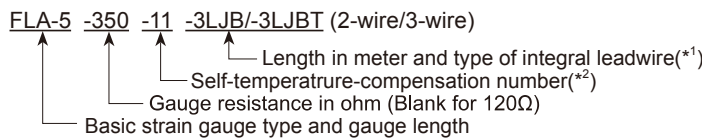
GENERAL USE

Gauge pattern	Basic type	Gauge size L W	Backing L W	Resist- ance Ω
---------------	------------	-------------------	----------------	-------------------

These gauges employ Cu-Ni alloy foils for the grid and epoxy resin for the backing. The epoxy resin backing exhibits excellent electrical insulation performance, and is color-coded to identify the objective material for self-temperature-compensation. Various types of strain gauges such as "for residual stress measurement" are available in addition to general use gauges.



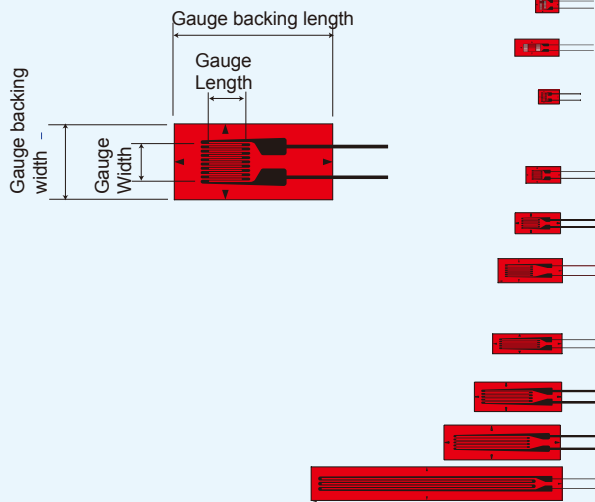
Example of type number designation



- *1 : Not mentioned for gauges without leadwire
- *2 : The following numbers are available for F series gauges
 - 11: Mild steel (11ppm/°C)
 - 17: Stainless steel, Copper alloy (17ppm/°C)
 - 23: Aluminium (23ppm/°C)

Single element : FLG/FLA/FLK

Each package contains 10 gauges.



FLG-02	0.2	1.4	3.5	2.5	120
FLG-1	1	1.1	6.5	2.5	120
FLA-03	0.3	1.4	3	2	120
FLA-05	0.5	1.2	5	2.2	120
FLA-1	1	1.3	5	2.5	120
FLA-2	2	1.5	6.5	3	120
FLA-3	3	1.7	8.8	3.5	120
FLA-3-60	3	1.2	8	3	60
FLA-5	5	1.5	10	3	120
FLA-6	6	2.2	12.5	4.3	120
FLA-10	10	2.5	16.7	5	120
FLA-30	30	2	36.1	5.1	120
FLK-1	1	0.7	4.5	1.4	120

Source: TML F-Series.

Figure F 2: String Potentiometers – Specifications of draw-wire sensors Messotron MSZ-P1



Draw-wire sensors MSZ-P1

Ranges: Up to 50 inches
Precision Potentiometric Output
Low Cost • Fast Delivery

P1

- Handy Mounting Bracket** : Mounts easily and quickly in several directions
- Designed for Cable Misalignment** : Long cable life, even when installation isn't perfect
- Polycarbonate Enclosure** : Withstands impacts and chemicals
- "Free-Release" Tolerant** : Greatly reduces damage due to mis-handling of cable



Specification Summary:

GENERAL
 Full Stroke Range Options.....0-4.75, 0-12.5, 0-25, 0-50 inches
 Output Signal voltage divider (potentiometer)
 Linearity..... ±0.25 to ±1.00% *see ordering information*
 Repeatability ± 0.05% full stroke
 Resolution essentially infinite
 Measuring Cable0.019-in. dia. nylon-coated stainless steel
 Enclosure Material polycarbonate
 Sensor plastic-hybrid precision potentiometer
 Weight3 oz. (w/o mounting bracket) max.

ELECTRICAL
 Input Resistance 10K ohms, ±10%
 Power Rating, Watts.....2.0 at 70°F derated to 0 at 250°
 Recommended Maximum Input Voltage..... 30 V (AC/DC)
 Output Signal Change Over Full Stroke Range..... 94% ±4% of input voltage

ENVIRONMENTAL
 Enclosure IP 50
 Operating Temperature0° to 160°F (-18° to 71°C)
 Vibrationup to 10 G's to 2000 Hz maximum

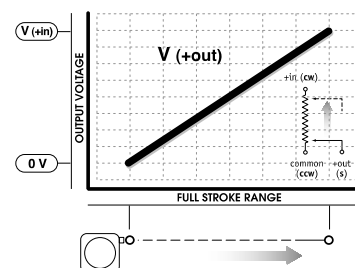
The P1 String Pot is a compact, economical and durable device that utilizes a flexible cable, a spring-loaded spool, and a potentiometer to detect and measure linear position.

The P1 is designed for tight spaces, high-cycle applications and generously allows cable misalignment. With 4 different measurement ranges and handy mounting brackets, the P1 is a perfect solution for many applications, from light industrial to OEM.

Ordering Information:

Item Number	P1-4	P1-12	P1-25	P1-50
full stroke range	4.75 in.	12.5 in.	25 in.	50 in.
accuracy (% of f.s.)	1.00%	0.25%	0.25%	0.25%
potentiometer cycle life	2.5M cycles	500K cycles	500K cycles	250K cycles
cable tension (±25%)	7 oz.	7 oz.	7 oz.	7 oz.

Output Signal



Source: Messotron MSZ-P1 User Manual.

Figure F 3: Proximity probes – Specifications of proximity sensors Messotron MNS5-M18



Proximity sensors

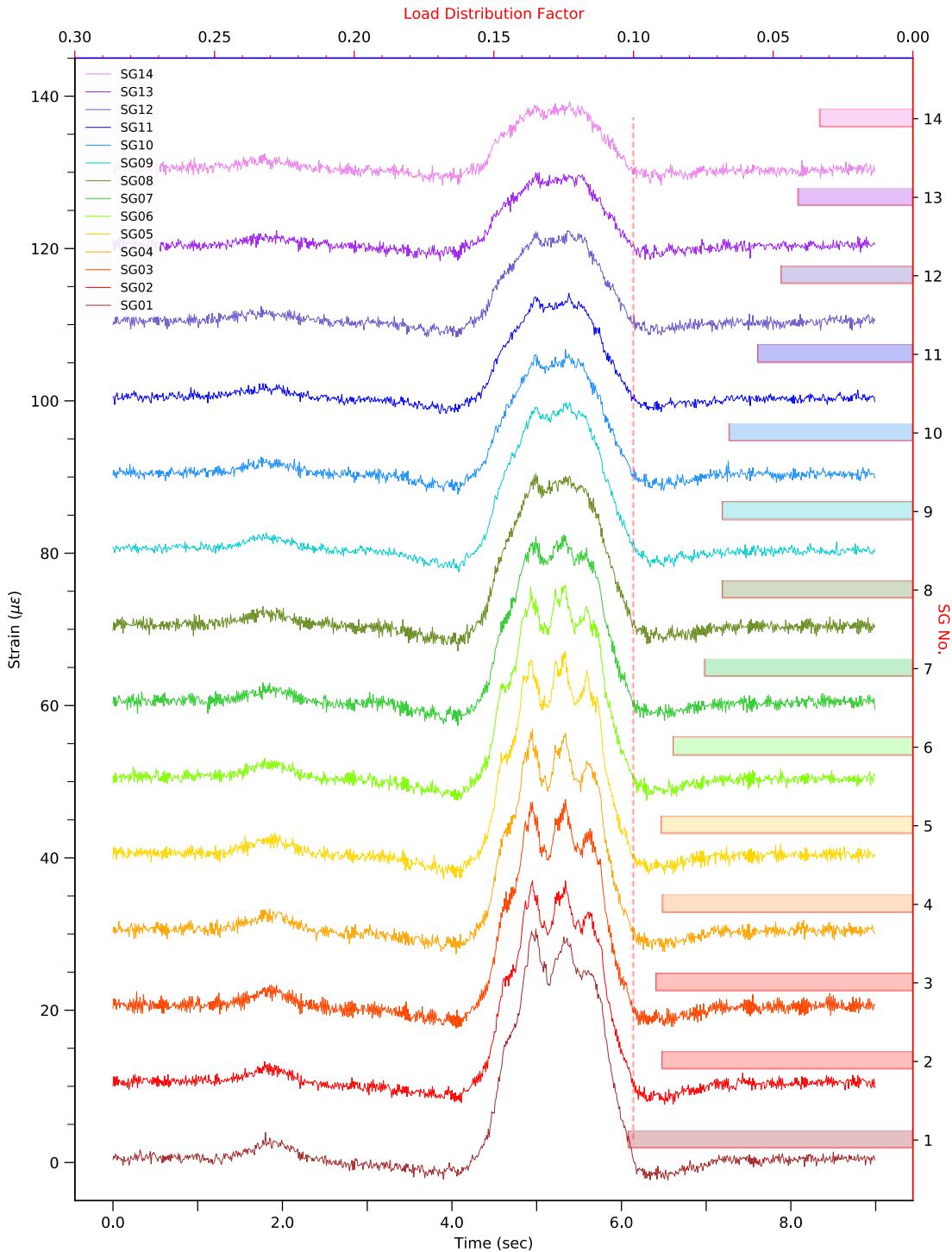
Proximity sensors (up to 15 mm measuring range)

Model	MNS2-G6,5	MNS2-M8	MNS3-M12	MNS5-M18	MNS12-M30
					
Sensing principle	inductive	inductive	inductive	inductive	inductive
Mounting	flush	flush	flush	flush	non-flush
Measuring range [mm]	0,5 ... 2,0	0,5 ... 2,0	0,25 ... 3,0	0,5 ... 5,0	3 ... 15
Case diameter [mm]	6,5 (no thread)	M8	M12	M18	M30
Linearity [% FS]	3%	3%	5%	5%	5%
Supply	11 ... 35 VDC	11 ... 35 VDC	11 ... 35 VDC	11 ... 35 VDC	11 ... 35 VDC
Dynamic range	400 Hz	400 Hz	500 (400) Hz	500 (400) Hz	300 Hz
Voltage output version 0 ... 10 (1 ... 9) VDC					
Current output version 4 ... 20 mA	-	-			
Wire					
Connector	-				
Key feature	Very compact	-	-	-	Large range
Optional versions	extended case	extended case	Non-flush mounting	Non-flush mounting	1) flush mounting, 2) add. 4bit digital output 3) parallel U/I output

Source: Messotron, 'Eddy current sensors with integrated electronics – Data Sheets'.

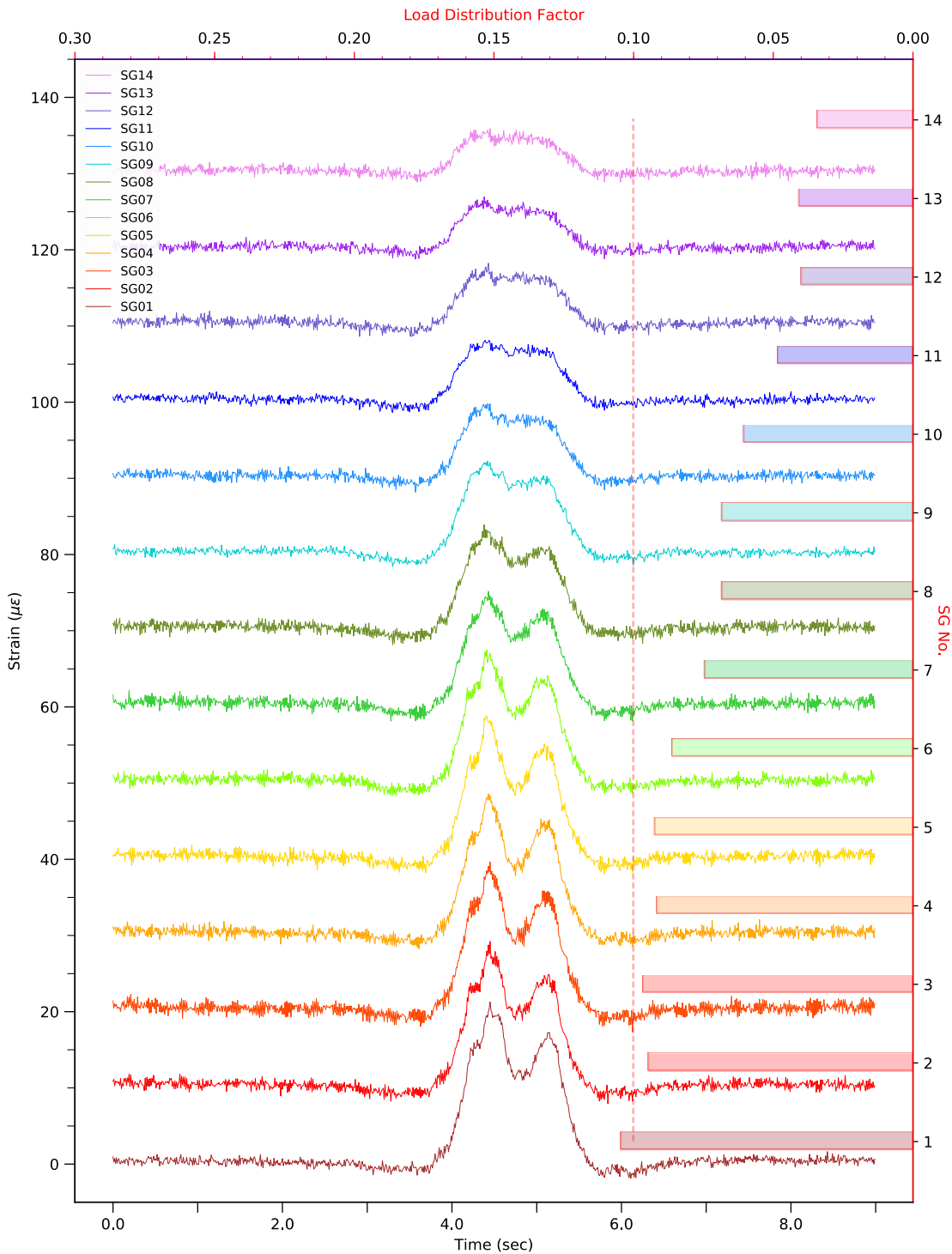
APPENDIX G IN-SERVICE MONITORING – KEY EVENTS

Figure G 1: Strain measured for Event # 1



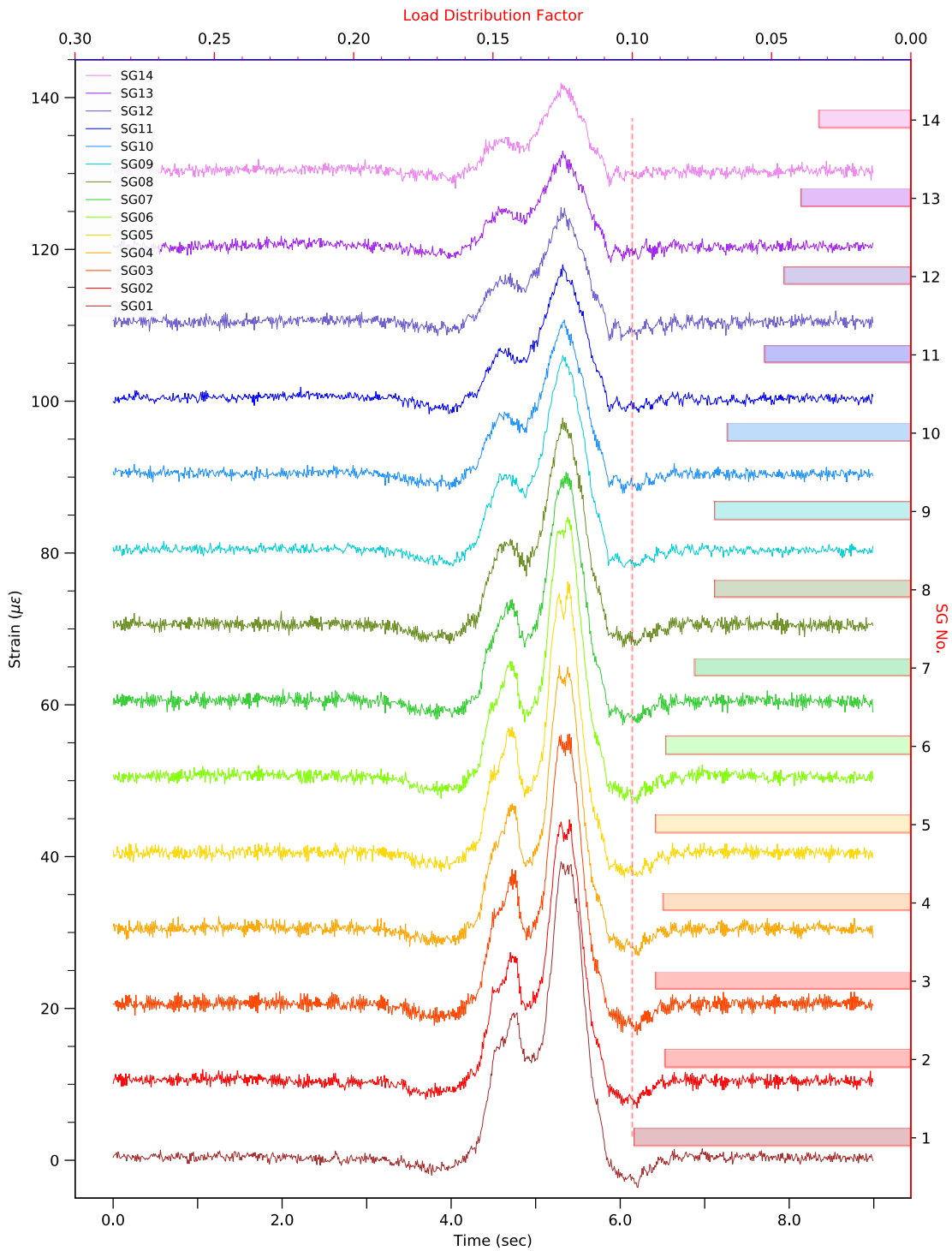
Notes: Day Friday 3 March 2017 – Start time 02:57:46 – Max strain: 30.63 $\mu\epsilon$ – LDF: 10.16% (DU1). The strain time histories recorded by each strain gauge (SG) on the deck soffit in midspan (SG1–15) are stacked with an offset of 10 $\mu\epsilon$, with SG 1 at the bottom. Each SG number matches the deck unit (DU) N, to which it is attached to, as indicated by the labels on the right vertical axis. The related load distribution factor (LDF) is plotted on the right with values indicated by the top horizontal axis. The vertical red dashed line marks LDF = 10%. For SG layout see Figure 7.3.

Figure G 2: Strain measured for Event # 2



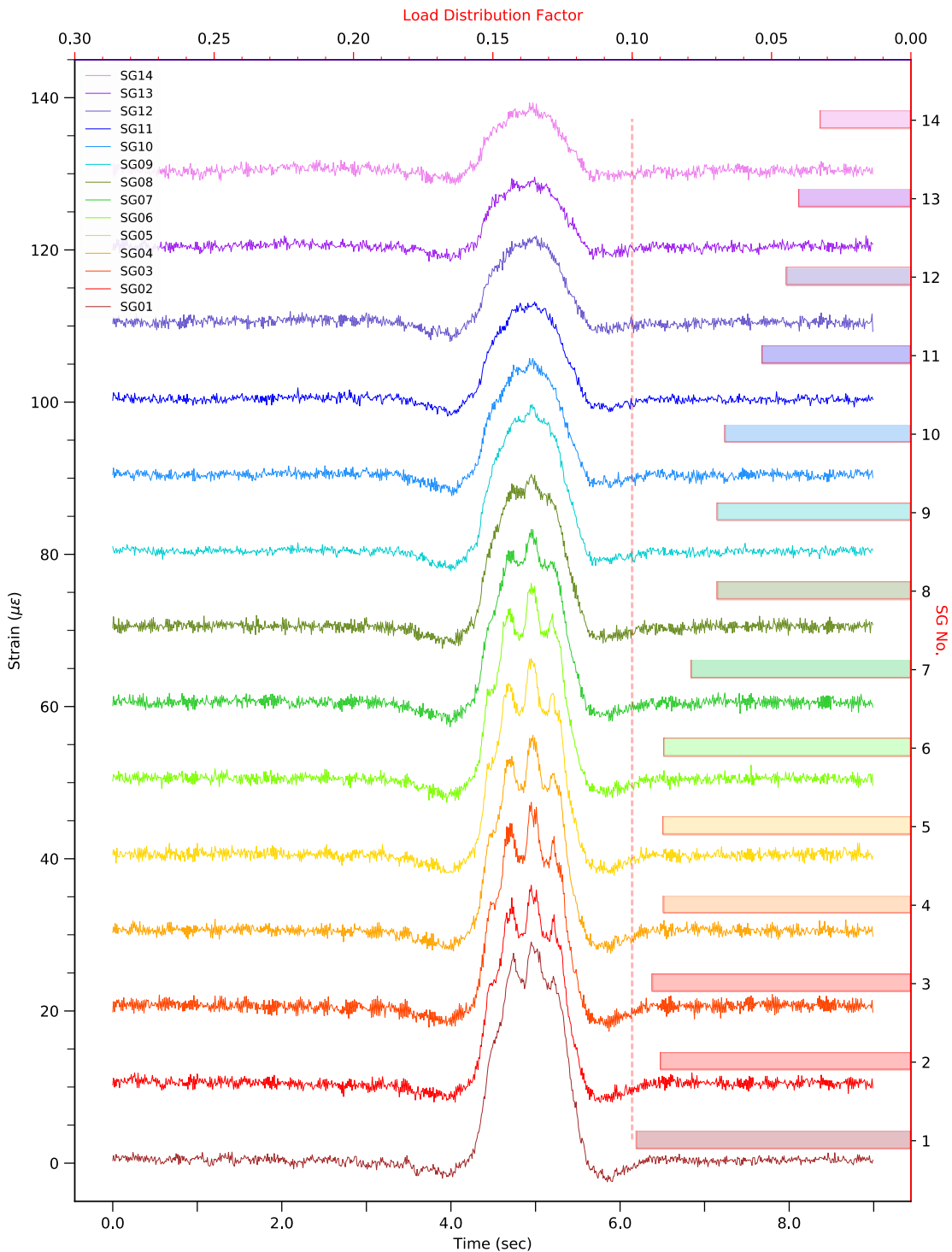
Notes: Day Friday 3 March 2017 – Start time 02:51:07 – Max strain: 21.27 $\mu\epsilon$ – LDF: 10.45% (DU1). The strain time histories recorded by each strain gauge (SG) on the deck soffit in midspan (SG1–15) are stacked with an offset of 10 $\mu\epsilon$, with SG 1 at the bottom. Each SG number matches the deck unit (DU) N, to which it is attached to, as indicated by the labels on the right vertical axis. The related load distribution factor (LDF) is plotted on the right with values indicated by the top horizontal axis. The vertical red dashed line marks LDF = 10%. For SG layout see Figure 7.3.

Figure G 3: Strain measured for Event # 3



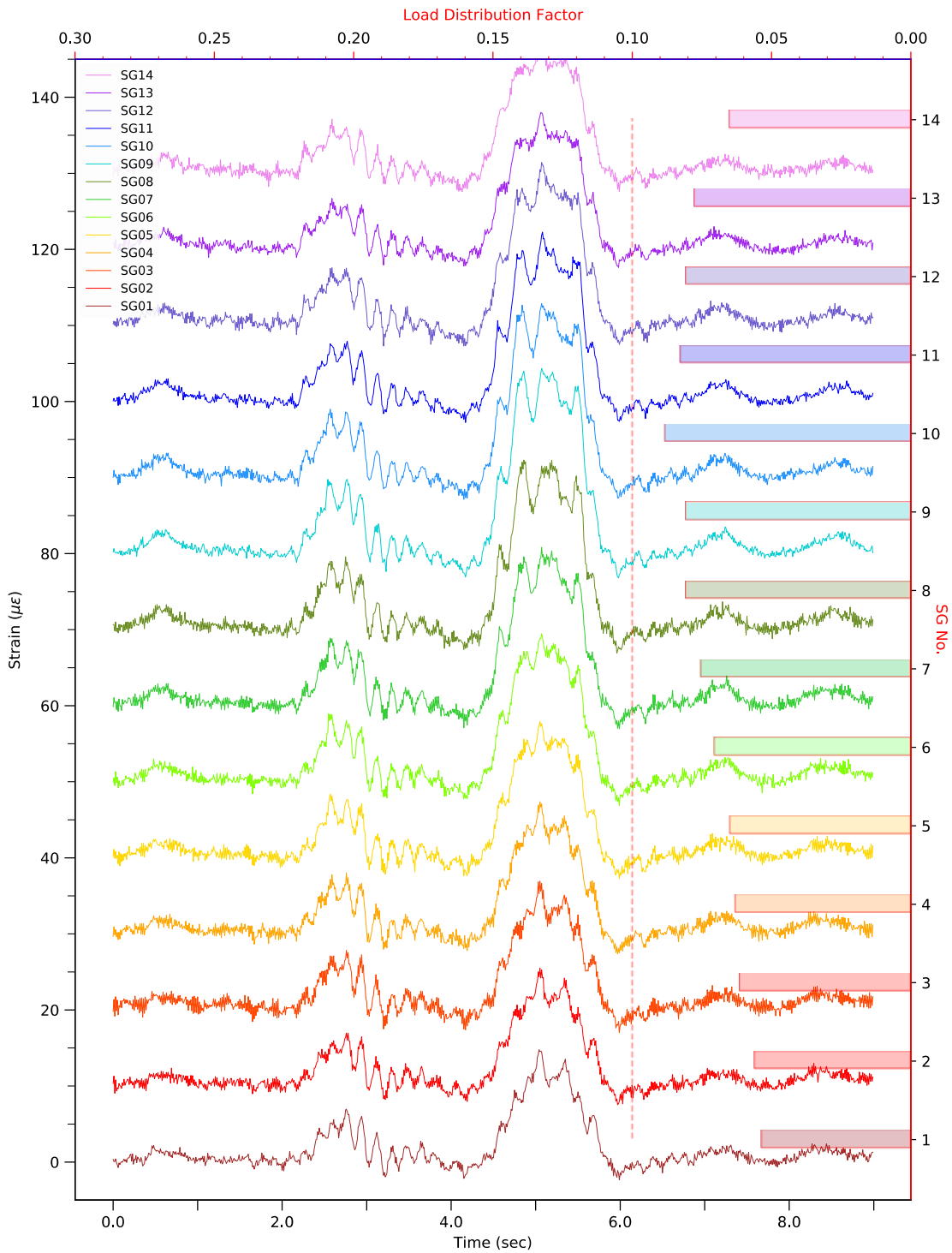
Notes: Day Thursday 2 March 2017 – Start time 20:14:46 – Max strain: 39.231 $\mu\epsilon$ – LDF: 9.93% (DU1). The strain time histories recorded by each strain gauge (SG) on the deck soffit in midspan (SG1–15) are stacked with an offset of 10 $\mu\epsilon$, with SG 1 at the bottom. Each SG number matches the deck unit (DU) N, to which it is attached to, as indicated by the labels on the right vertical axis. The related load distribution factor (LDF) is plotted on the right with values indicated by the top horizontal axis. The vertical red dashed line marks LDF = 10%. For SG layout see Figure 7.3.

Figure G 4: Strain measured for Event # 4



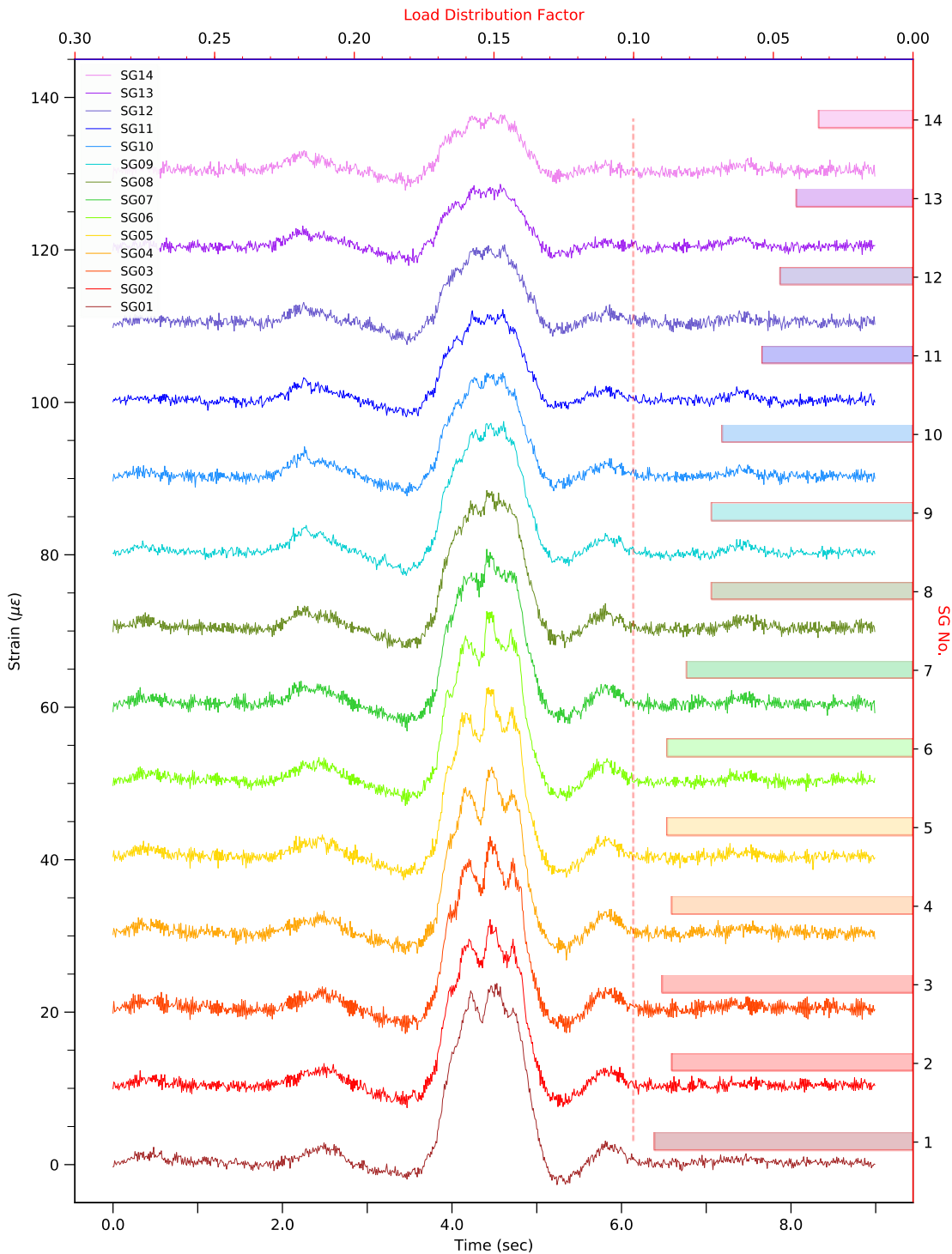
Notes: Day Thursday 2 March 2017 – Start time 20:18:59 – Max strain: 29.067 $\mu\epsilon$ – LDF: 9.82% (DU1). The strain time histories recorded by each strain gauge (SG) on the deck soffit in midspan (SG1–15) are stacked with an offset of 10 $\mu\epsilon$, with SG 1 at the bottom. Each SG number matches the deck unit (DU) N, to which it is attached to, as indicated by the labels on the right vertical axis. The related load distribution factor (LDF) is plotted on the right with values indicated by the top horizontal axis. The vertical red dashed line marks LDF = 10%. For SG layout see Figure 7.3.

Figure G 5: Strain measured for Event # 5



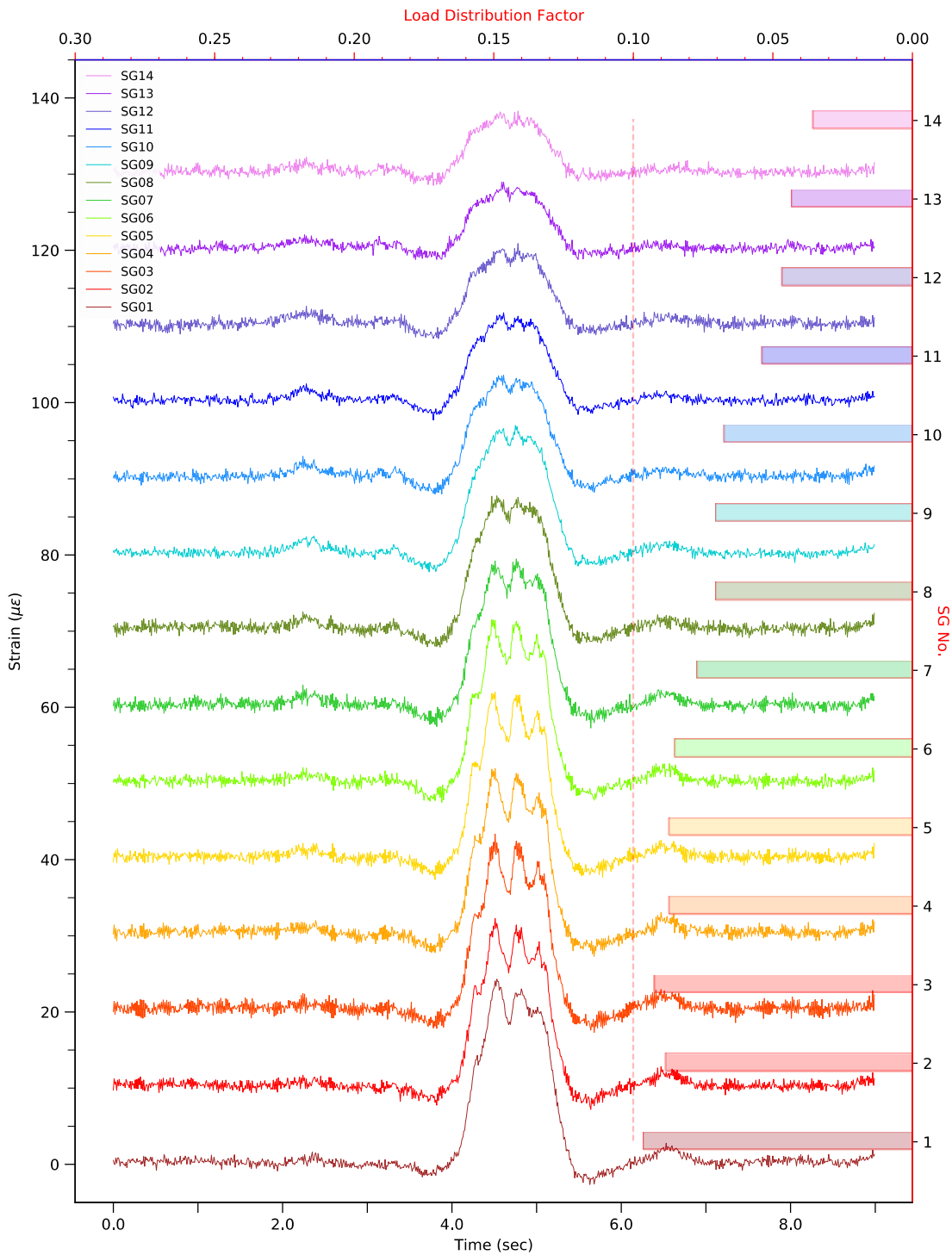
Notes: Day Thursday 2 March 2017 – Start time 19:13:38 – Max strain: 24.345 $\mu\epsilon$ – LDF: 8.81% (DU10). The strain time histories recorded by each strain gauge (SG) on the deck soffit in midspan (SG1–15) are stacked with an offset of 10 $\mu\epsilon$, with SG 1 at the bottom. Each SG number matches the deck unit (DU) N, to which it is attached to, as indicated by the labels on the right vertical axis. The related load distribution factor (LDF) is plotted on the top horizontal axis with values indicated by the top horizontal axis. The vertical red dashed line marks LDF = 10%. For SG layout see Figure 7.3.

Figure G 6: Strain measured for Event # 6



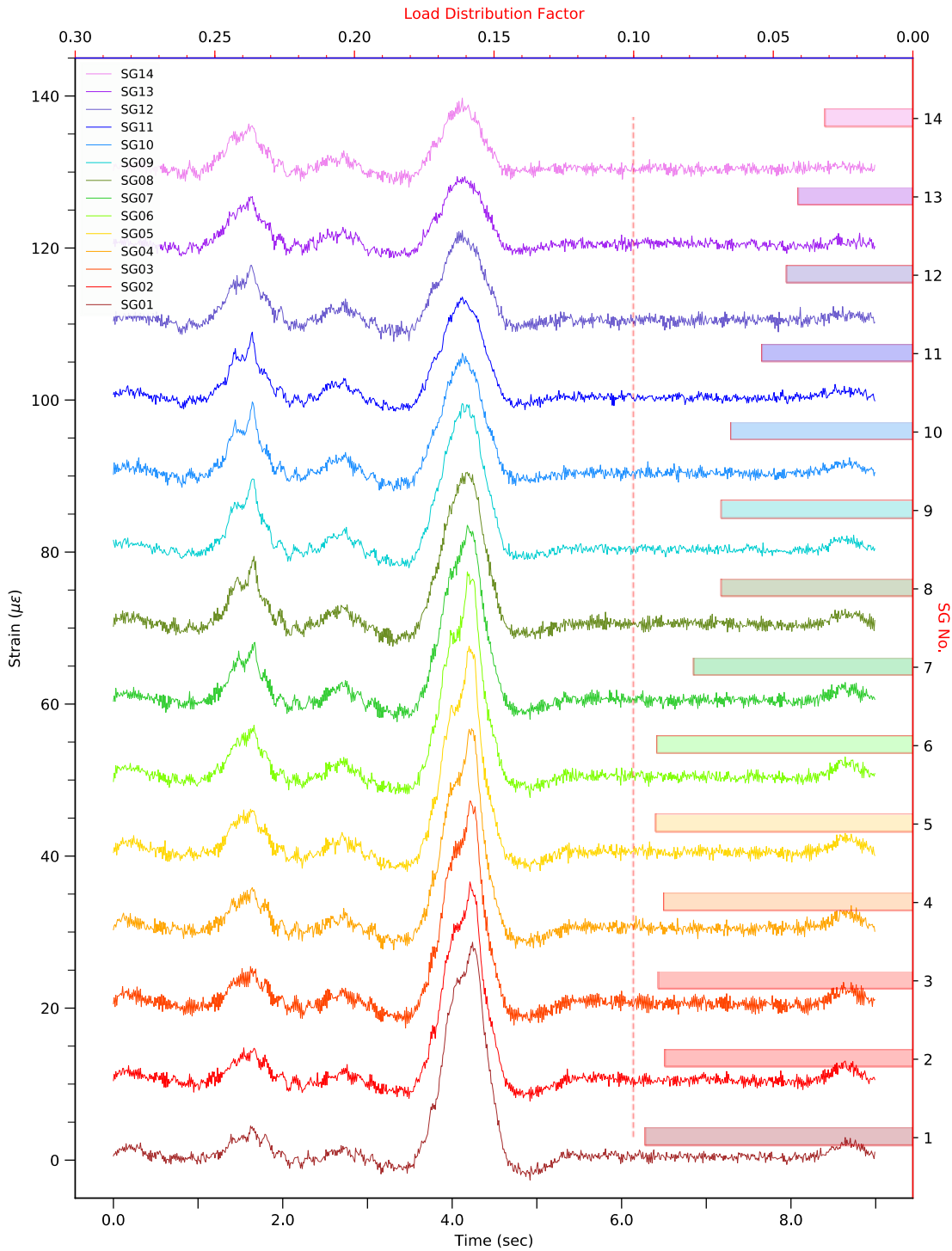
Notes: Day Thursday 2 March 2017 – Start time 19:04:25 – Max strain: 23.767 $\mu\epsilon$ – LDF: 9.25% (DU1). The strain time histories recorded by each strain gauge (SG) on the deck soffit in midspan (SG1–15) are stacked with an offset of 10 $\mu\epsilon$, with SG 1 at the bottom. Each SG number matches the deck unit (DU) N, to which it is attached to, as indicated by the labels on the right vertical axis. The related load distribution factor (LDF) is plotted on the right with values indicated by the top horizontal axis. The vertical red dashed line marks LDF = 10%. For SG layout see Figure 7.3.

Figure G 7: Strain measured for Event # 7



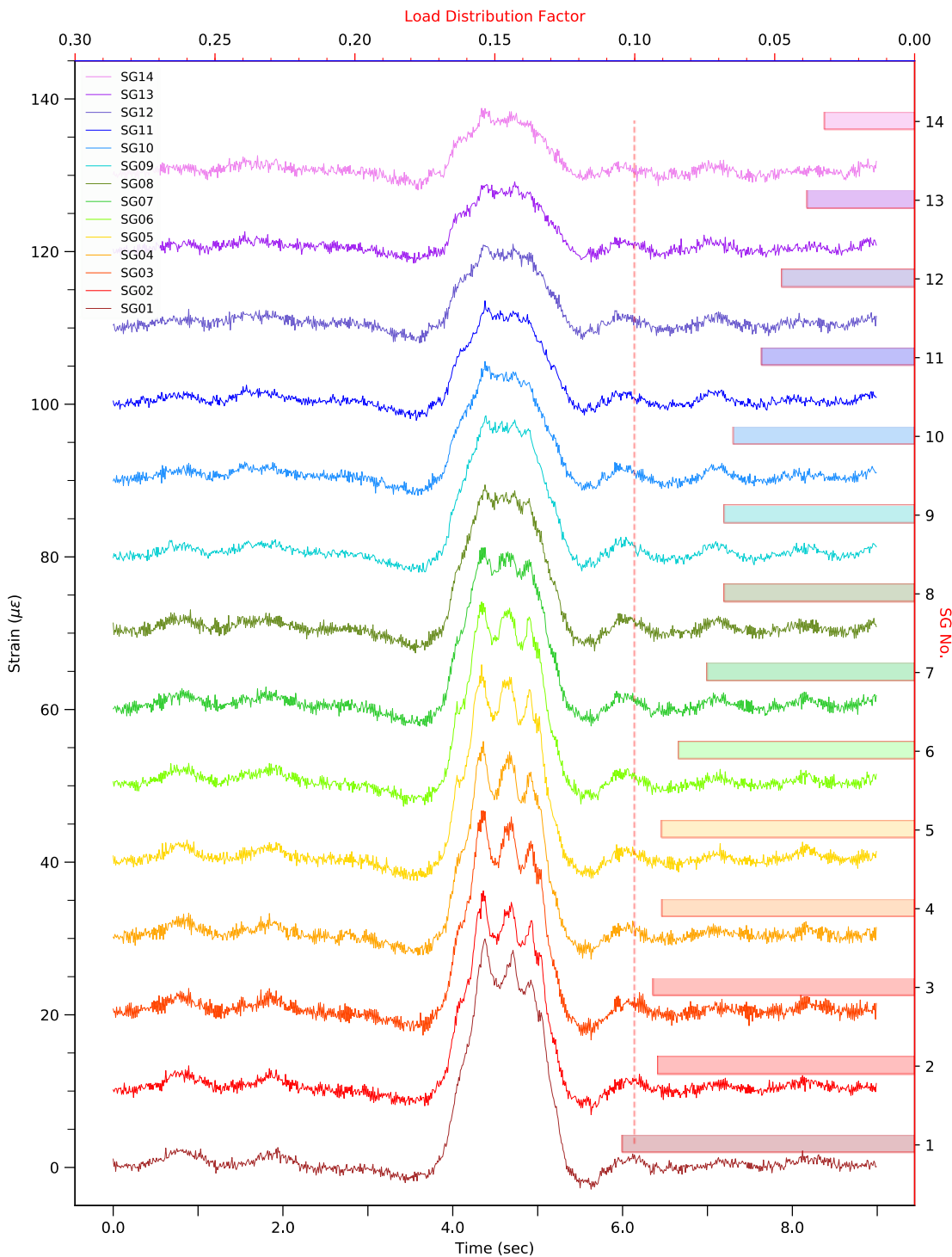
Notes: Day Thursday 2 March 2017 – Start time 19:04:25 – Max strain: 23.767 $\mu\epsilon$ – LDF: 9.25% (DU1). The strain time histories recorded by each strain gauge (SG) on the deck soffit in midspan (SG1–15) are stacked with an offset of 10 $\mu\epsilon$, with SG 1 at the bottom. Each SG number matches the deck unit (DU) N, to which it is attached to, as indicated by the labels on the right vertical axis. The related load distribution factor (LDF) is plotted on the right with values indicated by the top horizontal axis. The vertical red dashed line marks LDF = 10%. For SG layout see Figure 7.3.

Figure G 8: Strain measured for Event # 8



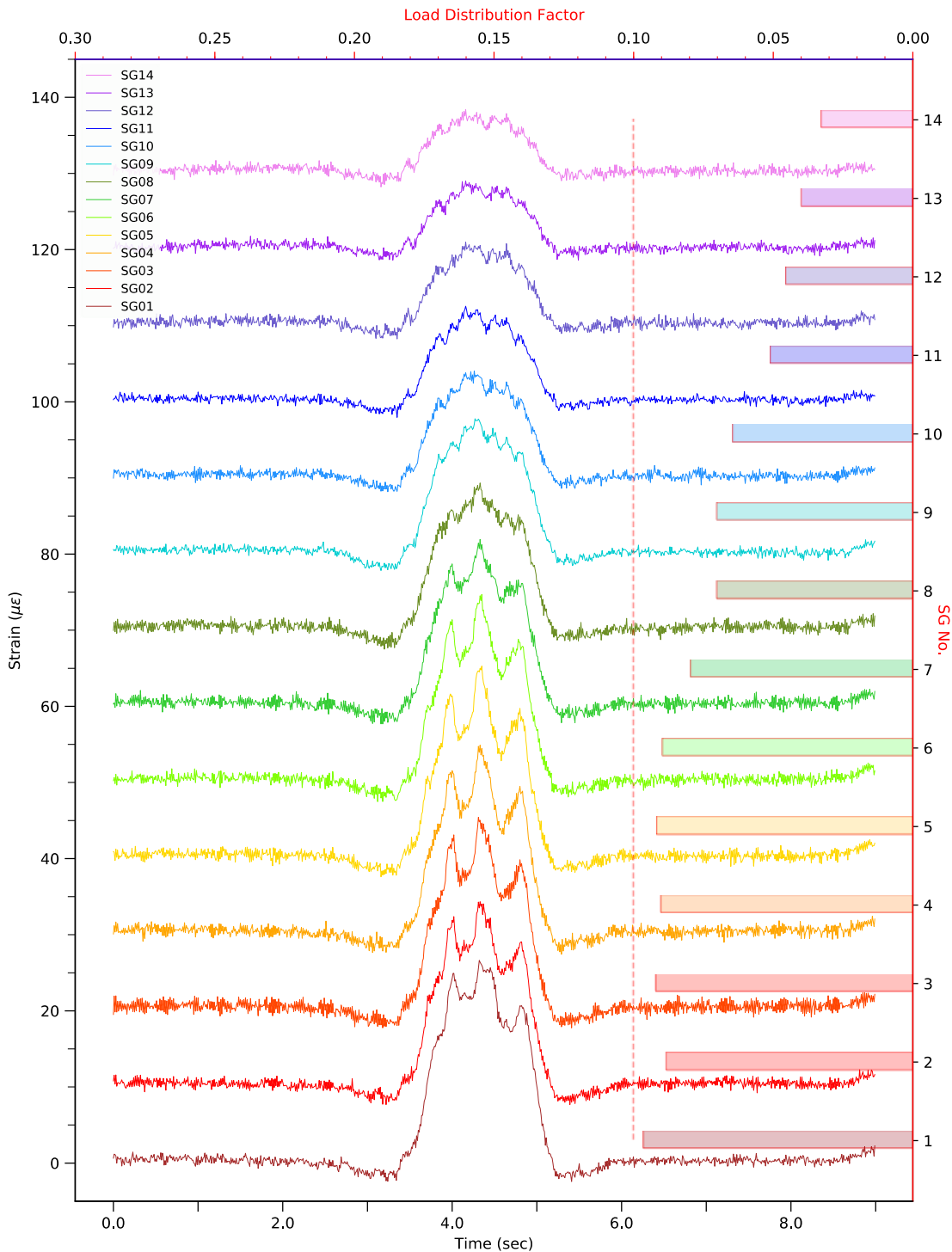
Notes: Day Thursday 2 March 2017 – Start time 19:55:51 – Max strain: 28.670 µε – LDF: 9.56% (DU1). The strain time histories recorded by each strain gauge (SG) on the deck soffit in midspan (SG1–15) are stacked with an offset of 10 µε, with SG 1 at the bottom. Each SG number matches the deck unit (DU) N, to which it is attached to, as indicated by the labels on the right vertical axis. The related load distribution factor (LDF) is plotted on the right with values indicated by the top horizontal axis. The vertical red dashed line marks LDF = 10%. For SG layout see Figure 7.3.

Figure G 9: Strain measured for Event # 9



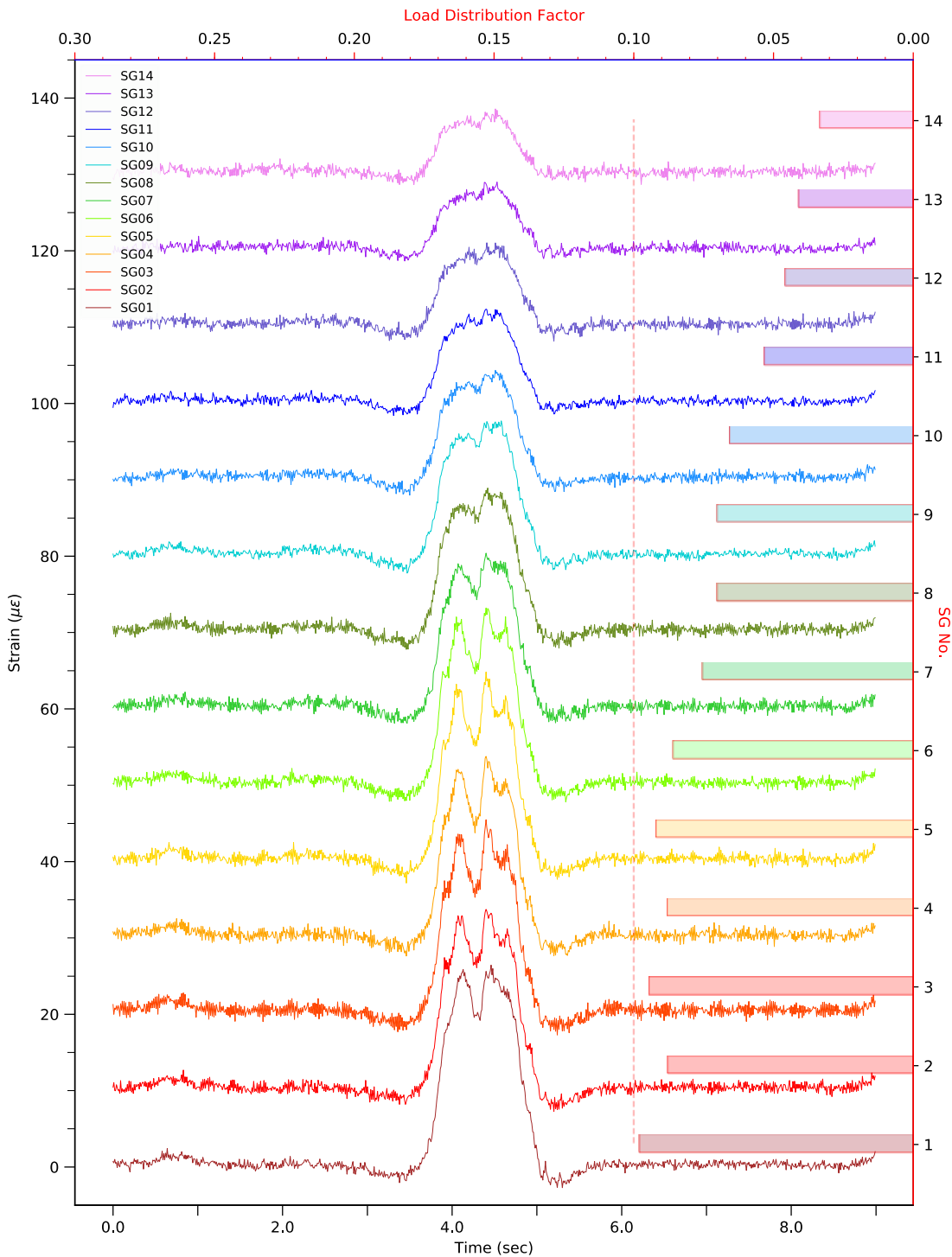
Notes: Day Thursday 2 March 2017 – Start time 20:03:38 – Max strain: 29.941 $\mu\epsilon$ – LDF: 10.44% (DU1). The strain time histories recorded by each strain gauge (SG) on the deck soffit in midspan (SG1–15) are stacked with an offset of 10 $\mu\epsilon$, with SG 1 at the bottom. Each SG number matches the deck unit (DU) N, to which it is attached to, as indicated by the labels on the right vertical axis. The related load distribution factor (LDF) is plotted on the right with values indicated by the top horizontal axis. The vertical red dashed line marks LDF = 10%. For SG layout see Figure 7.3.

Figure G 10: Strain measured for Event # 10



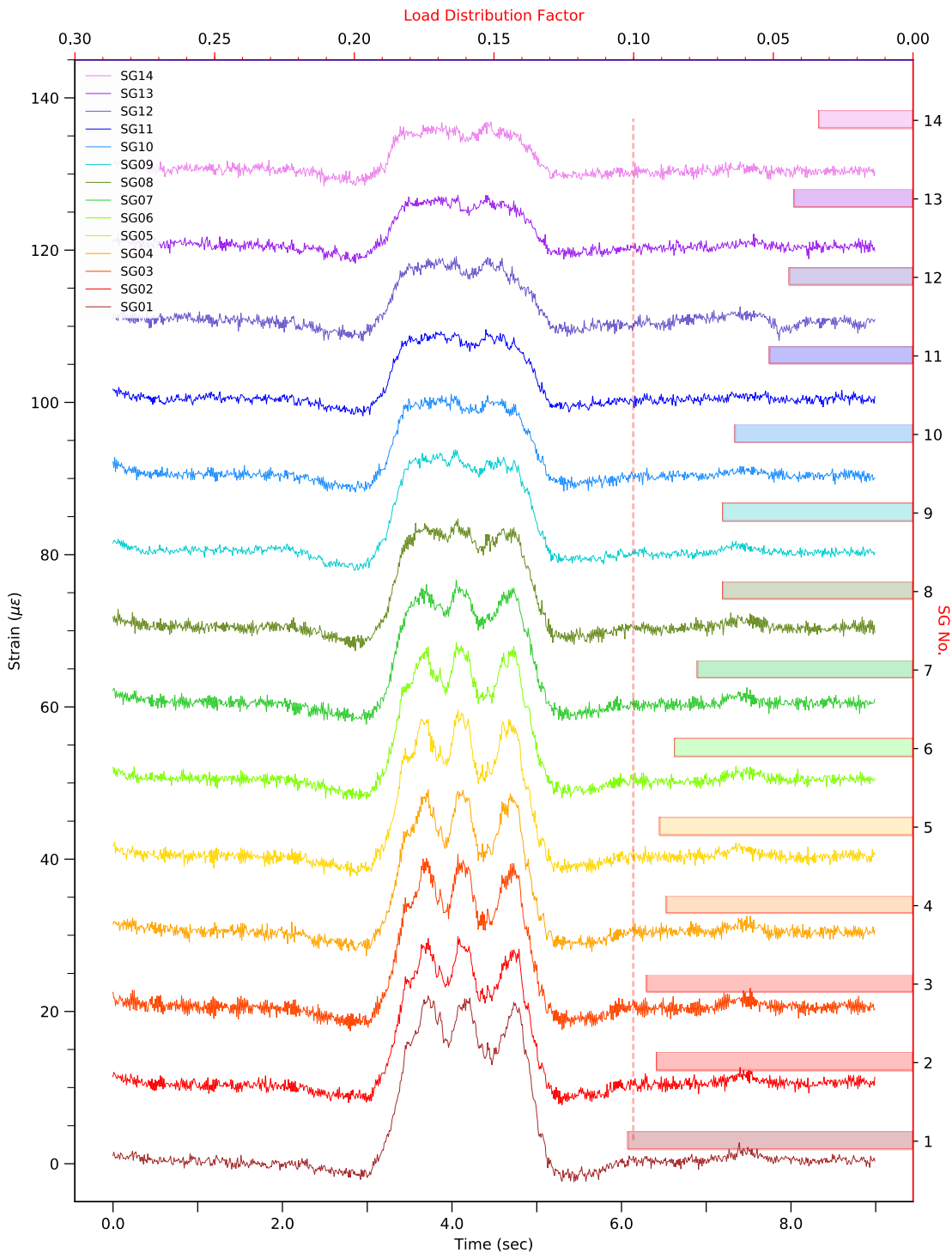
Notes: Day Thursday 2 March 2017 – Start time 20:25:49 – Max strain: 26.640 $\mu\epsilon$ – LDF: 9.64% (DU1). The strain time histories recorded by each strain gauge (SG) on the deck soffit in midspan (SG1–15) are stacked with an offset of 10 $\mu\epsilon$, with SG 1 at the bottom. Each SG number matches the deck unit (DU) N, to which it is attached to, as indicated by the labels on the right vertical axis. The related load distribution factor (LDF) is plotted on the right with values indicated by the top horizontal axis. The vertical red dashed line marks LDF = 10%. For SG layout see Figure 7.3.

Figure G 11: Strain measured for Event # 11



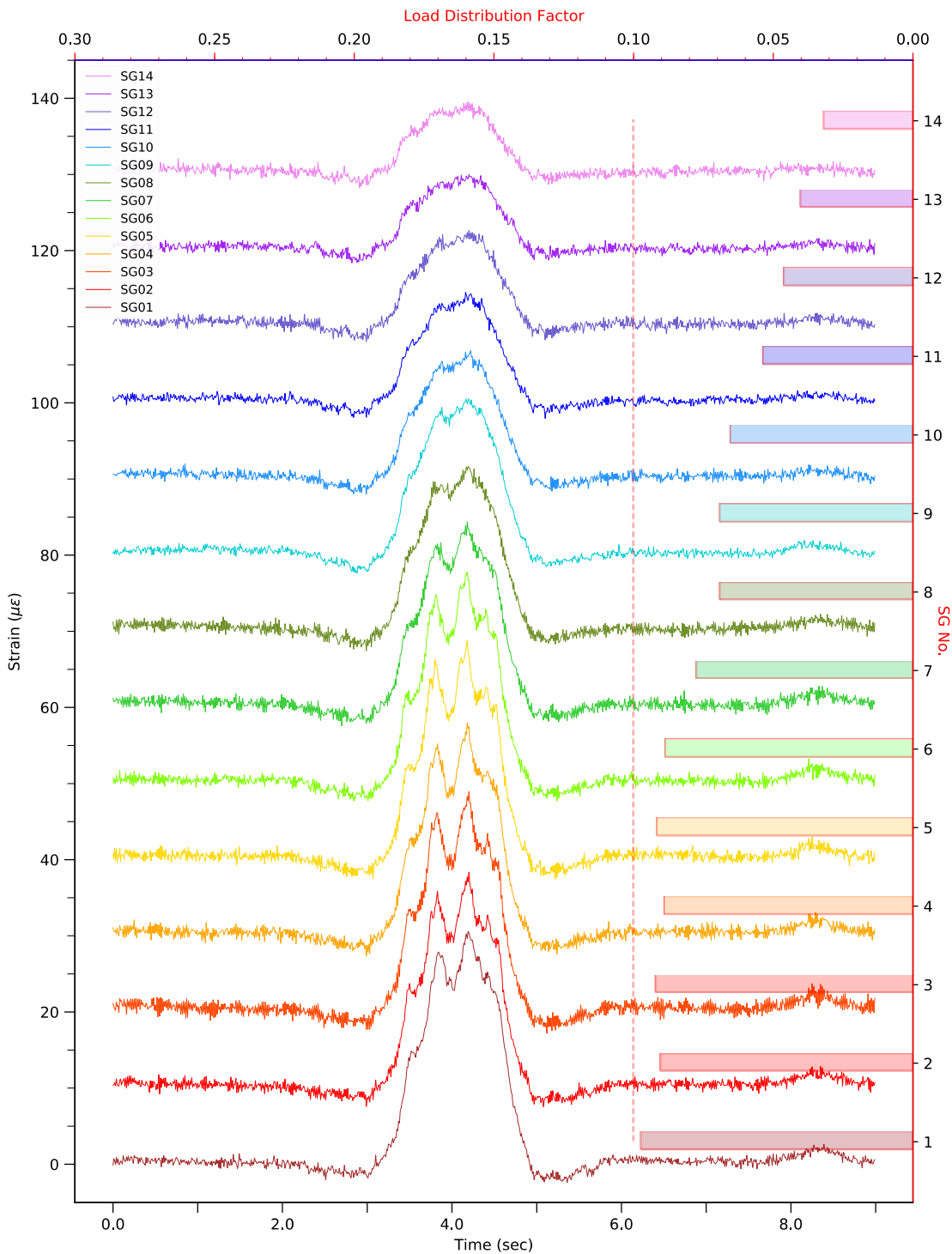
Notes: Day Thursday 2 March 2017 – Start time 20:26:56 – Max strain: 26.448 $\mu\epsilon$ – LDF: 9.79% (DU1). The strain time histories recorded by each strain gauge (SG) on the deck soffit in midspan (SG1–15) are stacked with an offset of 10 $\mu\epsilon$, with SG 1 at the bottom. Each SG number matches the deck unit (DU) N, to which it is attached to, as indicated by the labels on the right vertical axis. The related load distribution factor (LDF) is plotted on the right with values indicated by the top horizontal axis. The vertical red dashed line marks LDF = 10%. For SG layout see Figure 7.3.

Figure G 12: Strain measured for Event # 12



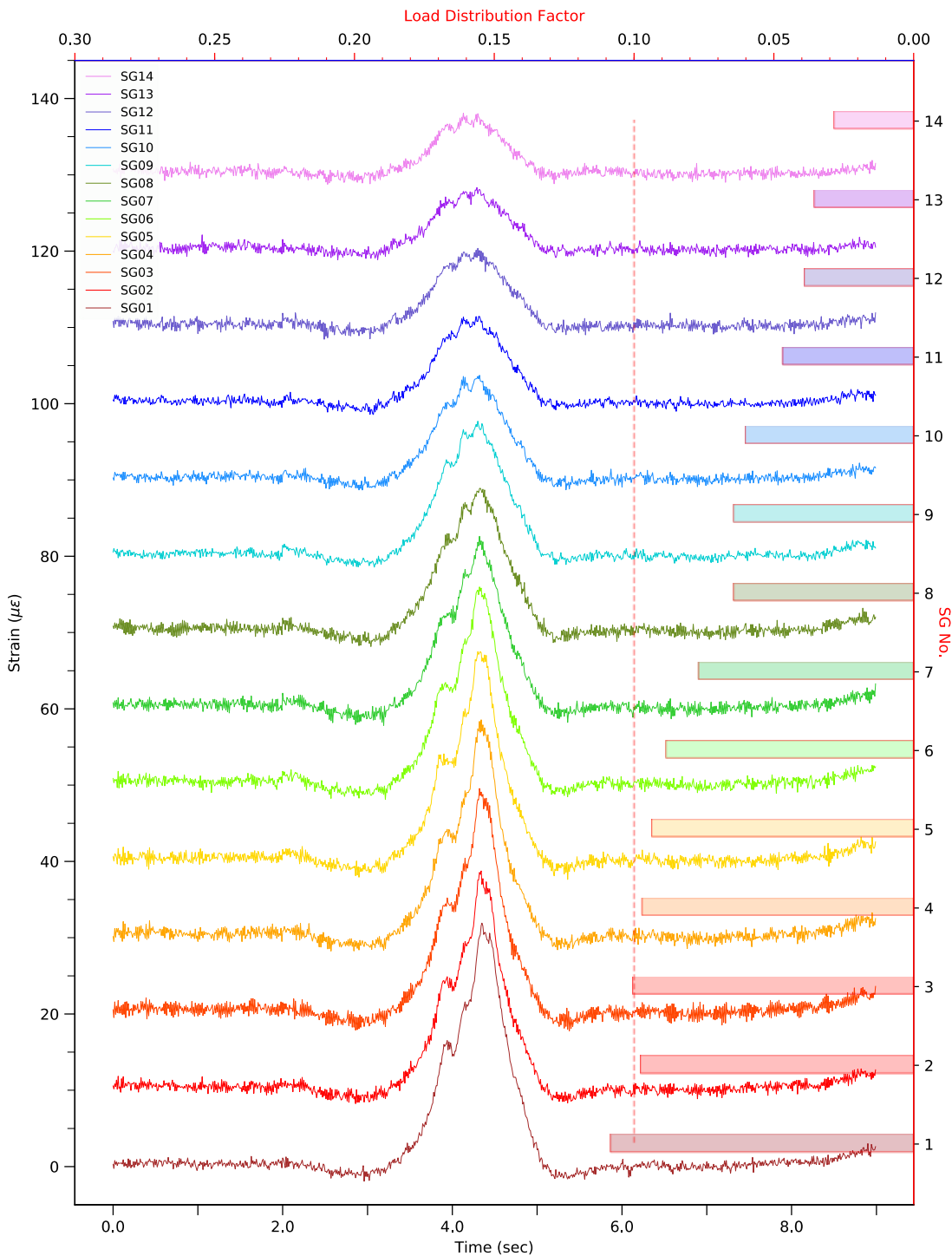
Notes: Day Thursday 2 March 2017 – Start time 20:33:34 – Max strain: 22.035 $\mu\epsilon$ – LDF: 10.17% (DU1). The strain time histories recorded by each strain gauge (SG) on the deck soffit in midspan (SG1–15) are stacked with an offset of 10 $\mu\epsilon$, with SG 1 at the bottom. Each SG number matches the deck unit (DU) N, to which it is attached to, as indicated by the labels on the right vertical axis. The related load distribution factor (LDF) is plotted on the right with values indicated by the top horizontal axis. The vertical red dashed line marks LDF = 10%. For SG layout see Figure 7.3.

Figure G 13: Strain measured for Event # 13



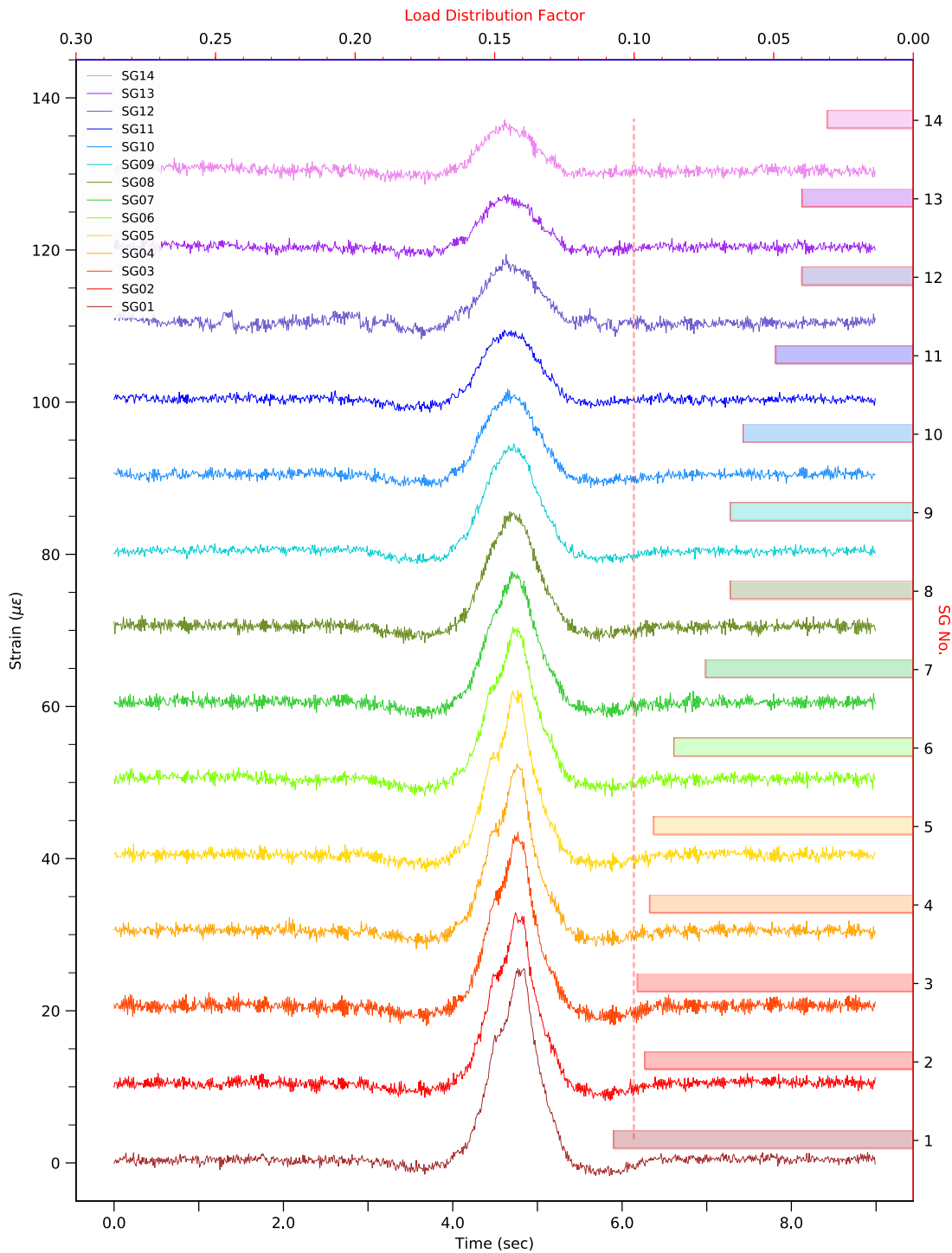
Notes: Day Thursday 2 March 2017 – Start time 21:06:23 – Max strain: 30.547 µε – LDF: 9.71% (DU1). The strain time histories recorded by each strain gauge (SG) on the deck soffit in midspan (SG1–15) are stacked with an offset of 10 µε, with SG 1 at the bottom. Each SG number matches the deck unit (DU) N, to which it is attached to, as indicated by the labels on the right vertical axis. The related load distribution factor (LDF) is plotted on the right with values indicated by the top horizontal axis. The vertical red dashed line marks LDF = 10%. For SG layout see Figure 7.3.

Figure G 14: Strain measured for Event # 14



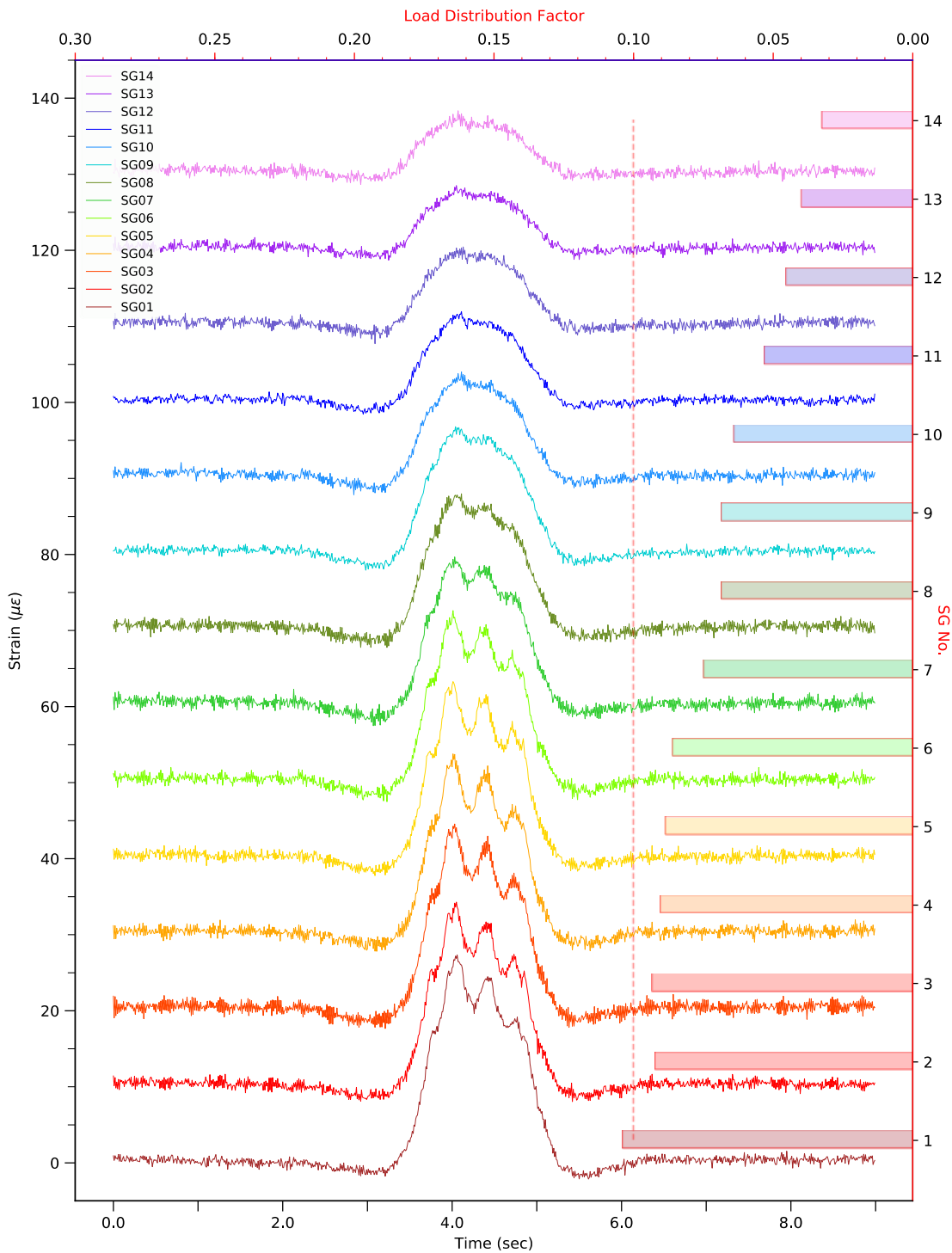
Notes: Day Thursday 2 March 2017 – Start time 21:26:33 – Max strain: 31.907 $\mu\epsilon$ – LDF: 10.84% (DU1). The strain time histories recorded by each strain gauge (SG) on the deck soffit in midspan (SG1–15) are stacked with an offset of 10 $\mu\epsilon$, with SG 1 at the bottom. Each SG number matches the deck unit (DU) N, to which it is attached to, as indicated by the labels on the right vertical axis. The related load distribution factor (LDF) is plotted on the right with values indicated by the top horizontal axis. The vertical red dashed line marks LDF = 10%. For SG layout see Figure 7.3.

Figure G 15: Strain measured for Event # 15



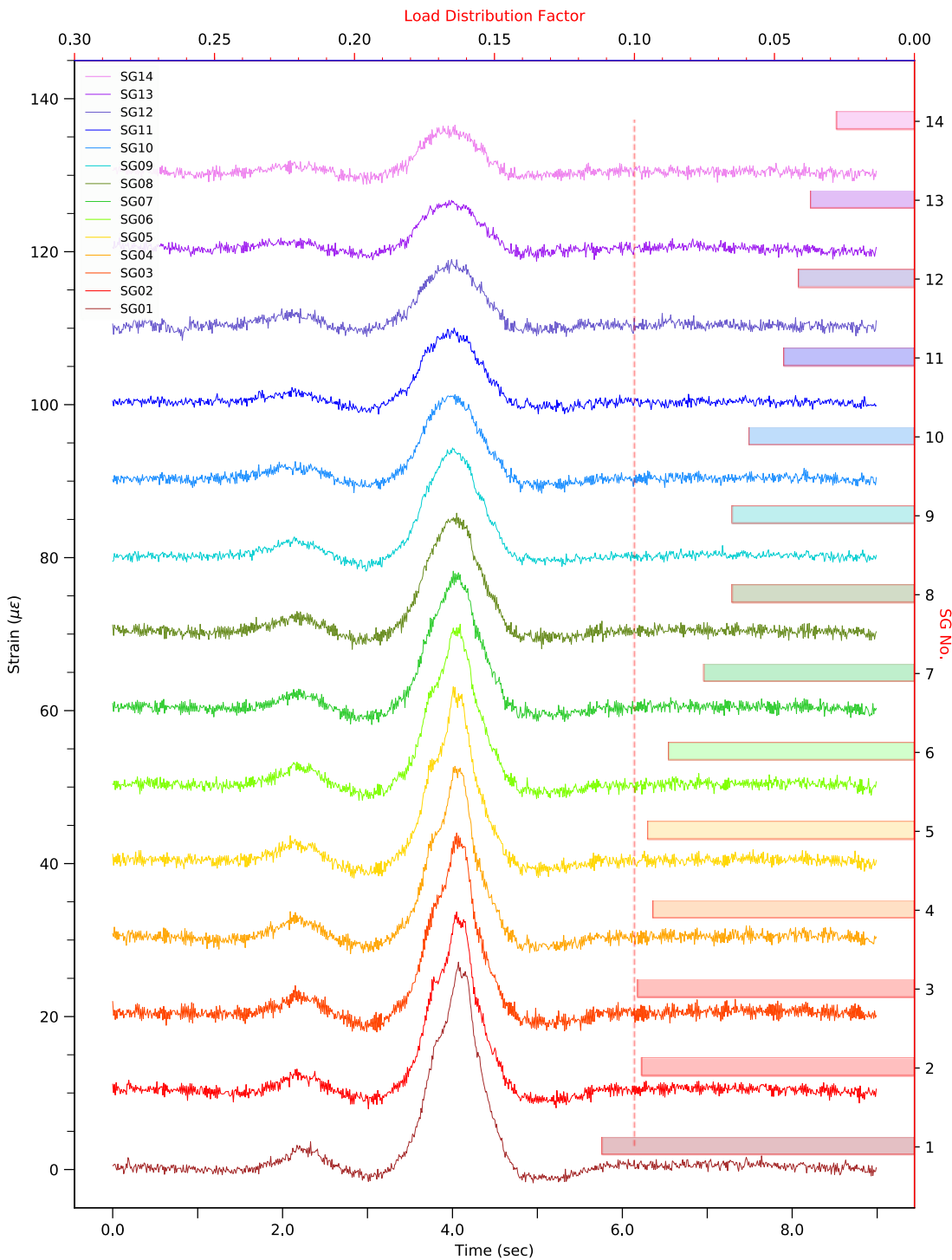
Notes: Day Thursday 2 March 2017 – Start time 21:39:10 – Max strain: 25.571 $\mu\epsilon$ – LDF: 10.73% (DU1). The strain time histories recorded by each strain gauge (SG) on the deck soffit in midspan (SG1–15) are stacked with an offset of 10 $\mu\epsilon$, with SG 1 at the bottom. Each SG number matches the deck unit (DU) N, to which it is attached to, as indicated by the labels on the right vertical axis. The related load distribution factor (LDF) is plotted on the right with values indicated by the top horizontal axis. The vertical red dashed line marks LDF = 10%. For SG layout see Figure 7.3.

Figure G 16: Strain measured for Event # 16



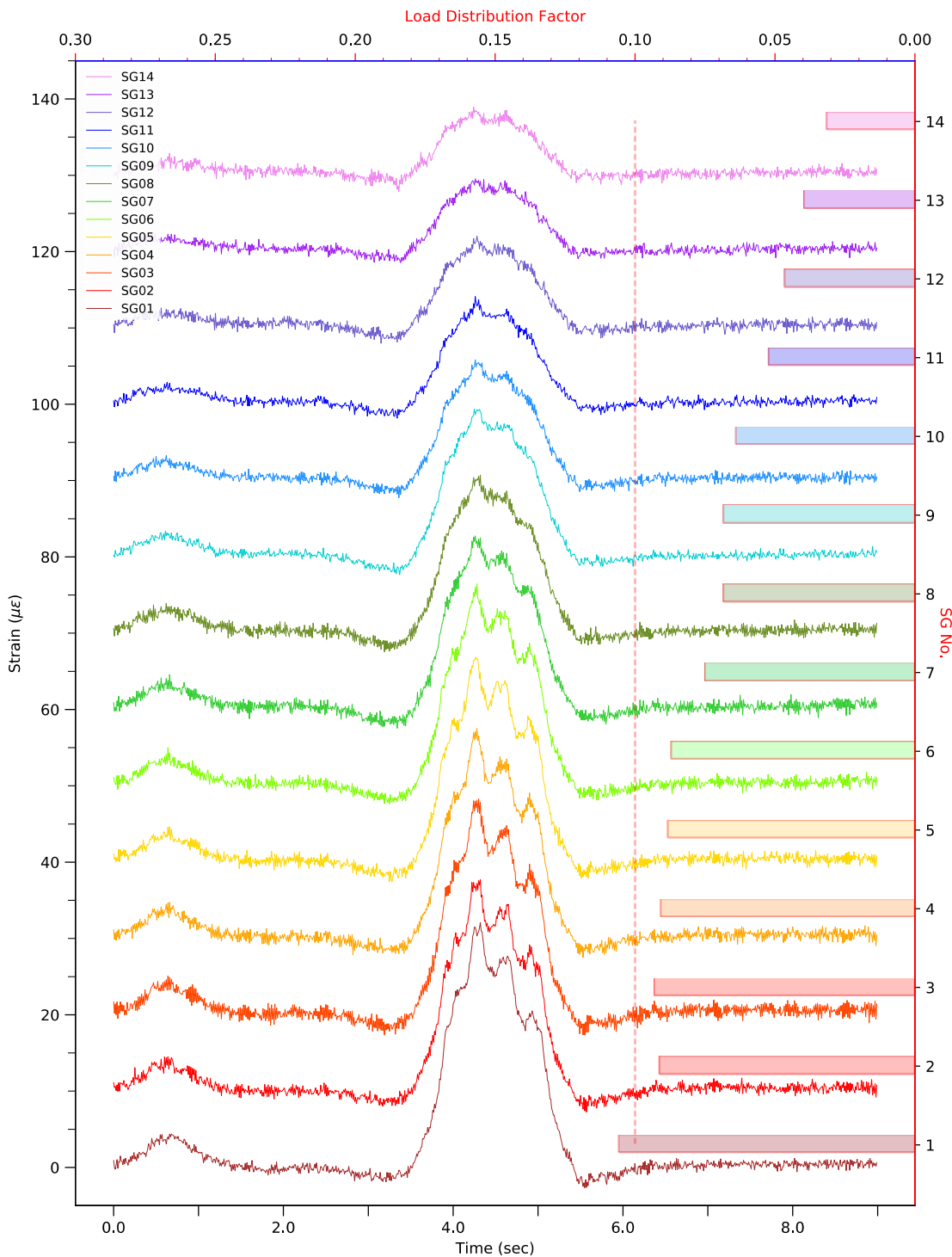
Notes: Day Thursday 2 March 2017 – Start time 22:44:16 – Max strain: 27.329 µε – LDF: 10.38% (DU1). The strain time histories recorded by each strain gauge (SG) on the deck soffit in midspan (SG1–15) are stacked with an offset of 10 µε, with SG 1 at the bottom. Each SG number matches the deck unit (DU) N, to which it is attached to, as indicated by the labels on the right vertical axis. The related load distribution factor (LDF) is plotted on the right with values indicated by the top horizontal axis. The vertical red dashed line marks LDF = 10%. For SG layout see Figure 7.3.

Figure G 17: Strain measured for Event # 17



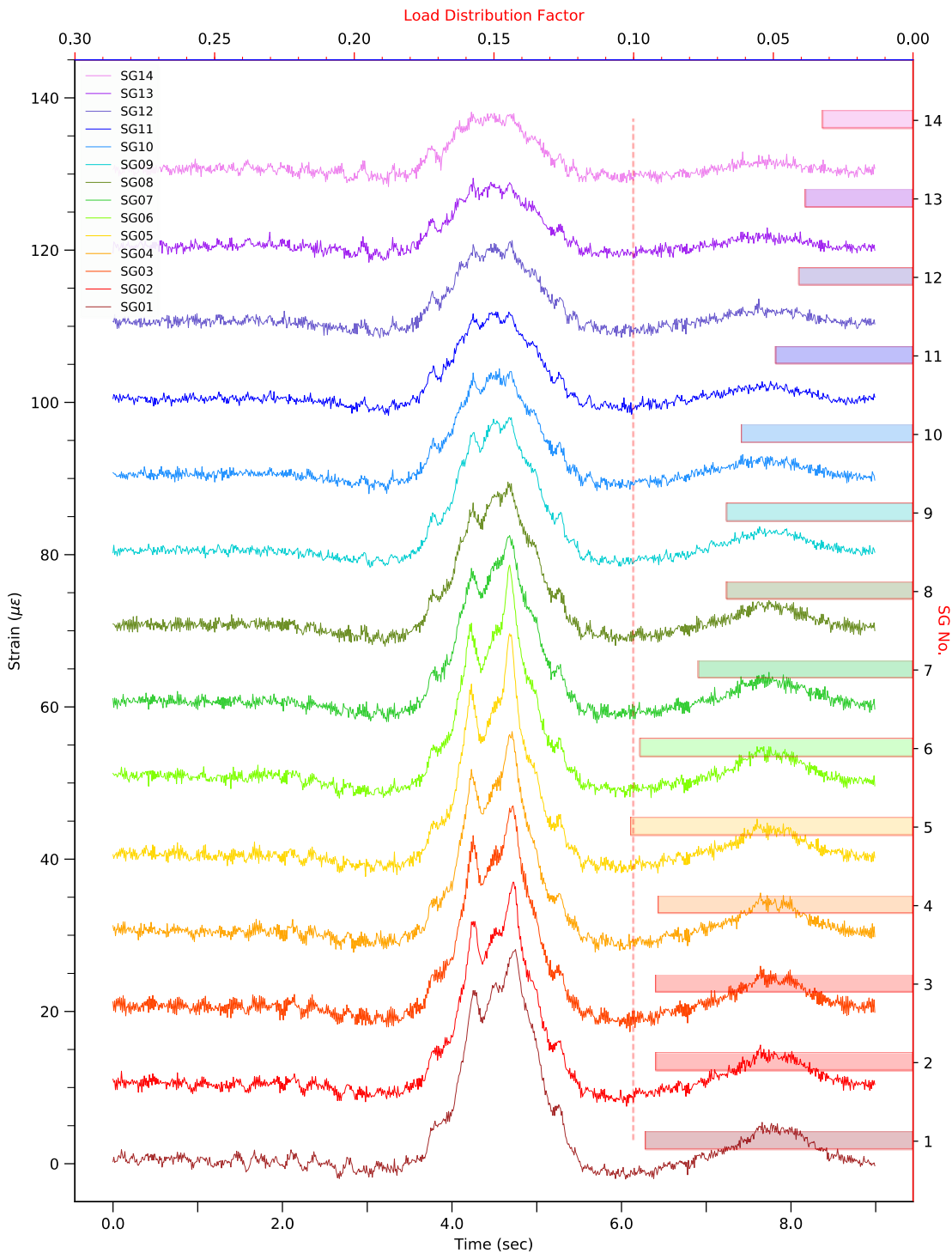
Notes: Day Thursday 2 March 2017 – Start time 22:41:18 – Max strain: 27.130 µε – LDF: 11.15% (DU1). The strain time histories recorded by each strain gauge (SG) on the deck soffit in midspan (SG1–15) are stacked with an offset of 10 µε, with SG 1 at the bottom. Each SG number matches the deck unit (DU) N, to which it is attached to, as indicated by the labels on the right vertical axis. The related load distribution factor (LDF) is plotted on the right with values indicated by the top horizontal axis. The vertical red dashed line marks LDF = 10%. For SG layout see Figure 7.3.

Figure G 18: Strain measured for Event # 18



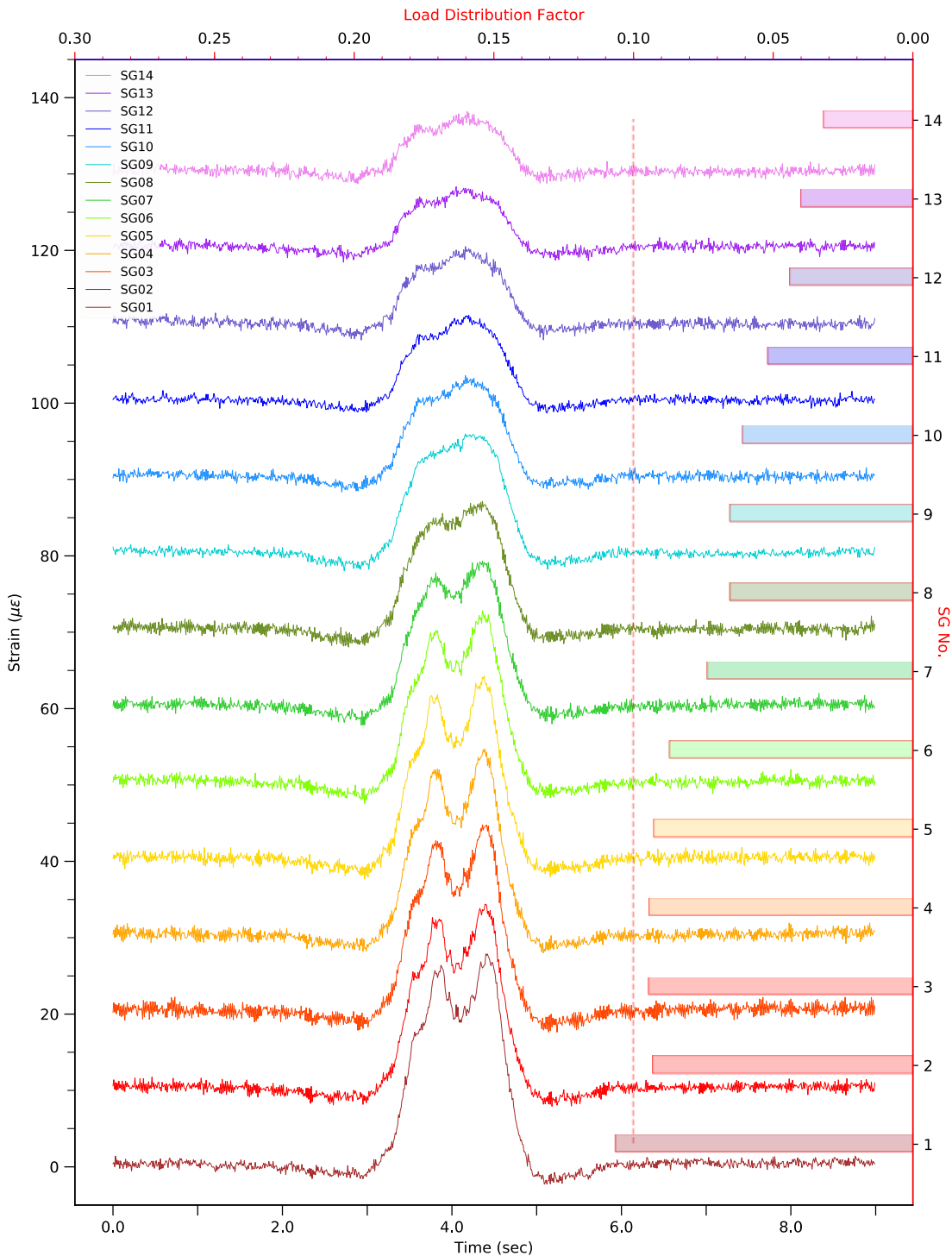
Notes: Day Thursday 2 March 2017 – Start time 23:50:42 – Max strain: 32.074 $\mu\epsilon$ – LDF: 10.56% (DU1). The strain time histories recorded by each strain gauge (SG) on the deck soffit in midspan (SG1–15) are stacked with an offset of 10 $\mu\epsilon$, with SG 1 at the bottom. Each SG number matches the deck unit (DU) N, to which it is attached to, as indicated by the labels on the right vertical axis. The related load distribution factor (LDF) is plotted on the right with values indicated by the top horizontal axis. The vertical red dashed line marks LDF = 10%. For SG layout see Figure 7.3.

Figure G 19: Strain measured for Event # 19



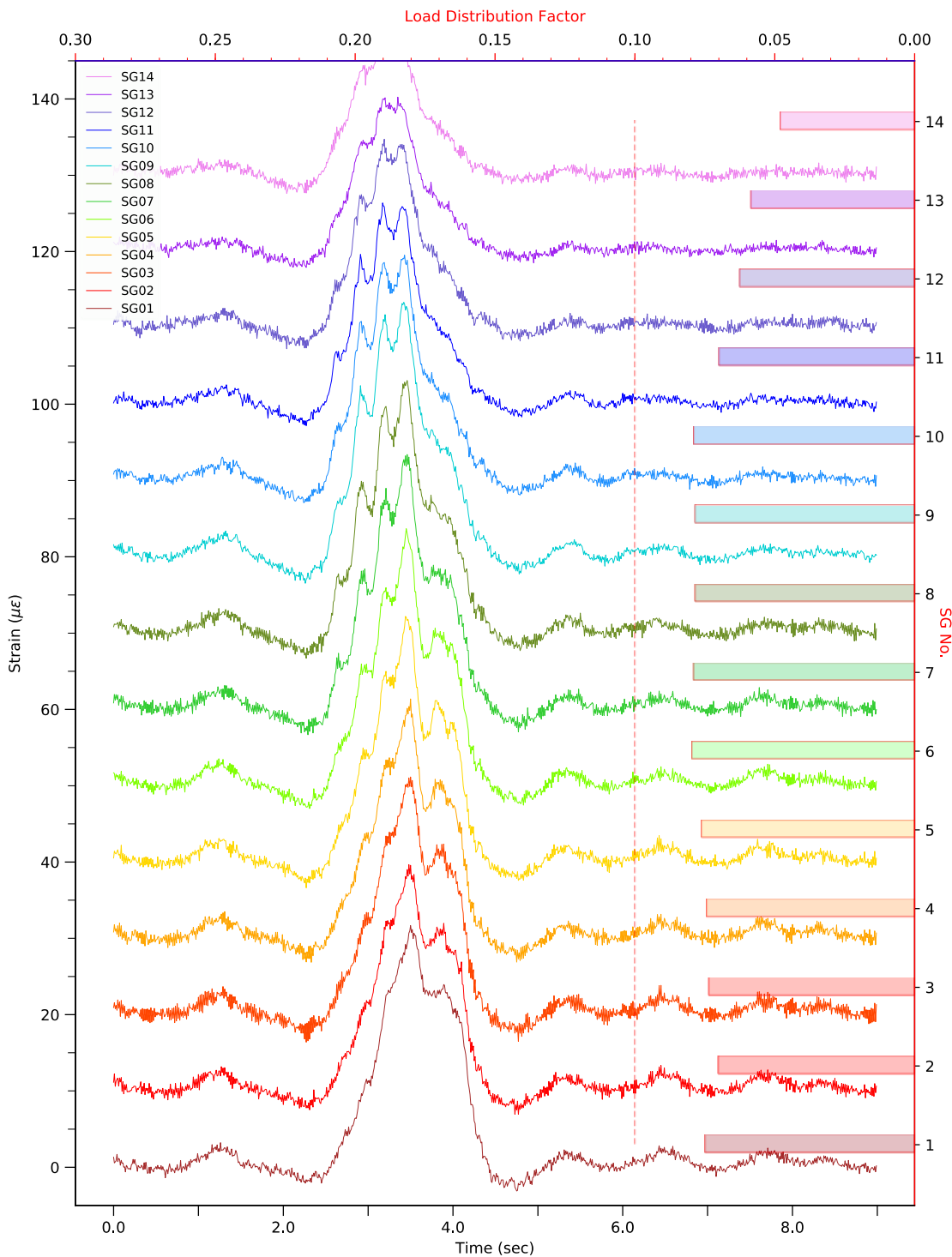
Notes: Day Friday 2 March 2017 – Start time 00:45:07– Max strain: 29.616 $\mu\epsilon$ – LDF: 10.08% (DU5). The strain time histories recorded by each strain gauge (SG) on the deck soffit in midspan (SG1–15) are stacked with an offset of 10 $\mu\epsilon$, with SG 1 at the bottom. Each SG number matches the deck unit (DU) N, to which it is attached to, as indicated by the labels on the right vertical axis. The related load distribution factor (LDF) is plotted on the right with values indicated by the top horizontal axis. The vertical red dashed line marks LDF = 10%. For SG layout see Figure 7.3.

Figure G 20: Strain measured for Event # 20



Notes: Day Friday 2 March 2017 – Start time 02:14:51– Max strain: 27.880 $\mu\epsilon$ – LDF: 10.62% (DU1). The strain time histories recorded by each strain gauge (SG) on the deck soffit in midspan (SG1–15) are stacked with an offset of 10 $\mu\epsilon$, with SG 1 at the bottom. Each SG number matches the deck unit (DU) N, to which it is attached to, as indicated by the labels on the right vertical axis. The related load distribution factor (LDF) is plotted on the right with values indicated by the top horizontal axis. The vertical red dashed line marks LDF = 10%. For SG layout see Figure 7.3.

Figure G 21: Strain measured for Event # 27



Notes: Day Friday 2 March 2017 – Start time 12:22:43 – Max strain: 33.685 µε – LDF: 7.95% (DU6). The strain time histories recorded by each strain gauge (SG) on the deck soffit in midspan (SG1–15) are stacked with an offset of 10 µε, with SG 1 at the bottom. Each SG number matches the deck unit (DU) N, to which it is attached to, as indicated by the labels on the right vertical axis. The related load distribution factor (LDF) is plotted on the right with values indicated by the top horizontal axis. The vertical red dashed line marks LDF = 10%. For SG layout see Figure 7.3.

APPENDIX H LOAD TESTING – SUPPLEMENTARY INFORMATION

The following general observations were made during the performance load tests:

- The wind was slight during the load tests.
- Temperature effects were minimal, while all sensors were reset to zero after each run. Each set of runs (3 repeats) lasted up to 6 minutes. The temperature variation of a concrete structure within such timeframes is negligible.
- The test vehicle moved across the bridge in nearly-static mode, i.e. with travelling speed of 2.5–5 km/h.

Representative time histories of strains, deflections and joint relative movements are reported in the next sections. It is noted that these measurements are presented prior to baseline correction.

H.1 Strain Gauges

Figure H 1 and Figure H 2 present representative waveforms of strains measured at top and bottom of DU9 in the undamaged stage and damaged stage D4A, respectively, due to the same test vehicle (62.5 t). The following comments can be made:

- Consistent measurements were obtained between the three repeats (forward and backward) within each run.
- There were small discrepancies in the maximum readings between the repeats, indicating possible slight variations in the lateral locations of the test vehicle.
- All readings returned to zero when the test vehicle was out of the bridge, indicating that the bridge behaved elastically.

H.2 Deflections

Similar to Appendix H.1, representative waveforms of deflections measured at the bottom of DU7 and DU12 in the undamaged stage and damaged stage D4A, respectively, due to the same test vehicle (62.5 t) are presented in Figure H 3 and Figure H 4.

H.3 Joint Movements

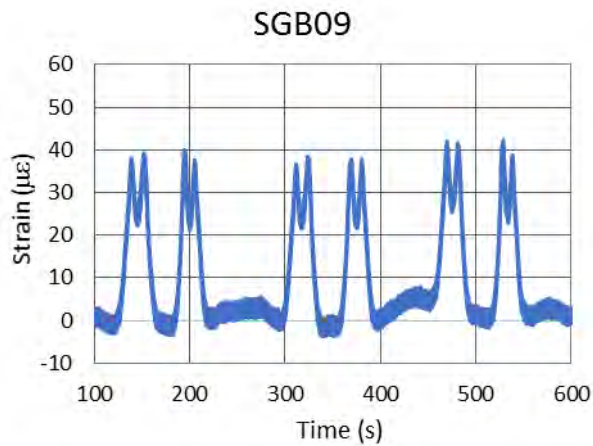
Figure H 5 and Figure H 6 present representative waveforms of the movement of the joints measured between DU11 and DU12, and between DU14 and DU15 in the undamaged stage and damaged stage D4A, respectively, due to the same test vehicle (62.5 t).

H.4 Peak Actions in Different Testing Scenarios

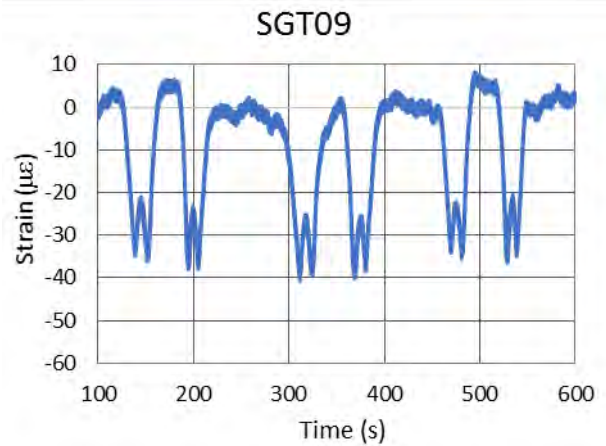
The following peak actions are presented in this Appendix:

- Summary of peak results for all test runs (Table H 1 and Table H 2)
- Peak strains in the midspan and quarterspan sections of all DUs (Figure H 7–Figure H 14).
- Peak deflections in the midspan and quarterspan sections of all DUs (Figure H 15–Figure H 18).
- Peak joint movements in the midspan and quarterspan sections of all DUs (Figure H 19–Figure H 20).

Figure H 1: Strain time histories, Run 2.1-2.3 (62.5 t) in midspan

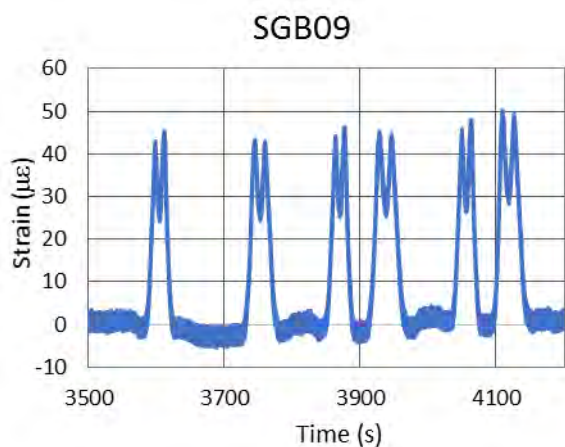


(a) Strains at soffit of DU9

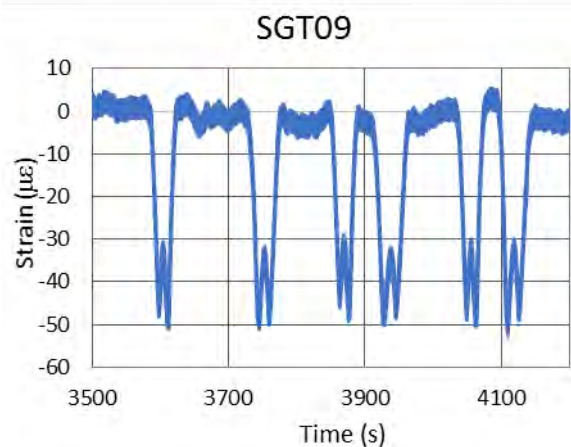


(b) Strains on top fibre of DU9

Figure H 2: Strain time histories, Run 8.1-8.3 (62.5 t) in midspan

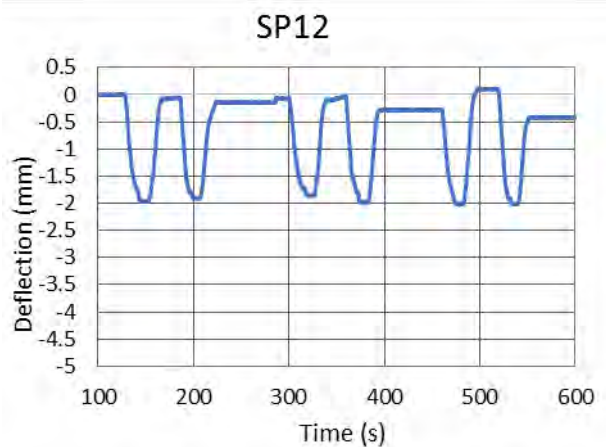
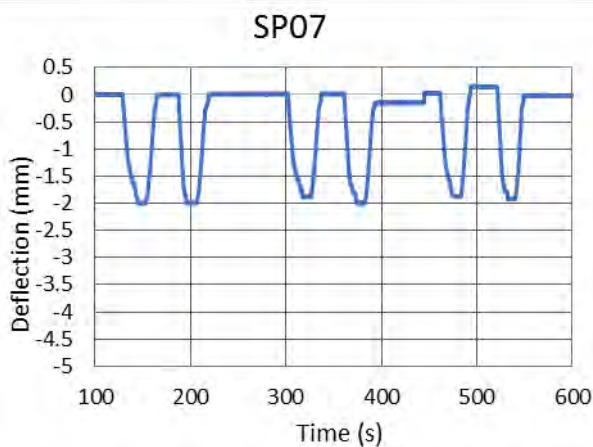


(a) Strains at soffit of DU9



(b) Strains on top fibre of DU9

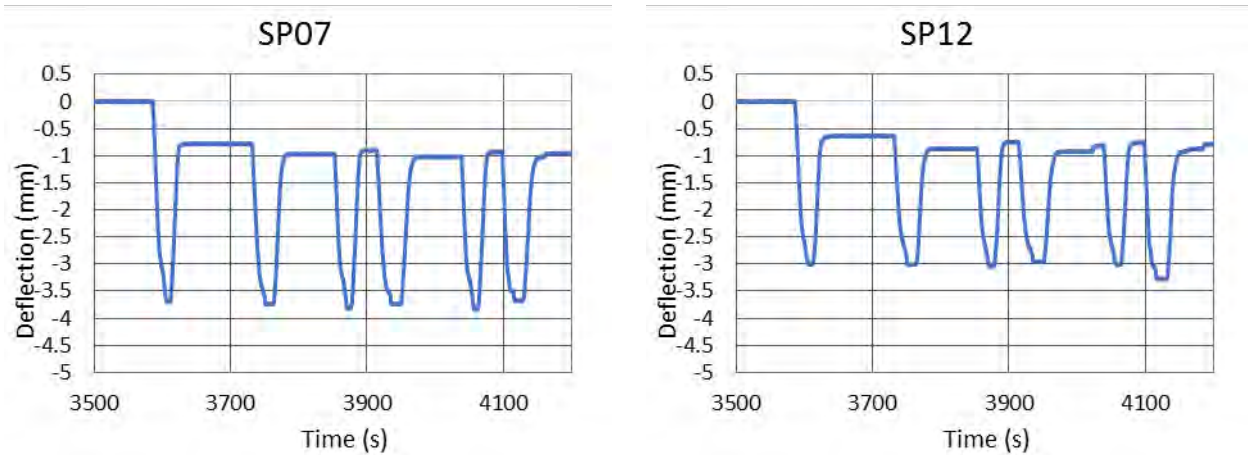
Figure H 3: Deflection time histories, Run 2.1-2.3 (62.5 t) in midspan



(a) Deflection at soffit of DU7

(b) Deflection at soffit of DU12

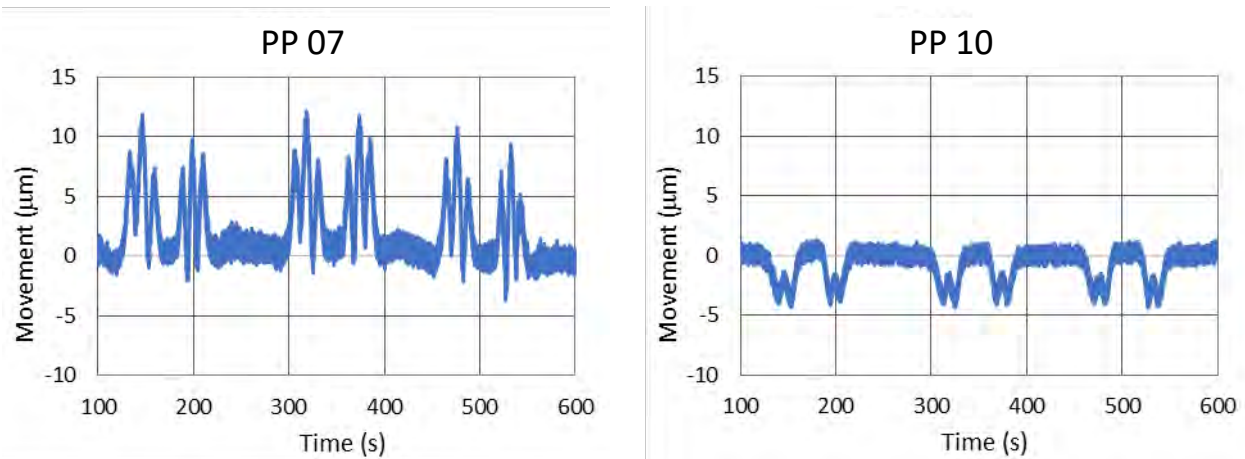
Figure H 4: Deflection time histories Run 8.1-8.3 (62.5 t) in midspan



(a) Deflection at soffit of DU7

(b) Deflection at soffit of DU12

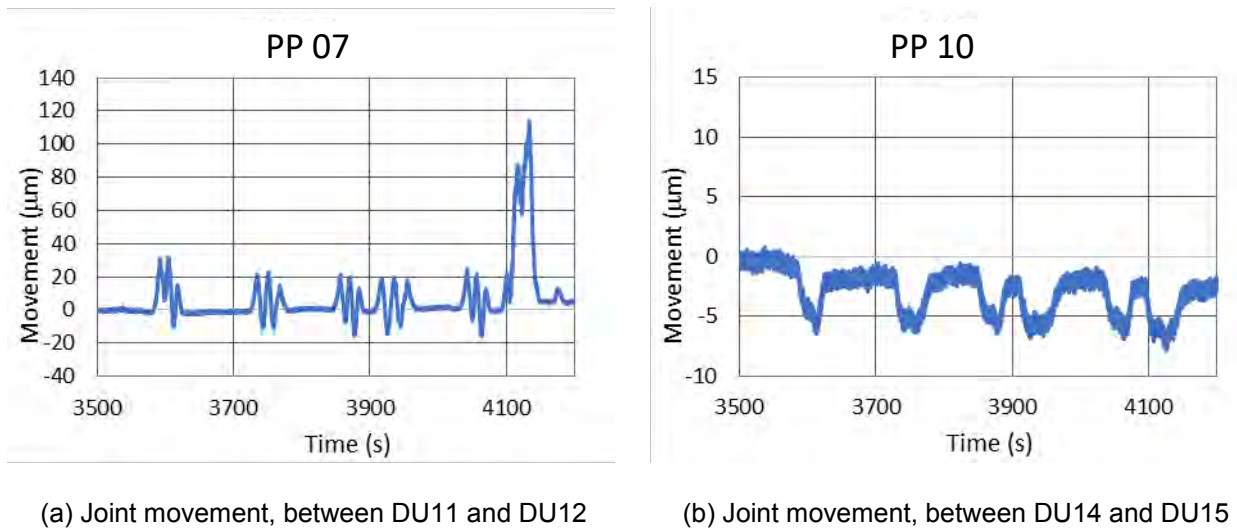
Figure H 5: Joint movement time histories, Run 2.1-2.3 (62.5 t) in midspan



(a) Joint movement, between DU11 and DU12

(b) Joint movement, between DU14 and DU15

Figure H 6: Joint movement time histories, Run 8.1-8.3 (62.5 t) in midspan



(a) Joint movement, between DU11 and DU12

(b) Joint movement, between DU14 and DU15

Table H 1: Peak measurements, runs along the central path

Measurement\ Runs	Unit	Run 1	Run 2	Run 3	Run 4	Run 5	Run 6	Run 7	Run 8	Run 9	Run 10
Strain at soffit, quarterspan 1	$\mu\epsilon$	34	41	51	40	44	47	42	46	39	42
Strain at soffit, midspan	$\mu\epsilon$	31	43	61	46	53	47	48	53	52	56
Strain at top fibre,	$\mu\epsilon$	-27	-36	-60	-43	-41	-52	-54	-45	-44	-73
Strain at top fibre, midspan	$\mu\epsilon$	-32	-48	-68	-51	-56	-60	-59	-63	-63	-67
Maximum gap opening	μm	120	157	204	134	276	454	418	390	451	430
Maximum gap closing	μm	-4	-5	-8	-20	-19	-30	-205	-218	-203	-209
Deflection, quarterspan 1	Mm	-0.9	-1.4	-2.6	-1.6	-1.8	-1.7	-1.7	-2.0	-2.0	-2.2
Deflection, midspan	mm	-1.7	-2.3	-3.6	-2.5	-2.7	-2.9	-2.6	-2.9	-3.4	-3.5

Table H 2: Peak measurements, runs along the northern path

Measurement\ Runs	Unit	Run 1	Run 2	Run 3	Run 4	Run 5	Run 6	Run 7	Run 8	Run 9	Run 10
Strain at soffit, quarterspan 1	$\mu\epsilon$	27	39	50	38	40	38	39	43	40	44
Strain at soffit, midspan	$\mu\epsilon$	31	49	66	47	51	50	54	59	58	58
Strain at top fibre,	$\mu\epsilon$	-29	-45	-64	-44	-41	-45	-50	-49	-44	-62
Strain at top fibre, midspan	$\mu\epsilon$	-32	-57	-64	-47	-51	-50	-59	-60	-62	-61
Maximum gap opening	μm	122	174	241	152	153	172	236	188	217	229
Maximum gap closing	μm	-6	-6	-9	-15	-20	-139	-23	-169	-140	-161
Deflection, quarterspan 1	Mm	-0.8	-1.6	-2.4	-1.6	-1.8	-1.7	-1.7	-2.1	-2.4	-2.4
Deflection, midspan	mm	-1.6	-2.5	-3.6	-2.4	-2.8	-2.8	-2.8	-3.4	-3.6	-3.4

Figure H 7: Maximum tensile strains measured in midspan, runs along the central path

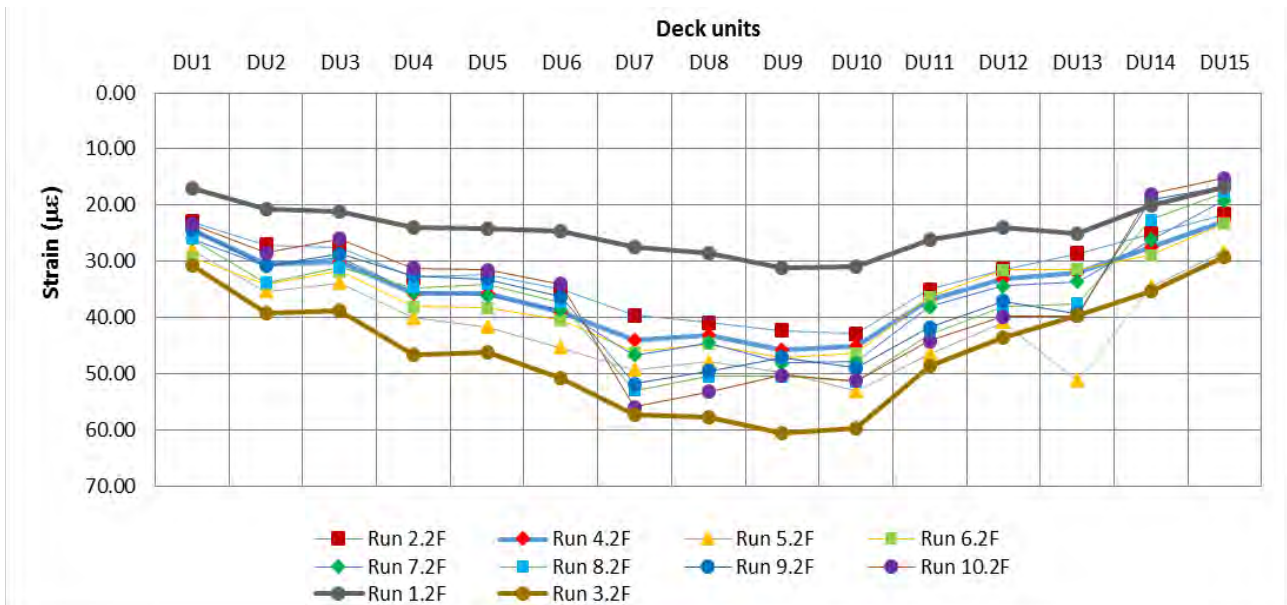


Figure H 8: Maximum tensile strains measured in midspan, runs along the northern path

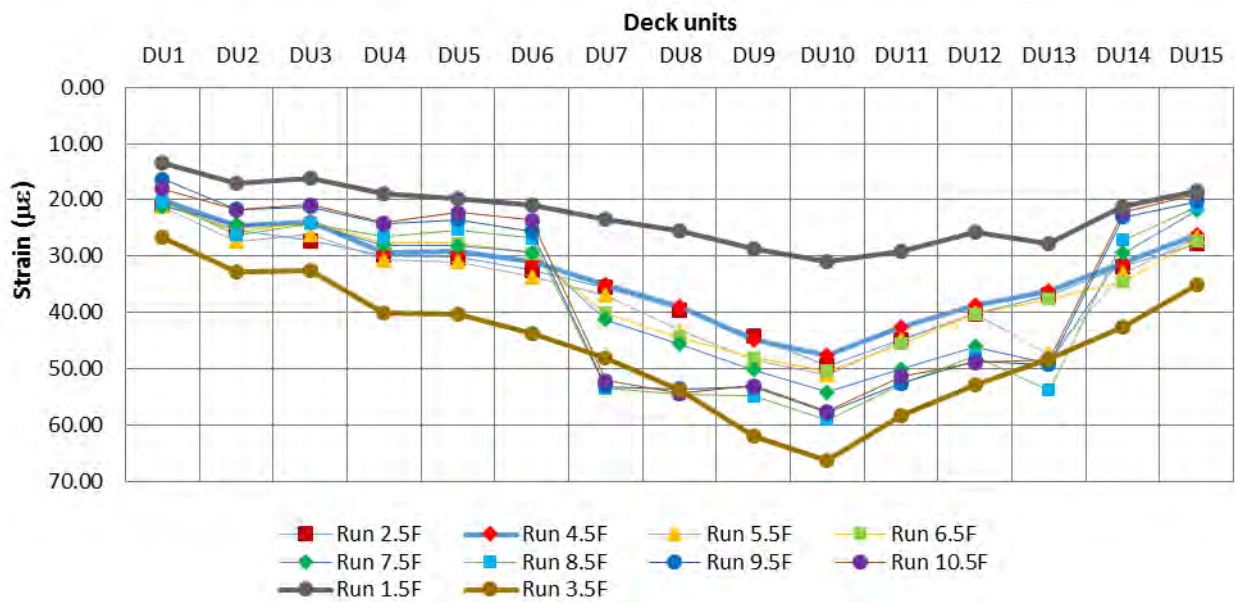


Figure H 9: Maximum tensile strains measured at the quarterpan section, runs along the central path

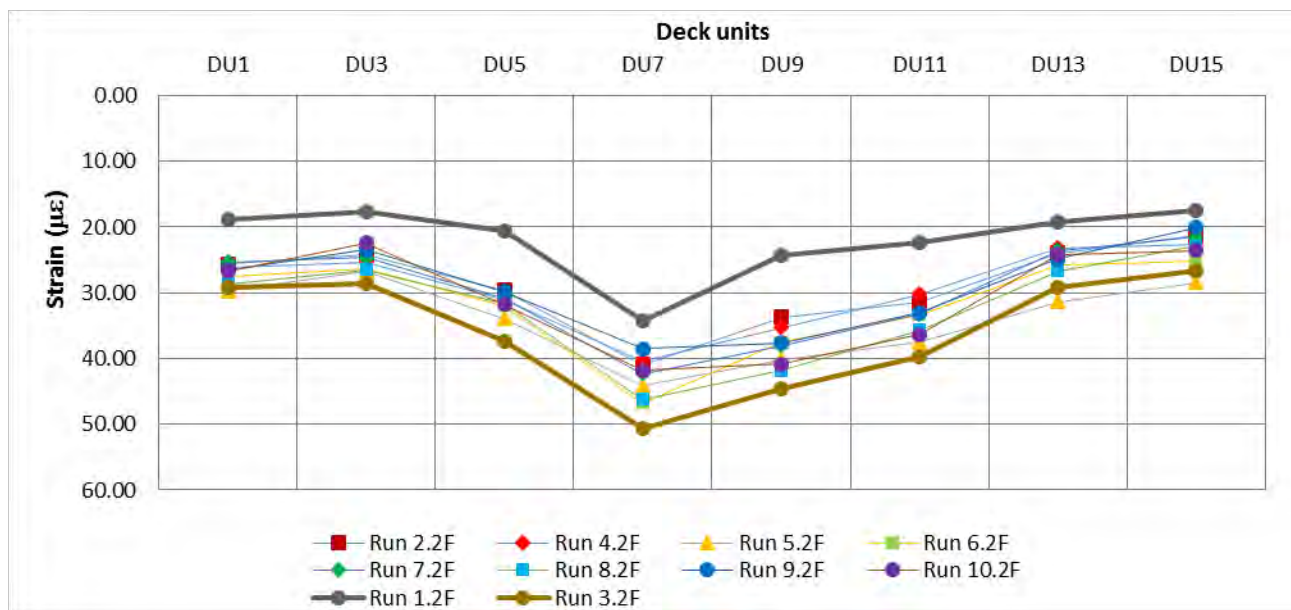


Figure H 10: Maximum tensile strains measured in quarter span, runs along the northern path

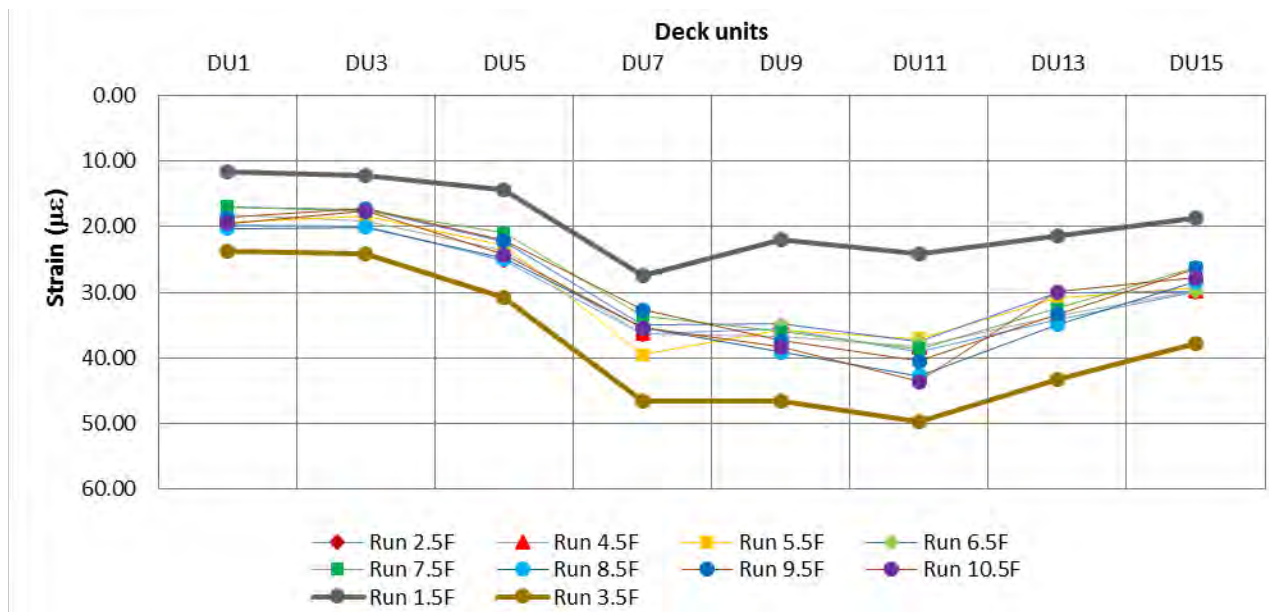


Figure H 11: Maximum compressive strains measured in midspan, runs along the central path

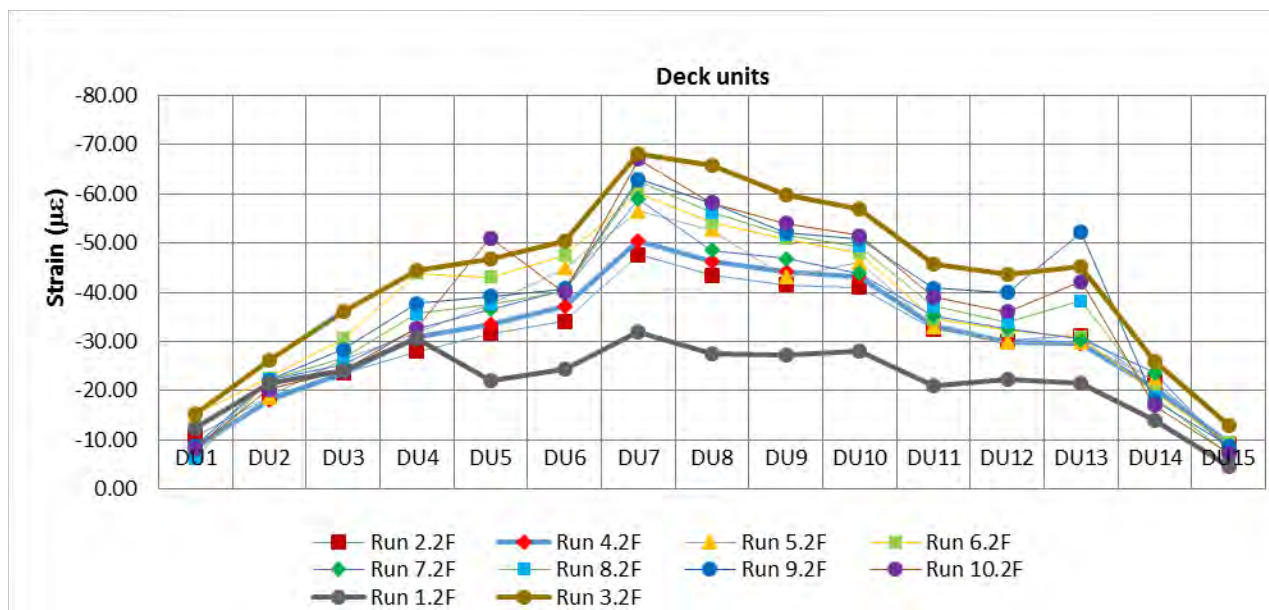


Figure H 12: Maximum compressive strains measured in midspan, runs along the northern path

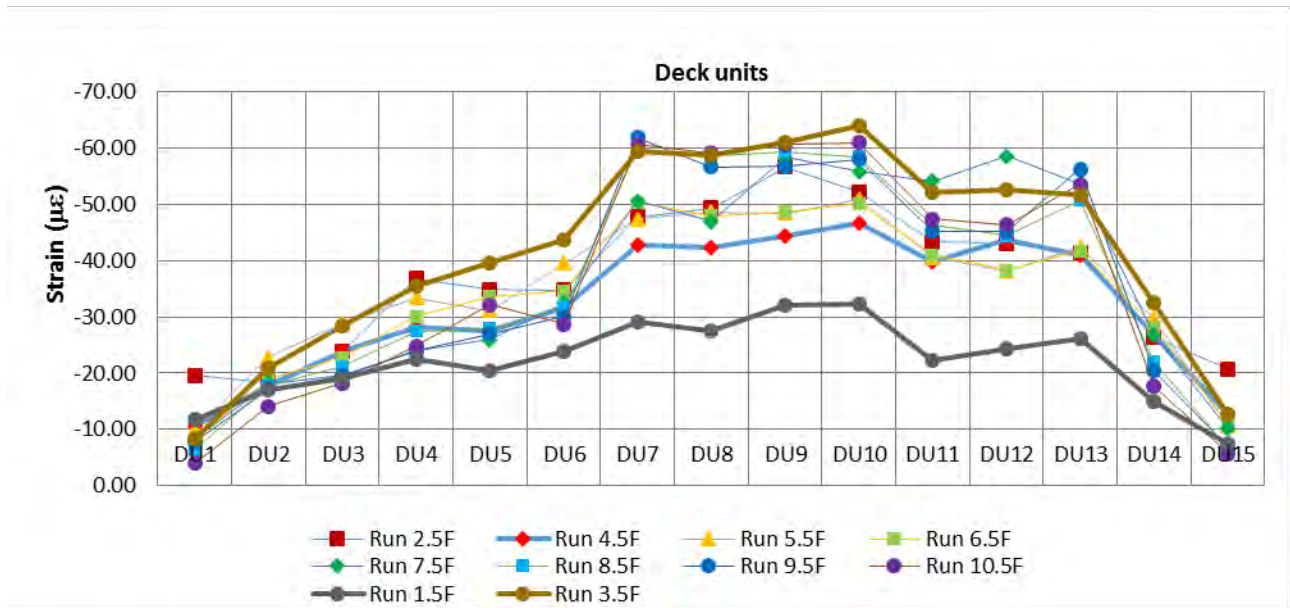


Figure H 13: Maximum compressive strains measured in quarter span, runs along the central path

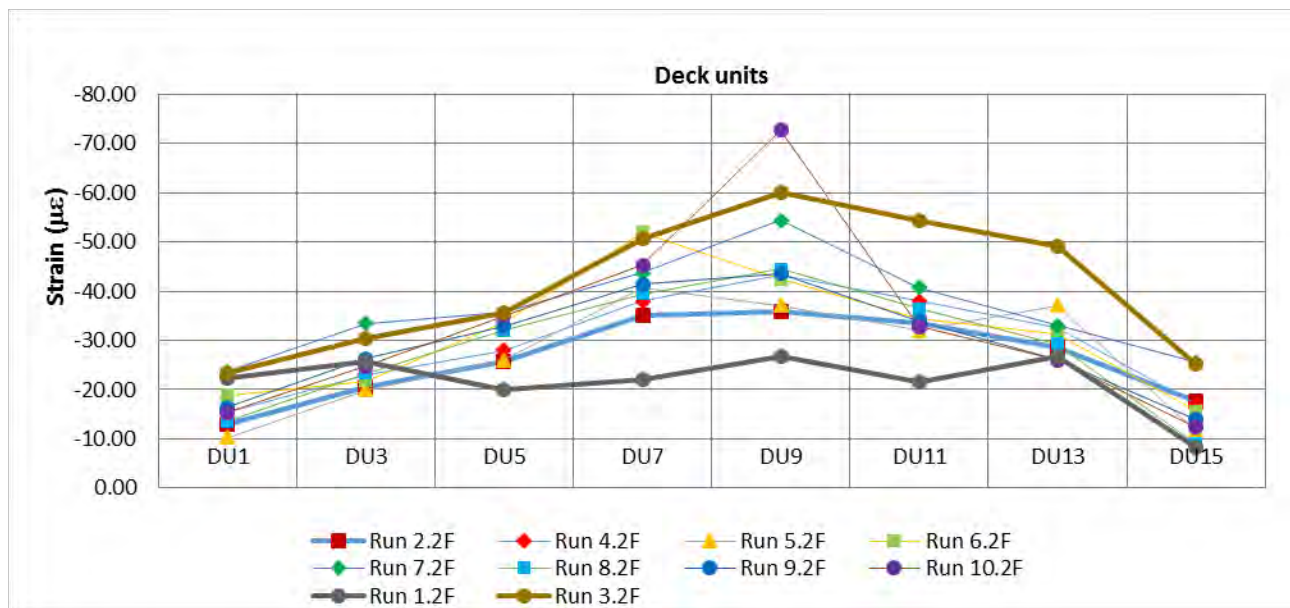


Figure H 14: Maximum compressive strains measured in quarter span, runs along the northern path

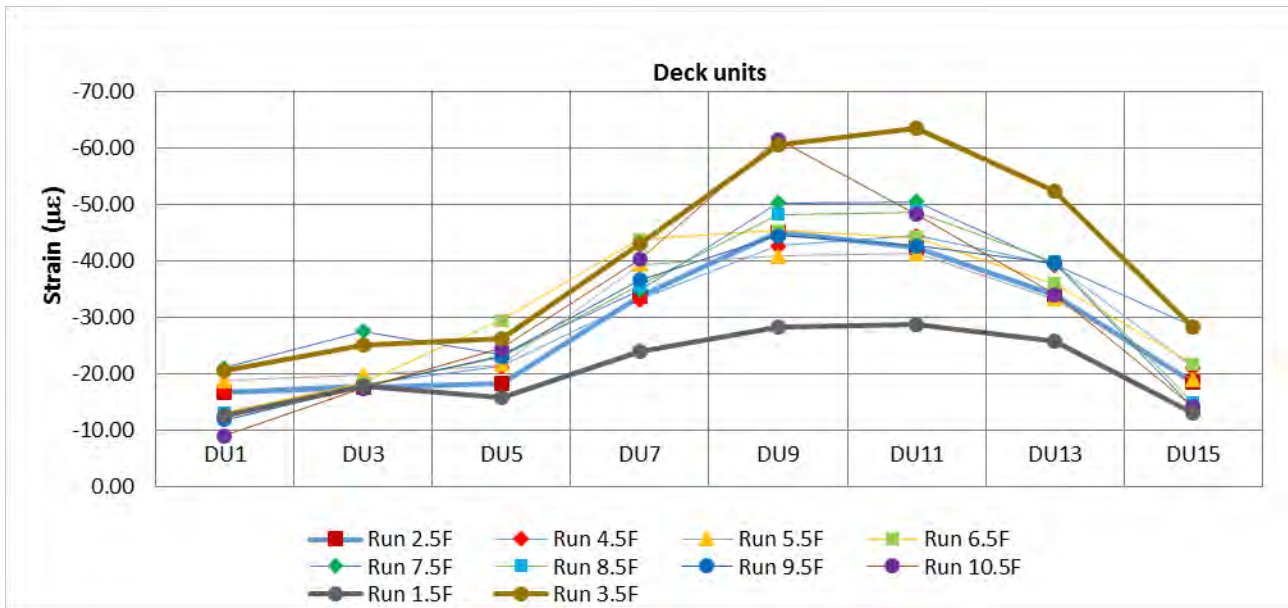


Figure H 15: Maximum deflections measured in midspan, runs along the central path

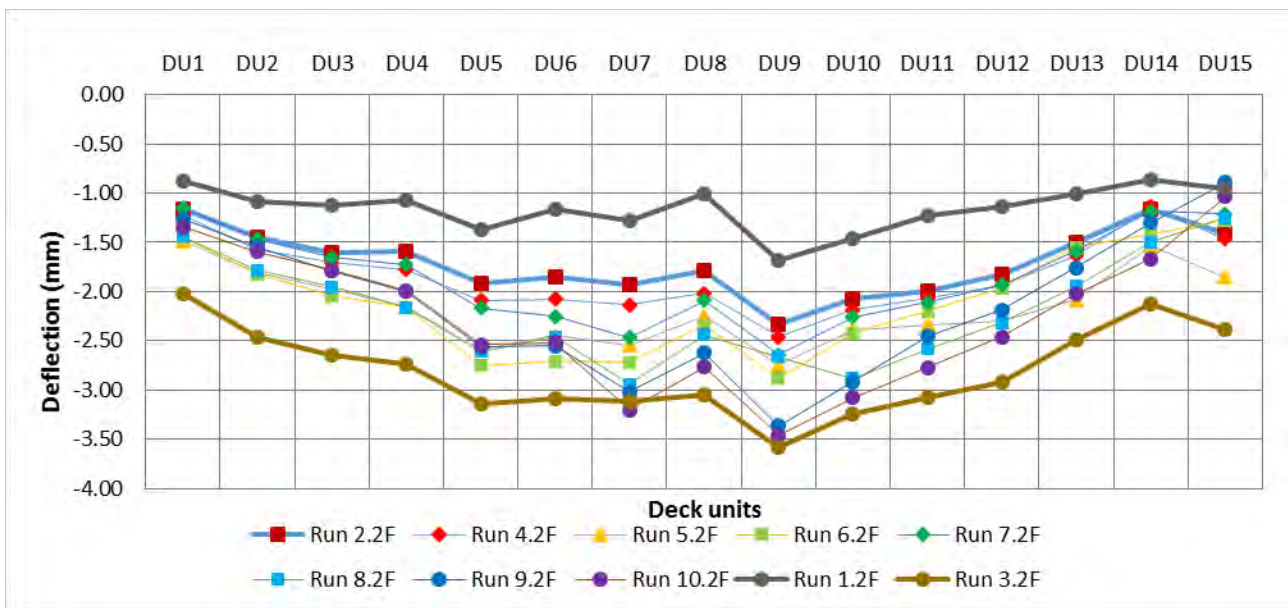


Figure H 16: Maximum deflections measured in midspan, runs along the northern path

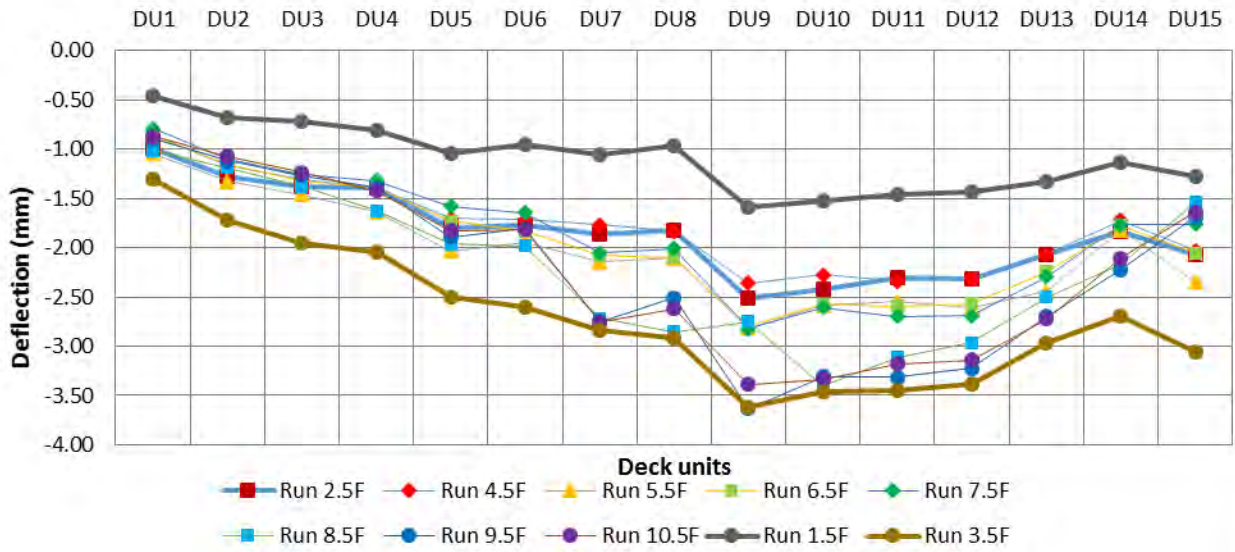


Figure H 17: Maximum deflections measured in quarter span, runs along the central path

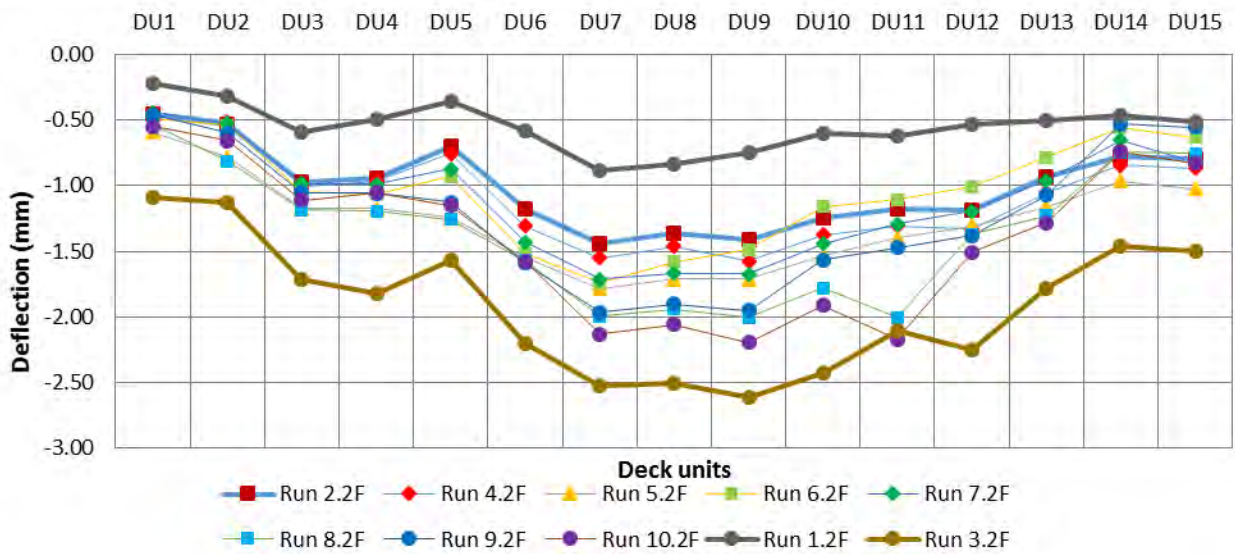


Figure H 18: Maximum deflections measured in quarter span, runs along the northern path

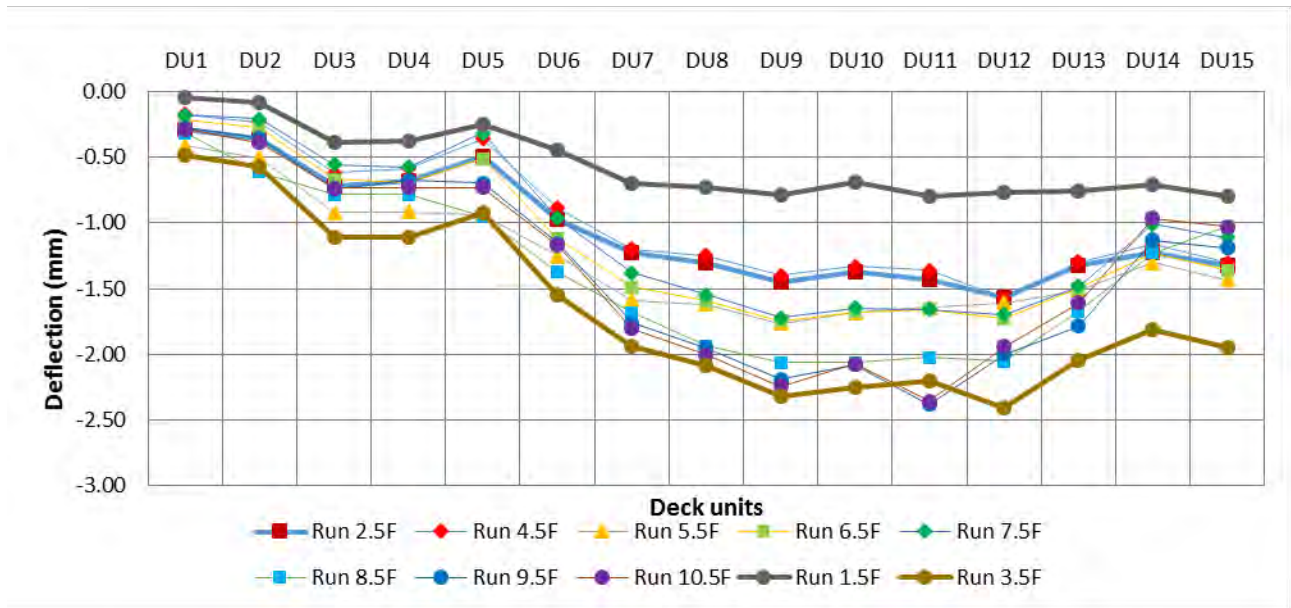


Figure H 19: Maximum joint movement measured in midspan, runs along the central path

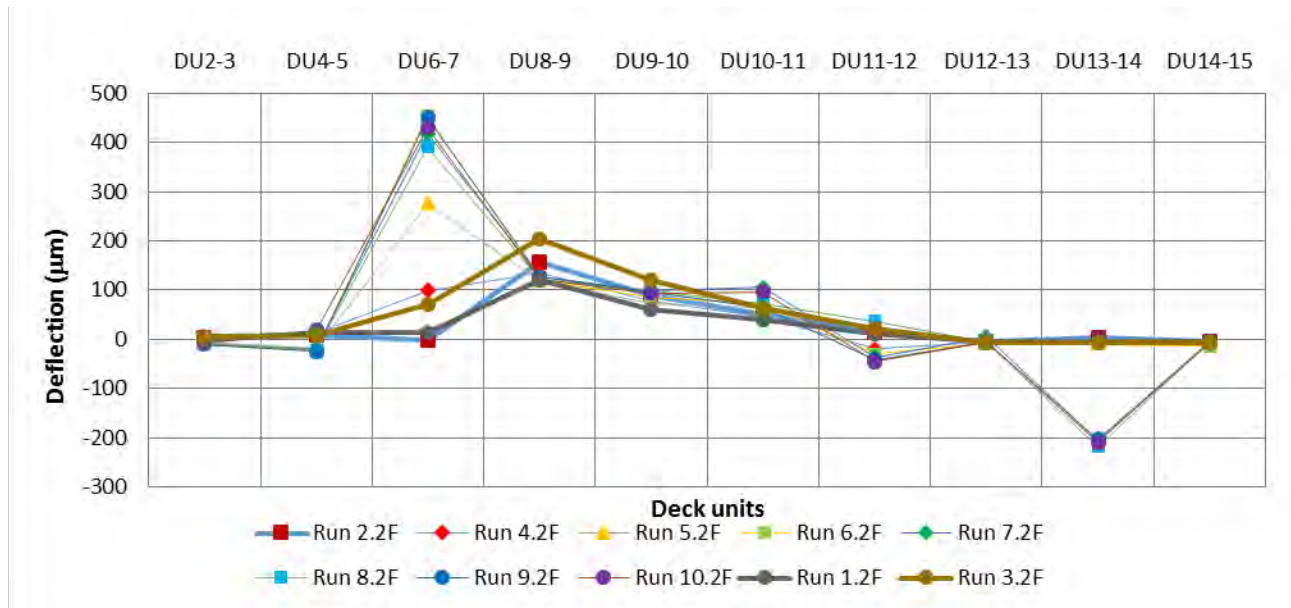


Figure H 20: Maximum joint movement measured in midspan, runs along the northern path

